STALL PROPAGATION IN AXIAL COMPRESSORS

ALAN H. STENNING

B.Sc., University of Glasgow
(1950)

S.M., Massachusetts Institute of Technology
(1951)

SUBMITTED IN PARTIAL FULFILLMENT
OF THE REQUIREMENTS FOR THE
DEGREE OF DOCTOR OF SCIENCE

at the

MASSACHUSETTS INSTITUTE OF TECHNOLOGY
June, 1955

Signature of Author.....
Department of Mechanical Engineering, May 10, 1955

Certified by.....
Thesis Supervisor

Accepted by.....
Chairman, Departmental Committee on Graduate Students

m e
Thesis
1955

MASS. INST. TECH.
SEP 28 1955
LIBRARY

Gas Turbine Laboratory
Mass. Inst. of Technology
May 10, 1955

Professor J. H. Keenan
Chairman, Committee on Graduate Students
Mechanical Engineering Department
Massachusetts Institute of Technology
Cambridge, Massachusetts

Dear Professor Keenan:

I submit herewith a thesis entitled "Stall Propagation in Axial Compressors" in partial fulfillment of the requirements for the degree of Doctor of Science at the Massachusetts Institute of Technology.

Very truly yours,

Alan H. Stenning

ABSTRACT

STALL PROPAGATION IN AXIAL COMPRESSORS

(Submitted to the Department of Mechanical Engineering on May 10, 1955, in partial fulfillment of the requirements for the degree of Doctor of Science in Mechanical Engineering).

A theory of stall propagation in a cascade of airfoils of high solidity has been developed which includes the effects of finite blade chord and of the boundary layer response to changes in angle of attack. The theory is valid for small perturbations in velocity about a mean flow condition with finite pressure rise across the cascade, provided that the pressure fluctuations behind the cascade are much smaller than those ahead of the cascade. The solution for the velocity of stall propagation indicates that the velocity increases with the wave length of the stall cell, tending towards a limiting value for very large stall cells. The wave length of the stall cells at the beginning of rotating stall is dependent on the magnitude of the boundary layer time delay.

The theory predicts propagation velocities within 25% over a wide range of wave lengths for a stationary circular cascade and a rotating blade row which have been tested. The experiments have confirmed that an increase in wave length is accompanied by an increase in propagation velocity if other parameters are unchanged.

Thesis Supervisor: Edward S. Taylor
Title: Professor of Aircraft Engines

ACKNOWLEDGEMENTS

The author is grateful to the students and members of the Gas Turbine Laboratory staff who participated in the experimental investigation. A. R. Kriebel designed the test cascade and was responsible for the success of the high speed schlieren photography. S. R. Montgomery and Lt. J. J. Braun U.S.N. investigated the stall characteristics of the single-stage compressor and provided the data on stall propagation in the rotor. The original idea of using a circular cascade came from Professor E. S. Taylor, who has guided the project since its initiation. Professor Harold E. Edgerton gave generously of his time and lent much equipment.

The investigation was sponsored by the National Advisory Committee for Aeronautics under Contract NAw - 6375.

TABLE OF CONTENTS

		Page
1.	INTRODUCTION	2
2.	A THEORY OF ROTATING STALL	
	2.1 Background	5
	2.2 An Analysis of Stall Propagation in a Cascade	9
	2.3 Discussion of the Results	25
3.	AN EXPERIMENTAL INVESTIGATION OF ROTATING STALL	
	3.1 The Stationary Cascade	26
	3.1.1 Instrumentation	28
	3.1.2 Cascade Performance	30
	3.1.3 Rotating Stall in the Cascade	33
	3.1.4 Effect of Cascade Solidity on Rotating Stall	41
	3.1.5 Comparison of Theory with Experiment	44
	3.2 The Single-Stage Axial Compressor	46
	3.2.1 Rotating Stall in the Free-Vortex Stage	46
4.	CONCLUSIONS AND SUGGESTIONS FOR FURTHER RESEARCH	49
	Nomenclature	51
	Appendices	53
	Bibliography	59
	Figures	60

1. INTRODUCTION

In 1941, an investigation of diffusers for centrifugal compressors was made by Whittle's group, who were at that time developing the first British jet engine. They constructed a low-speed research rig with an observation window to study, with tufts of thread, the flow pattern at the diffuser entrance. In one type of diffuser the observation was made that at low mass flow rates a region of flow reversal travelled around the diffuser in the direction of wheel rotation, causing flow separation on each diffuser blade in turn. The velocity of the travelling stall was approximately one-sixth of the rotor tip speed. This was the first recorded example of the phenomenon now known as "rotating stall". (Ref. 1) The phenomenon apparently attracted little attention at the time and no further reference to it can be found, although in the light of recent discoveries it is possible that rotating stall was the cause of some blading failures in the early Whittle engines.

Several years later, at a time when compressor blade failures had become one of the major problems in the development of the axial jet engine, rotating stall was rediscovered. Although the phenomenon was noted independently by several researchers, the first detailed study was apparently made by a research group working under the direction of H. W. Emmons at Harvard. (Ref. 2) Using hot-wire techniques to investigate flow conditions in an axial compressor Emmons' group found, when the compressor was throttled, that regions of low velocity appeared, travelling around the annulus in the direction of wheel rotation but at a lower speed. It was then apparent that blade failures previously unexplained were probably caused by vibratory stresses

induced by rotating stall.

Later investigations of rotating stall in single-stage and multi-stage compressors have been carried out at the California Institute of Technology (Ref. 3) and by the N.A.C.A. (Ref. 4)

The origin of rotating stall may readily be explained from consideration of the flow changes associated with blade stall. When a cascade of airfoils operates close to the stalled condition, a local increase in angle of attack on one airfoil may initiate stall on that blade. Due to the increased blockage effect of the separation region, some fluid spills around the affected channel, increasing the angle of attack on the blade above the stalled airfoil and decreasing the angle of attack on the blade below, so that the stalled region propagates along the blade row as shown in Figure 1.

The main concern of the compressor designer is the frequency with which stalled regions pass the compressor blades. It is desirable to be able to predict this frequency for a given compressor and, if necessary, to alter it to avoid blade resonance. Investigations of rotating stall in axial compressors have yielded a bewildering variety of results, with no apparent order, so that at present the desired goal is not in sight. Some success has been attained in predicting the velocity of propagation of the stalled regions, but no means has been found of predicting the number of stalled regions present in a given compressor, and this number must be known before the exciting frequency can be calculated.

The investigation described in this report was undertaken in the belief that a thorough study of stall propagation in the simplest

possible case (the single, two-dimensional cascade) was essential before approaching the more practical, but many times more complicated, problem of rotating stall in the axial compressor. Previous analyses of stall propagation in single cascades considered only disturbances of large wave length and were unable to give any clues to the reasons for the appearance of stalled regions of varying wave lengths as the inlet angle to the blade-row was changed. An analysis which included the effects of finite blade chord was therefore carried out and accompanied by experimental work on a single cascade and on a single-stage compressor to determine the validity of the available theories and the effects which must be included in a successful theory.

2. A THEORY OF ROTATING STALL

2.1 Background

Theoretical investigations of rotating stall have previously been undertaken by Emmons, Sears and Marble. In each case, the equations of motion were linearized, so that the analyses are strictly valid only for small perturbations in velocity about a mean flow condition.

In any analysis of stall propagation, the results obtained depend on the assumptions made about (a) the nature of the flow field after the cascade, (b) the form of the cascade characteristic and (c) the relative importance of the different dynamic effects which govern the velocity of propagation of disturbances along the cascade. The possible choices which can be made will be discussed before reviewing the three theories.

The flow field immediately behind a stalled cascade in steady flow consists of streams of fluid which have suffered little loss in stagnation pressure, separated by regions of low stagnation pressure shown in Figure 2. Downstream, mixing occurs between the high and low velocity regions, and at a distance of ten chord-lengths or so from the cascade the velocity is approximately uniform across the wake. In analyzing stall propagation, some approximation to the real conditions after the cascade in the unsteady flow must be made. Emphasis may be placed on the flow field immediately behind the cascade, by considering the flow to consist of a number of free jets entering a region of constant pressure. Alternatively, the region where mixing is complete may be considered to be of greater importance and the velocity distribution downstream assumed continuous throughout the field. The true condition lies between

these two extremes and may be closer to one or other of them depending on the size of the propagating stall regions relative to the blade chord. If the disturbance is very large relative to the blade chord, then its effect will be felt far downstream, and well beyond the mixing region. For this case, the mixing region can be neglected and the downstream flow field considered as a continuum. On the other hand, if the disturbance affects only two or three blades, it may be damped out within the mixing region and the downstream pressure changes will be small. The assumption of free jets discharging into a constant pressure chamber is then to be preferred.

The cascade performance may be represented by a curve of pressure coefficient, circulation, or effective discharge coefficient as a function of inlet angle to the cascade. This function may be continuous or discontinuous, and considerable disagreement exists as to which representation is the more accurate. This question will probably be settled only when dynamic measurements of cascade performance can be made.

In the most general case, three factors influence the speed of propagation of a disturbance along a cascade of airfoils in the stalled condition. These are: (a) the time required for movement of the separation point on the airfoil after a change in inlet angle, which will be called the boundary layer time delay, (b) the inertia of the fluid between the blades and (c) the inertia of the fluid outside the cascade. The relative importance of these effects depends on the size of the stall region with respect to the blade chord, because the boundary layer time delay and the inertia of the fluid within the blades are proportional

to the blade chord, while the inertia of the fluid affected by the disturbance outside the cascade is proportional to the wave length of the disturbance. In consequence, when disturbances covering many blades are considered, the boundary layer time delay and the inertia of the fluid within the cascade can be neglected.

The first analytical treatment of the problem was made by Emmons, in 1951.(Ref. 2) He showed that the cascade could be represented as a series of channels in parallel, with variable area outlets to represent the blockage effect of the separation regions. By investigating the stability of small disturbances ahead of the cascade, Emmons showed that if a critical value of rate of change of effective outlet area with angle of attack were obtained, disturbances would propagate unchanged along the cascade. For lower values of the derivative, disturbances died out, while for higher values they were amplified. The propagation velocity was governed by an arbitrarily assumed time delay between changes in angle of attack and changes in the flow field ahead of the cascade. Pressure variations behind the cascade were assumed negligible and the cascade characteristic was assumed to be a continuous function of inlet angle. Emmons did not solve the dynamic equations of motion and therefore was unable to predict the velocity of propagation.

Sears, in 1953 (Ref. 5), considered the case of disturbances large with respect to the blade chord and obtained the first complete solution. He assumed the existence of stalled regions moving with steady velocity along the cascade and calculated their velocity and the conditions required to produce them. The velocity field downstream of the cascade was considered to be continuous. Sears failed, however, to realize the

full consequences of the assumption of large stall cells and introduced a boundary layer phase lag which he believed to be of prime importance in influencing stall propagation. Although he obtained a solution showing stall propagation occurring with zero boundary layer phase lag, in his conclusions Sears still stated that "the speed of propagation of this phenomenon is determined by viscous effects." The cascade characteristic was represented as a continuous function of inlet angle, and the mean flow condition was considered to be one with no pressure rise across the cascade and no turning of the flow. The latter assumption is not a good one, because rotating stall commences in a cascade at an angle of attack only slightly greater than that corresponding to the peak of the pressure coefficient curve.

Marble, in 1954 (Ref. 6), noted the inconsistency in Sears' analysis with regard to the boundary layer delay, and presented a theory for large stall cells in which the inertia of the fluid outside the blade row was considered to be of much greater importance than either the boundary layer time delay, or the inertia of the fluid between the blades. In addition, by a very ingenious method, he was able to treat the effect of a discontinuity in the cascade pressure rise characteristic and show how the shape of the propagating wave changed as the mean inlet angle to the cascade increased. The propagation velocities obtained were the same as those predicted by Sears for zero boundary layer phase lag. Marble's theory, like Sears', is valid only for a mean flow condition with very small pressure rise across the cascade, since a finite step in pressure is accompanied by finite velocity changes and the theory is based on the assumption of small perturbations in velocity.

In summation, the theories presented by Sears and Marble should predict the velocity of propagation of stalled regions along a cascade in cases where the stalled regions are so large that the effects of the boundary layer delay, the inertia of the fluid within the blades, and the mixing region after the cascade can be neglected. They give no clues to the reasons for the appearance of different numbers of stall cells in a compressor as the compressor is throttled, and they are valid only if the cascade pressure coefficient is small when rotating stall commences.

In 1954, the author presented a theory which treated the case where the inertia of the fluid within the cascade could not be neglected, allowing also a finite pressure rise across the cascade when rotating stall commenced. (Ref. 7) A later development of the theory includes the boundary layer delay and offers a possible explanation of the varying number of stall cells which appear when a compressor is throttled. The complete analysis is presented in the following section.

2.2 Analysis of Stall Propagation in a Cascade

The main objective of the analysis is a consideration of stall propagation when the boundary layer time delay and the inertia of the fluid within the cascade cannot be neglected in comparison with the free stream inertia. As has already been suggested, for this case (which is one frequently encountered in practice) the pressure fluctuations downstream of the cascade should be small compared with the upstream fluctuations, so that the assumption that the flow behind the cascade consists of free jets discharging into a constant pressure region appears to be the more accurate one.

The model representation of the cascade and the method of attack employed are similar to that used by Emmons. The advantage of this method is that it uses the classic techniques of stability analysis to determine whether disturbances will be amplified or will die away, and thus gives a good physical understanding of the phenomenon.

Representation of the Cascade

The analysis is based on the model shown in Figure 3, with the cascade simulated by a series of channels of length L arranged in parallel, with variable area outlets. The fluid enters the cascade at (1) with entrance angle β_1, is turned to β_2 at (3) in a short distance, and leaves the channel at (2). The assumption is made that the effect of stall is to produce a discrete region of flow separation, so that the wake behind the cascade consists of a number of free jets discharging into a region of constant pressure.

The ratio of exit area to inlet area $\frac{A_2}{A_3}$ is defined to be a function of β_1.

$$\frac{A_2}{A_3} = \alpha = F\,(\cot\beta_1)$$

The assumption is made that local changes in α lag behind local changes in β_1 exponentially as shown in Figure 4, so that for step changes in β_1

$$\delta\alpha = (\delta\alpha)_{ss}\left[1 - e^{-t/\tau}\right]$$

where $(\delta\alpha)_{ss}$ is the steady state change in α corresponding to the change in β_1 and τ is the time constant of the boundary layer time delay. Thus, in general, when β_1 changes continually

$$\tau \frac{\partial(\delta\alpha)}{\partial t} = (\delta\alpha)_{ss} - \delta\alpha$$

at any instant where $(\delta\alpha)_{ss}$ is the steady state value of $\delta\alpha$

corresponding to the value of β_1 at that instant or $\delta\alpha = \frac{(\delta\alpha)_{ss}}{\tau D + 1}$ using operational notation where D denotes $\frac{\partial}{\partial t}$.

This representation of the boundary layer response is an extreme over-simplification of a complex phenomenon which is not yet fully understood. It is, of course, not possible to consider the changes in effective exit area as independent of the fluid velocity in the passage since the fluid itself forms the "gate." However, the response assumed gives the simplest model which includes the boundary layer delay and should at least yield some information on the effect of this delay.

A_2/A_3 is equivalent to the ratio

$$\frac{\text{actual flow through cascade}}{\text{ideal flow for same } (p_{o_1} - p_2) \text{ with no losses}}$$

and is obtainable, for a real cascade, from test results.

It can be seen that $\alpha = \frac{A_2}{A_3}$ is a measure of the "swallowing capacity" of the cascade and must therefore be important when the possibility of flow spillage around the entrance is considered. For a real cascade, it can be shown that α is equivalent to

$$\frac{\cos\beta_1}{\cos\beta_2 \sqrt{1 - C_p}}$$

for a rectilinear cascade, where C_p is the pressure coefficient (See Appendix I).

Additional assumptions are that the fluid is incompressible and frictionless, and that changes in β_2 in the unsteady flow can be neglected. The blades are considered to be very close together, so that α may be taken as a continuous function of y.

For the initial analysis, the boundary layer response is assumed fast compared with the inertia delays, so that τ is taken as zero.

The effect of the boundary layer delay is considered later.

Solution in the Field Before the Cascade

The cascade lies on the y-axis in the x-y plane. The fluid is considered to be incompressible. Perturbations are considered from a steady flow with inlet angle β_1 and velocity components c_x, c_y.

Since the flow entering the cascade is irrotational a velocity potential can be used.

In the unsteady flow,

$u = c_x + \varphi_x$

$v = c_y + \varphi_y$

$\Phi = c_x x + c_y y + \varphi$

Where Φ is the total velocity potential and φ is the perturbation potential

From continuity, $\frac{\partial u}{\partial x} + \frac{\partial v}{\partial y} = 0$; i.e. $\varphi_{xx} + \varphi_{yy} = 0$. Solutions to this equation are obtainable in the form:

$$\varphi = \sum_{n=1}^{\infty} \left[a_n(t) \cos \frac{n\pi y}{b} + b_n(t) \sin \frac{n\pi y}{b} \right] e^{\frac{n\pi x}{b}} \qquad (1)$$

representing periodic disturbances of half-wave length b and satisfying the boundary condition,

$$\varphi_x = \varphi_y = 0 \quad \text{at} \quad x = -\infty$$

The stability of the disturbances depends on the time-dependent functions $a_n(t)$, $b_n(t)$, which are as yet undetermined. From consideration of the dynamic equations, we may find the conditions required for the disturbances to be damped, amplified, or propagated unchanged along the cascade.

From Euler's equation for unsteady flow

$$\Phi_t + H = \text{constant}$$

where

$$H = \frac{c^2}{2} + \frac{p}{\rho} = \frac{u^2 + v^2}{2} + \frac{p}{\rho}$$

For small perturbations from the steady flow,

$$\varphi_t + c\,\delta c + \frac{\delta p}{\rho} = 0 \qquad (2)$$

Equations (1) and (2) are valid in the region $-\infty < x < 0$

Entry to the Cascade

The distance (1) - (3) is assumed small so that inertia effects between (1) and (3) may be neglected.

Thus,
$$\frac{c_1^2}{2} + \frac{p_1}{\rho} = \frac{c_3^2}{2} + \frac{p_3}{\rho}$$

$$c_1 \delta c_1 + \frac{\delta p_1}{\rho} = c_3 \delta c_3 + \frac{\delta p_3}{\rho} \qquad (3)$$

At (1), equation (2) may be rewritten

$$(\varphi_t)_1 + c_3 \delta c_3 + \frac{\delta p_3}{\rho} = 0 \qquad (4)$$

Momentum Effects in the Cascade

Considering the flow between (3) and (2) as one-dimensional, the momentum equation in the ℓ-direction is

$$\frac{\partial c}{\partial t} + c\frac{\partial c}{\partial \ell} + \frac{1}{\rho}\frac{\partial p}{\partial \ell} = 0$$

Integrating with respect to ℓ from (3) to (2), with the assumption that $c = c_3$ between (3) and (2) and the change in velocity from c_3 to c_2 takes place in a short distance

$$L\frac{\partial c_3}{\partial t} + \frac{c_2^2}{2} - \frac{c_3^2}{2} + \frac{p_2}{\rho} - \frac{p_3}{\rho} = 0$$

For small perturbations from a steady flow,

$$L\frac{\partial(\delta c_3)}{\partial t} + c_2 \delta c_2 - c_3 \delta c_3 - \frac{\delta p_3}{\rho} = 0 \qquad (5)$$

if p_2 does not change. Eliminating $(c_3 \delta c_3 + \frac{\delta p_3}{\rho})$ between (4) and (5),

$$L\frac{\partial(\delta c_3)}{\partial t} + (\varphi_t)_1 + c_2 \delta c_2 = 0 \qquad (6)$$

From continuity,

$$A_3 c_3 = A_2 c_2$$

$$A_3 \delta c_3 = A_2 \delta c_2 + c_2 \delta A_2$$

Thus, $$\delta c_2 = \frac{A_3}{A_2}\delta c_3 - c_2\frac{\delta A_2}{A_2}$$

and $$c_2\delta c_2 = \left(\frac{A_3}{A_2}\right)^2 c_3\delta c_3 - \left(\frac{A_3}{A_2}\right)^2 c_3^2\cdot\frac{\delta A_2}{A_2}$$

Also from continuity $u = c_3\cos\beta_2$ so that $\delta u = \varphi_x = \delta c_3\cos\beta_2$.

Substitution for c_3, δc_3 yields

$$c_2\delta c_2 = \left(\frac{A_3}{A_2}\right)^2\frac{c_x\varphi_x}{\cos^2\beta_2} - \left(\frac{A_3}{A_2}\right)^2\frac{c_x^2}{\cos^2\beta_2}\cdot\frac{\delta A_2}{A_2}$$

By substituting this expression for $c_2\delta c_2$ in (6) we obtain, at point (1), the following equation

$$\varphi_t + \frac{L}{\cos\beta_2}\varphi_{xt} + \frac{c_x\varphi_x}{\alpha^2\cos^2\beta_2} - \frac{c_x^2}{\alpha^2\cos^2\beta_2}\cdot\frac{\delta A_2}{A_2} = 0 \qquad (7)$$

But,

$$\frac{\delta A_2}{A_2} = \frac{\delta\alpha}{\alpha} = \frac{1}{\alpha}\frac{d\alpha}{d(\cot\beta_1)}\delta(\cot\beta_1)$$

$$= \frac{\alpha'}{\alpha}\delta(v/u) \quad \text{where } \alpha' = \frac{d\alpha}{d(\cot\beta_1)}$$

$$= \frac{\alpha'}{\alpha}\cdot\frac{\varphi_x - \cot\beta_1\varphi_y}{c_y}$$

Thus, at (1)

$$\varphi_t + \frac{L}{\cos\beta_2}\varphi_{xt} + \frac{c_x\varphi_x}{\alpha^2\cos^2\beta_2}\left[1 - \frac{\cot\beta_1\alpha'}{\alpha}\right] + \frac{\cot^2\beta_1\,\alpha'}{\alpha^3\cos^2\beta_2}c_x\varphi_y = 0 \qquad (8)$$

This equation must be satisfied by φ at the entrance to the cascade; that is, at $x = 0$. Substituting the solution for φ into (8) and separating coefficients of $\cos\frac{n\pi y}{b}$, $\sin\frac{n\pi y}{b}$ two simultaneous differential equations are obtained in $a_n(t)$ and $b_n(t)$

$$a_n\left[\left(\cos\beta_2 + \frac{Ln\pi}{b}\right)D + \frac{n\pi}{b}\cdot\frac{c_x}{\alpha^2\cos\beta_2}\left(1 - \frac{\cot\beta_1\alpha'}{\alpha}\right)\right]$$

$$+ b_n\left[\frac{n\pi}{b}\cdot\frac{\cot^2\beta_1\,\alpha' c_x}{\alpha^3\cos\beta_2}\right] = 0$$

$$b_n\left[\left(\cos\beta_2 + \frac{L n\pi}{b}\right)D + \frac{n\pi}{b}\cdot\frac{Cx}{\alpha^2\cos\beta_2}\left(1 - \frac{\cot\beta_1\alpha'}{\alpha}\right)\right]$$

$$- a_n\left[\frac{n\pi}{b}\cdot\frac{\cot^2\beta_1\,\alpha'\,Cx}{\alpha^3\cos\beta_2}\right] = 0$$

Assuming solutions of the form $a_n = A_n e^{\lambda_n t}$

$$b_n = B_n e^{\lambda_n t}$$

the characteristic equation

$$\left[\left(\cos\beta_2 + \frac{L n\pi}{b}\right)\lambda_n + \frac{n\pi}{b}\frac{Cx}{\alpha^2\cos\beta_2}\left(1 - \frac{\cot\beta_1\alpha'}{\alpha}\right)\right]^2$$

$$+\left[\frac{n\pi}{b}\,\frac{\cot^2\beta_1\,\alpha'\,Cx}{\alpha^3\cos\beta_2}\right]^2 = 0 \qquad (9)$$

is obtained.

The roots of this equation may represent oscillatory disturbances which are damped out, amplified, or persist unchanged depending on the value of the damping term containing $\left(1 - \frac{\cot\beta_1\alpha'}{\alpha}\right)$. If $\alpha' < \frac{\alpha}{\cot\beta_1}$, the disturbance will die away. If $\alpha' > \frac{\alpha}{\cot\beta_1}$, it will be amplified beyond the range in which a linearized analysis is valid. If $\alpha' = \frac{\alpha}{\cot\beta_1}$ (Figure 5), the disturbance will persist and a_n, b_n will be of the form $A_n\cos\omega_n t + B_n\sin\omega_n t$, $A_n \sin\omega_n t - B_n \cos\omega_n t$ respectively. The potential function then represents waves travelling along the cascade. At this point, the characteristic equation becomes,

$$\lambda_n^2 + \left[\frac{\frac{n\pi}{b}\cot\beta_1\ Cx}{\alpha^2\cos\beta_2\left(\frac{L n\pi}{b} + \cos\beta_2\right)}\right]^2 = 0$$

representing waves of frequency.

$$\omega_n = \frac{\frac{n\pi}{b}\cot\beta_1\ Cx}{\alpha^2\cos\beta_2\left[\frac{L n\pi}{b} + \cos\beta_2\right]} \qquad \text{radians/sec}$$

The velocity of wave propagation of the nth harmonic along the cascade V_n = frequency x wave length.

$$= \frac{\omega_n}{2\pi} \cdot \frac{2b}{n}$$

$$V_n = \frac{\cot\beta_1 \, c_x}{\alpha^2 \cos\beta_2 \left(\frac{Ln\pi}{b} + \cos\beta_2 \right)}$$

$$\frac{V_n}{c_x} = \frac{\cot\beta_1}{\alpha^2 \cos\beta_2 \left(\frac{Ln\pi}{b} + \cos\beta_2 \right)}$$

This result indicates that the velocity of stall propagation increases with the size of the stall cell, the limiting value of $\frac{V}{c_x}$ for stall cells covering many blades being: $\frac{\cot \beta_1}{\alpha^2 \cos^2 \beta_2}$. In Figures (6) and (7) $\frac{\alpha^2 V}{c_x}$ is plotted against β_1 for cascades with 10^o and 15^o turning and different values of $\frac{\pi L}{b}$. The velocity of propagation is taken as the velocity of the fundamental component of the wave. The expression for $\frac{U_n}{c_x}$ includes the number of the harmonic n and indicates that higher harmonics travel more slowly than the primary wave. This is not in accord with experience and shows that a linearized analysis is inadequate in this respect.

The propagation velocity may be conveniently related to the cascade pressure rise (which is a more familiar parameter than α) by replacing α with its equivalent $\frac{\cos\beta_1}{\cos\beta_2 \sqrt{1 - C_p}}$.

Then we obtain

$$\frac{V_n}{c_x} = \frac{\cot\beta_1 \, (1 - C_p)}{\cos^2\beta_1 \left(\frac{Ln\pi}{b\cos\beta_2} + 1 \right)}$$

$$\frac{V_n}{C_x} = \frac{2(1-C_p)}{\sin 2\beta_1 \left(\frac{Ln\pi}{b\cos\beta_2} + 1\right)}$$

For stall cells covering many blades, this expression reduces to

$$\frac{V}{C_x} = \frac{2(1-C_p)}{\sin 2\beta_1}$$

It should be noted that, with the boundary layer time delay neglected, no limitation is placed on the wave length of the disturbances. Consideration of the boundary layer delay permits prediction of the size of the wave in addition to the velocity.

Interference Effect of a Blade Row Upstream of the Cascade

With the assumption that pressure changes downstream of the cascade may be neglected, it is not possible to treat the interference effect of an additional blade row behind the cascade. Upstream interference effects are, however, very easily determined. If a row of closely spaced blades of very large chord is situated distance p from the cascade (Figure 8), then the perturbation velocity φ_x will be forced to zero at x = -p because of the high inertia of the fluid within the guide vanes. In any practical case, φ_x will not be zero at x = -p because of the finite chord of the guide vanes, but this approximation will permit an estimation of upstream interference. A solution for φ may then be found in the form

$$\varphi = \sum_{n=1}^{\infty} \left[a_n(t)\cos\frac{n\pi y}{b} + b_n(t)\sin\frac{n\pi y}{b}\right]\left[e^{\frac{n\pi x}{b}} + e^{\frac{-n\pi}{b}(x+2p)}\right]$$

satisfying the condition $\varphi_x = 0$ at x = -p. Substitution of this solution into equation (8) as before gives, for the case of undamped waves, when $\alpha' = \frac{\cot\beta_1}{\alpha}$

$$\omega_n = \frac{\left(\frac{n\pi}{b}\right)\cot\beta_1 C_x}{\alpha^2\cos\beta_2\left[\frac{Ln\pi}{b}\frac{\left(1-e^{\frac{-2n\pi p}{b}}\right)}{\left(1+e^{\frac{-2n\pi p}{b}}\right)} + \cos\beta_2\right]}$$

$$\frac{V_n}{c_x} = \frac{\cot\beta_1}{\alpha^2\cos\beta_2\left[\frac{L_n\pi}{b}\frac{1-e^{-2n\pi\frac{p}{b}}}{1+e^{-2n\pi\frac{p}{b}}}+\cos\beta_2\right]}$$

The equivalent expression for propagation velocity in terms of the cascade pressure coefficient is

$$\frac{V_n}{c_x} = \frac{2(1-c_p)}{\sin 2\beta_1\left[\frac{L_n\pi}{b}\frac{1-e^{-2n\pi\frac{p}{b}}}{1+e^{-2n\pi\frac{p}{b}}}+1\right]}$$

Thus, interference increases the velocity of propagation for $\frac{L\pi}{b}$ of order unity but does not change it for disturbances with wave lengths large compared with the blade chord. If p/b is very small, then the coefficient of $\frac{Ln\pi}{b}$ is effectively zero and we may put $\frac{V_n}{c_x} = \frac{\cot\beta_1}{\alpha^2\cos^2\beta_2}$ which is the same result as that obtained without upstream interference when the wave length is large. The addition of a row of guide vanes upstream of the cascade therefore decreases the influence of the inertia of the fluid within the stalled cascade on the velocity of propagation.

An approximation to the velocity of stall propagation relative to the rotor in a single stage compressor with guide vanes close to the wheel thus may be obtained by putting $\frac{V}{c_x} = \frac{\cot\beta_1}{\alpha^2\cos^2\beta_2}$. This should be valid only when the blades are stalled from root to tip so that the flow is effectively two-dimensional.

Effects of the Boundary Layer Delay

The time constant τ of the boundary layer delay will now be included in the analysis to determine the additional limitations it imposes on stall propagation. Returning to equation (7)

$$\varphi_t + \frac{L}{\cos\beta_2}\varphi_{xt} + \frac{c_x\varphi_x}{\alpha^2\cos^2\beta_2} - \frac{c_x^2}{\alpha^2\cos^2\beta_2}\cdot\frac{\delta\alpha}{\alpha} = 0$$

and setting

$$\delta\alpha = \frac{\alpha'}{\tau D+1}\,\delta(\cot\beta_1)$$

the equation satisfied by φ at (1) is

$$\tau\varphi_{tt} + \frac{L\tau}{\cos\beta_2}\varphi_{xtt} + \varphi_t + \varphi_{xt}\left[\frac{L}{\cos\beta_2} + \frac{\tau c_x}{\alpha^2\cos^2\beta_2}\right] \tag{10}$$

$$+ \frac{c_x\varphi_x}{\alpha^2\cos^2\beta_2}\left[1 - \frac{\cot\beta_1\alpha'}{\alpha}\right] - \frac{\cot^2\beta_1\,\alpha'}{\alpha^3\cos^2\beta_2}\cdot c_x\varphi_y = 0$$

Inserting the solution for φ of equation (1) and separating the coefficients of $\cos\frac{n\pi y}{b}$, $\sin\frac{n\pi y}{b}$ gives two second order differential equations in a_n, b_n.

Taking solutions of the form $a_n = A_n e^{\lambda_n t}$

$$b_n = B_n e^{\lambda_n t}$$

a characteristic equation for λ_n is found

$$\left\{\left[\tau + \frac{n\pi}{b}\frac{L\tau}{\cos\beta_2}\right]\lambda_n^2 + \left[1 + \frac{n\pi}{b}\left(\frac{L}{\cos\beta_2} + \frac{\tau c_x}{\alpha^2\cos^2\beta_2}\right)\right]\lambda_n\right\}^2 \tag{11}$$

$$+ \frac{n\pi}{b}\frac{c_x}{\alpha^2\cos^2\beta_2}\left[1 - \frac{\cot\beta_1\alpha'}{\alpha}\right]$$

$$+ \left\{\frac{n\pi}{b}\frac{\cot^2\beta_1\,\alpha'\,c_x}{\alpha^3\cos^2\beta_2}\right\}^2 = 0$$

This equation will be examined to find the conditions for undamped oscillations in time.

Equation (11) is of form

$$\left[p_1\lambda_n^2 + p_2\lambda_n + p_3\right]^2 + p_4^2 = 0 \tag{12}$$

For undamped oscillations, $\lambda_n = \pm i\omega_n$ must be a root.

With $\lambda_n = +i\omega_n$ a solution

$$\left[-p_1\omega_n^2 + ip_2\omega_n + p_3\right]^2 + p_4^2 = 0 \tag{13}$$

With $\lambda_n = -i\omega_n$ a solution

$$\left[-p_1\omega_n^2 - ip_2\omega_n + p_3\right]^2 + p_4^2 = 0 \tag{14}$$

Subtracting (14) from (13) and factoring

$$2\left[-p_1\omega_n^2 + p_3\right]\left[2ip_2\omega_n\right] = 0$$

Thus if $\lambda_n = \pm i\omega_n$ is a root of equation (12)

then $\omega_n^2 = \frac{p_3}{p_1}$

Putting $\omega_n = \sqrt{\frac{p_3}{p_1}}$ in equation (13)

Then

$$\left[-p_3 + ip_2\sqrt{\frac{p_3}{p_1}} + p_3\right]^2 + p_4^2 = 0$$

$$-p_2^2 \cdot \frac{p_3}{p_1} + p_4^2 = 0$$

or
$$p_3/p_1 = (p_4/p_2)^2 \qquad (15)$$

The requirements for an undamped oscillatory solution to equation (12) are, therefore, that $\frac{p_3}{p_1} = (\frac{p_4}{p_2})^2$. With this requirement satisfied, two of the roots of the equation are $\pm i\omega_n$ where $\omega_n = \frac{p_4}{p_2}$.

A factor of the equation is then $\left[\lambda_n^2 + \left(\frac{p_4}{p_2}\right)^2\right]$ and the

remaining two roots satisfy the equation

$$\lambda_n^2 + 2\left(\frac{p_2}{p_1}\right)\lambda_n + \left[\left(\frac{p_4}{p_2}\right)^2 + \left(\frac{p_2}{p_1}\right)^2\right] = 0 \qquad (16)$$

For the remaining two roots to be stable the coefficient of λ_n in equation (16) must be positive; i.e. $(\frac{p_2}{p_1})$ must be positive.

It can be seen, therefore, that for equation (12) to have roots representing undamped oscillations of frequency ω_n:

1. All coefficients must be positive
2. $\frac{p_3}{p_1} = (\frac{p_4}{p_2})^2$

Under these circumstances, $\omega_n = \frac{p_4}{p_2}$

Applying these results to equation (11), the requirement for stall propagation is

$$\frac{\left[\frac{n\pi}{b}\ \frac{C_x}{\alpha^2\cos^2\beta_2}\left(1-\frac{\cot\beta_1\,\alpha'}{\alpha}\right)\right]}{\tau\left[1+\frac{n\pi}{b}\cdot\frac{L}{\cos\beta_2}\right]}$$

$$= \frac{\left[\frac{n\pi}{b}\ \frac{\cot^2\beta_1\ \alpha'\ C_x}{\alpha^3\ \cos^2\beta_2}\right]^2}{\left[1+\frac{n\pi}{b}\left(\frac{L}{\cos\beta_2}+\frac{\tau C_x}{\alpha^2\cos^2\beta_2}\right)\right]^2} \qquad (17)$$

and the frequency of the oscillations at any point in radians/second is

$$\omega_n = \frac{\frac{n\pi}{b}\ \frac{\cot^2\beta_1\ \alpha'\ C_x}{\alpha^3\ \cos^2\beta_2}}{1+\frac{n\pi}{b}\left(\frac{L}{\cos\beta_2}+\frac{\tau C_x}{\alpha^2\cos^2\beta_2}\right)} \qquad (18)$$

If $\tau = 0$ the same results are obtained as in the earlier analysis. The importance of this solution lies, not in the precise relationship, but in the fact that a relation is established between $\frac{L}{b}$, τ, α, α', β_1 and β_2 for stall propagation to be possible. More explicitly, since for a given cascade τ, α, α', and β_2 all depend on β_1, a relationship has been found between $\frac{L}{b}$ and β_1 for stall propagation. Thus, over a range of inlet angles, stall propagation can occur and the size of the stall cell will depend on the inlet angle. This result may explain the variation in size and number of stall cells found in an axial compressor stage over the working range of angle of attack.

It can be seen that with the boundary layer delay included in the analysis, stall propagation occurs with $(\frac{\cot\beta_1\alpha'}{\alpha})$ less than unity, so that the frequency of the disturbances is lower than the frequency of the stalls of the same wave length when the boundary layer is left out.

The boundary layer delay therefore has the effect of decreasing the velocities of propagation of the stalled regions. The boundary layer time constant should be approximately of the order $\frac{L}{c_3}$ so that the boundary layer delay may be of equal importance with the inertia delay of the fluid within the cascade, and will have little effect on the velocity of propagation of large stall cells.

Calculation of the Wave Length When Rotating Stall Commences

It is now possible, without making any additional assumptions, to predict the wave length of the disturbances when rotating stall commences. Because of the simple representation employed for the boundary layer response it would be unwise to attempt to derive numerical values from this result, but it is of interest inasmuch as the main features of the phenomenon can be reproduced with a simple model.

Returning to equation (17), which can be rewritten

$$\frac{\left[1-\frac{\cot\beta_1\alpha'}{\alpha}\right]}{\left[\frac{\tau\cot^4\beta_1\,\alpha'^2 C_x}{\alpha^4\cos^2\beta_2}\right]} = \frac{\frac{n\pi}{b}\left[1+\frac{n\pi}{b}\frac{L}{\cos\beta_2}\right]}{\left[1+\frac{n\pi}{b}\left(\frac{L}{\cos\beta_2}+\frac{\tau C_x}{\alpha^2\cos^2\beta_2}\right)\right]^2}$$

as the requirement for stall propagation to be possible, it can be seen that as the inlet angle β_1 to the cascade is increased and flow separation commences on the airfoils, α' will increase from almost zero to a positive quantity. The group on the left side of the equation (denoted below by A) will therefore have a value which begins as a large positive quantity at the design point and decreases as β_1 is increased. At any setting of β_1, the group on the right side of the equation (denoted by C) can have an infinite number of

values for each harmonic, depending on the value of b assumed. Considering only the primary component of the wave ($n = 1$), there will however be a maximum value of C corresponding to a wave length which might be considered as the wave length which is closest to being propagated. As β_1 is increased, the maximum possible value of C can be computed for each value of β_1 and compared with the value of A (see Figure 9), which will in general be larger than C. However, as β_1 is increased the difference between A and C shrinks until, at the critical value of β_1, the maximum value of C corresponds to the value of A at that point and stall propagation becomes possible for the wave length which yields this value of C. The problem is, therefore, the determination of the value of b which gives $(C)_{max}$.

For the primary component of the wave

$$C = \frac{\frac{\pi}{b}\left[1 + \frac{\pi}{b}\frac{L}{\cos\beta_2}\right]}{\left[1 + \frac{\pi}{b}\left(\frac{L}{\cos\beta_2} + \frac{\tau c x}{\alpha^2 \cos^2\beta_2}\right)\right]^2}$$

$$= \frac{\pi\left[b + \frac{\pi L}{\cos\beta_2}\right]}{\left[b + \pi\left(\frac{L}{\cos\beta_2} + \frac{\tau c x}{\alpha^2 \cos^2\beta_2}\right)\right]^2}$$

For a maximum (or minimum) value of C, $\frac{dC}{db} = 0$ and this occurs when

$$b = \frac{\pi L}{\cos\beta_2}\left[\frac{\tau}{\alpha^2 (L/c_0)} - 1\right]$$

A study of the expression for C shows that this value of b gives a maximum value of C, at a value of b which may be positive or negative depending on whether $\frac{\tau}{\alpha^2 (L/c_3)}$ is greater than, or less than unity.

There are now two possibilities. If $\frac{\tau}{\alpha^2(L/c_3)} > 1$, then for positive (i.e. real) values of b, C has a maximum when $b = \frac{\pi L}{\cos\beta_2}\left[\frac{\tau}{\alpha^2(L/c_3)} - 1\right]$ and this will be the value of b when stall propagation commences. If $\frac{\tau}{\alpha^2(L/c_3)} < 1$, then the maximum value of C for positive values of b occurs when b = 0, and stall propagation will commence with the smallest values of b that are physically possible. Thus, the wave length is governed by the ratio $\frac{\tau}{(L/c_3)}$ which is the ratio of the boundary layer time delay to the inertia delay of the fluid within the cascade.

Stall Propagation in a Circular, Radial Flow Cascade

For a radial outflow cascade, of the type used for the experimental study, an expression for propagation velocity may be derived in r-θ coordinates (See Appendix II).

With guide-vane interference effects included, but omitting the boundary layer time delay,

$$\frac{V}{c_{r_1}} = \left(\frac{r_1}{r_2}\right)^2 \frac{\cot\beta_1}{\alpha^2 \cos\beta_2 \left[\frac{Lm}{r_1}\frac{1-(R/r_1)^{2m}}{1+(R/r_1)^{2m}} + \cos\beta_2\right]}$$

where $\left(\frac{r_1}{r_2}\right)$ is the ratio $\frac{\text{inside radius of cascade}}{\text{outside radius of cascade}}$, R is the outside radius of the guide vanes, and m is the number of stall cells in the cascade. Consideration of the boundary-layer time delay yields lower values of $\frac{V}{c_{r_1}}$ than does the expression given above.

In terms of the cascade pressure coefficient

$$\frac{V}{c_{r_1}} = \frac{2(1-C_p)}{\sin 2\beta_1 \left[\frac{Lm}{r_1 \cos\beta_2}\frac{1-(R/r_1)^{2m}}{1+(R/r_1)^{2m}} + 1\right]}$$

and this reduces to the same form as for the rectangular cascade when the stall cells are very large, or the gap between the guide-vanes and the cascade is small.

2.3 Discussion of the Solutions

The most important point of difference between the present analysis and those of Sears and Marble is the assumption made here that downstream pressure fluctuations may be neglected. For the case considered by Sears (that with no pressure rise across the cascade when stall propagation occurs), $C_p = 0$ and the present analysis then yields for disturbances with large wave length $\frac{V}{c_x} = \frac{2}{\sin 2\beta_1}$. This is double the value obtained by Sears. Because C_p always lies in the range 0.3 to 0.6 when stall propagation commences, the values for propagation velocity given by the present theory in any practical case are never double Sears' values, but may be greater or less than those predicted by him depending on the pressure rise and whether the wave length of the disturbance is large with respect to the blade chord, or of the same order of magnitude.

The values of propagation velocity predicted when the boundary-layer delay is neglected should be larger than those obtained experimentally, with the difference most pronounced for the case of disturbances covering only a few airfoils, when the boundary-layer delay will have an important effect. An increase in the wave length of the stall cells should be accompanied by an increase in propagation velocity, if other variables are unchanged.

3. AN EXPERIMENTAL INVESTIGATION OF ROTATING STALL

Experimental work has been carried out using both a stationary cascade and a single stage axial compressor. This combination has proved exceedingly useful, because a wide range of stall wave lengths could be examined and the measured characteristics compared with theory. In addition, a comparison of phenomena observed in the two test rigs has given an indication of the value and limitations of the circular cascade as a research tool to reproduce effects found in turbomachines.

3.1 The Stationary Cascade

In order to obtain the simplest possible type of flow in which a stable rotating stall pattern could be observed, the cascade was constructed in the form of a circle between two flat plates (Figure 11). Air flows outwards through the cascade, and the angle of incidence of the air entering the blades is controlled by a set of variable-angle nozzles ahead of the cascade. There are fifty-four compressor blades and an equal number of nozzles. Provision has been made for removal of the wall boundary layers by suction through slots machined in the casing just after the nozzles. Air enters the test section through two pipes parallel with the central axis of the cascade and turns into the plane of the cascade before being accelerated in the nozzles. After leaving the cascade, the air is collected in a scroll and returned to the compressors.

Details of the test rig are shown in Figures 12 to 17 and a schematic of the flow circuit with fluid properties tabulated for a

typical operating condition is given in Figure 17. With the closed circuit arrangement, the Reynolds number and Mach number may be varied independently by changing the pressure level in the circuit. Reynolds numbers up to 300,000 (based on blade chord and conditions entering the cascade) and approach Mach numbers up to 0.8 are attainable.

The dimensions of the cascade blading are 1.71" length by 0.96" chord and the airfoil section is shown in Figure 18. The airfoil shape was obtained by conformal mapping of a rectilinear cascade into a circular cascade with radius ratio $\frac{\text{outside radius of cascade}}{\text{inside radius of cascade}}$ of 1.09. In the transformed cascade, the chord of the airfoil (defined as the straight line joining the centers of curvature of the leading and trailing edges) makes an angle of 42 degrees with the radius through the leading edge. The design point inlet air angle is 48.5° to the radius and the outlet air angle is 38°. The blades of the cascade are located in position by pins which fit into holes drilled in the casing on a circle of radius 8.23" (Figures 14 and 18). After the stagger angle has been set, the blades are clamped into position at one end with bar-clamps which fit over the ends of the pins and fasten adjacent blades together in pairs. It is thus possible to change the stagger of the cascade by loosening the clamps and resetting the blades. A different procedure is required for the three blades in the observation window since clamps would obscure the picture. These blades are retained in position by a wire soldered to their trailing edges and to the trailing edges of the clamped blades adjacent to the window.

At the commencement of the test program, difficulty was encountered with frequent torsion failures of the pins on the clamped ends of the

blades. In addition, blade vibration caused chipping of the optical flats around the pins (showing as a circular blemish on the Schlieren photographs) and the solder failed to hold the connecting wire to the blades in the window. These problems were ameliorated, though not completely solved, by cementing the blades to the casing on the clamped side and covering the pins of the blades in the test window with cement before inserting them in the window, thus increasing the damping and also cushioning the surface of the glass.

The design of the test rig and cascade is described in detail in References 8 and 9.

3.1.1 Instrumentation

The observations made in the cascade may be divided into two classes, measurements of mean or steady state values of pressure, velocity and flow direction, and observations of instantaneous values of these parameters and of the changes in the flow field around the airfoils in rotating stall.

To obtain mean values of static pressures before and after the cascade, three pressure taps were fitted before the cascade at 120° from each other on a circle of 7.69" radius, and three pressure taps mounted after the cascade between the first three on a circle of 8.94" radius. Total pressure probes were mounted in both inlet pipes to permit a total pressure traverse before the nozzles, and the test window could be removed and replaced by a small traversing gear to obtain a total pressure traverse ahead of the blades in the window.

The air angle leaving the cascade was measured with an uncertainty of $\pm 2^{\circ}$ using tufts attached to the connecting wire. The air angle entering the cascade was assumed equal to the nozzle outlet angle, since flow

deviation is small for nozzles and the nozzles were so close together that accurate measurement of the air angle could not be obtained. An error of the order $\pm 2^{\circ}$ is therefore possible in air inlet angle.

The mass flow through the cascade was obtained with an estimated accuracy of $\pm$ 1/2% using a standard A.S.M.E. orifice meter. The total temperature leaving the compressor was measured using a thermocouple with an accuracy of $\pm 2^{\circ}$F. From a knowledge of mass flow, air angle, total temperature and static pressure it was possible to compute the magnitude of the parameter $\frac{m\sqrt{T_o}}{A\,p}$ entering the cascade from which, using gas tables for compressible flow, the mean entry Mach number, velocity, and total pressure could be found. A check on the accuracy of this method of calculating the conditions entering the cascade was available, inasmuch as the mean total pressure obtained should be very close to the average value found from a total pressure traverse ahead of the cascade. A comparison of the two values at several operating points showed agreement within 0.5%, so that it was not necessary to make total pressure traverses ahead of the cascade at each operating condition to find the mean total pressure.

For observations in the unsteady flow, the main instrument used was the Gas Turbine Laboratory portable schlieren apparatus, which proved effective for entry Mach numbers to the cascade as low as 0.2. Schlieren photographs were taken using a General Radio 35 mm high speed camera, and a 16 mm Fastax camera, in conjunction with an Edgerton high speed stroboscopic flash unit operated at flash rates up to 6000 c.p.s. The schlieren photographs showed the propagation velocity and the frequency

of the rotating stalls, as well as the changes in air angle ahead of the cascade and the nature of the flow around the airfoils. A pair of hot wire instruments gave another method of calculating the propagation velocity and number of stall cells, and also showed qualitatively the nature of the velocity fluctuations. A barium crystal was used for comparisons of the pressure fluctuations before and after the cascade.

3.1.2 Cascade Performance

Before commencing the test program, total pressure traverses were made in the inlet pipes and ahead of the blades in the test window. The thickness of the boundary layer in each inlet pipe was of the order of 0.1" and outside the boundary layer a maximum variation in total pressure equal to 8% of the mean dynamic pressure was observed, so that the total variation in velocity outside the boundary layer did not exceed 4% of the mean velocity. Variation in mean total pressure between the two inlet pipes did not exceed 3% of the mean dynamic pressure in the inlet pipes. In spite of the uniformity of the conditions entering the test section, considerable asymmetry in static pressure around the cascade was observed after the nozzles, especially when the inlet angle β_1 to the cascade was low. At the design inlet angle, the total variation in static pressure around the cascade was 12% of the mean dynamic pressure leaving the nozzles. The asymmetry gradually disappeared as the rotating stall region was entered. These pressure variations were too large to be explainable by errors in nozzle throat area. Also, the scroll shape should have had little upstream effect since the velocity in the scroll was very low. The most plausible explanation of the pressure variation around the cascade appears to lie in the possible presence of regions of separated flow

within the duct which turned the flow leaving the inlet pipes into the plane of the cascade. Due to the space requirements of the schlieren apparatus, the duct was designed for no acceleration of the air as it turned, so that unfavorable pressure gradients in some areas may have caused flow separation before the nozzles. This effect would explain the decrease in the percentage asymmetry with increasing β_1, since upstream irregularities become less important as the pressure drop across the nozzles increases.

Ahead of the blades in the test window variations in total pressure outside the wall boundary layers and the nozzle wakes were less than 5% of the mean dynamic pressure entering the cascade. The thickness of the wall boundary layers was of the order of 0.050" and the width of the nozzle wakes was approximately 0.070".

The cascade performance was obtained in terms of the pressure rise across the cascade and the cascade outlet angle and is shown in Figures 19, 20 in which the cascade pressure coefficient C_p and the outlet angle β_2 to the radial direction are plotted versus β_1. It was found most convenient to operate the wind-tunnel compressors at constant rotational speed during a test run and vary the air angle entering the cascade. Because of the compressor characteristic, this procedure resulted in almost constant mass flow through the cascade at any one rotational speed, independent of nozzle angle, and in consequence the Mach number leaving the nozzles increased as the nozzles were closed. Each curve in Figure 19 corresponds to a constant value of the ratio $\frac{\text{compressor tip speed}}{\text{speed of sound in air entering compressor}}$ denoted by π_m, and in Figure 21 the Mach number entering the cascade is plotted

against β_1 for each of the three compressor speeds used. It can be seen in Figure 19 that for any value of β_1, there is a slight increase in C_p with increasing Mach number. Within experimental error, no change in β_2 with Mach number could be determined.

Starting at an inlet angle of 42°, the pressure coefficient increases with β_1 until at 48° the curve flattens out briefly before rising again. The explanation of this dip lies in the fact that the nozzle wakes wash over the airfoils at a value of β_1 equal to 49° and have a serious effect on the cascade performance. The pressure coefficient then rises once more until a peak value is attained at an inlet angle of 56°. Thereafter, the pressure coefficient falls, until when β_1 equals 59° the curve starts to flatten, has a minimum value at 60°, a second peak at 63°, and then falls off again. The nozzle wakes cross the airfoils a second time when β_1 attains a value of 60° and at this point some unsteadiness was observed in the nozzle and cascade wakes, but stall propagation did not begin until the nozzle wakes passed the cascade. Random stalls were observed at an inlet angle of 61°, and periodic rotating stall commenced at an inlet angle of 64°.

It has been suggested that the temporary rise in pressure coefficient after initiation of the unsteady flow may be partly due to the increase in the root-mean-square value of the velocity entering the cascade. For a given inlet angle and mass flow rate in an unsteady flow, the mean pressure rise across the cascade is proportional to the time mean value of $(\text{velocity})^2$, which increases as the velocity fluctuations become larger.

At the lowest compressor speed, the Mach number entering the cas-

cade does not exceed 0.35, so that compressibility effects should be small and the experimental results may be used to test the theory of Chapter 1. Using the method of Appendix I, α has been calculated for each inlet angle up to the point where rotating stall commences, and is plotted against $\cot\beta_1$ in Figure 22. At the point where rotating stall begins, the curve is practically a straight line, with a gradient very close to the value predicted by the theory, the tangent passing slightly below the origin instead of through it. This result is in agreement with experimental evidence for rectilinear cascades presented by Emmons in Reference 2. In the circular cascade, rotating stall started at a value of α of approximately 0.80. It is, of course, impossible to find values of α for higher angles of attack in the rotating stall region because of the unsteady flow, and the nozzle angle could not be increased sufficiently to pass through the unsteady flow region into a state of steady, fully stalled flow.

Spark schlieren photographs of the airfoils in the steady flow are presented in Figure 23, at inlet angles of 42°, 46°, 49.5°, 53.2°, 56.8° and 60.4°. The nozzle wakes and the cascade boundary layers are visible and the forward movement of the separation point with increasing β_1 can be observed.

3.1.3 Rotating Stall in the Cascade

As the nozzle angle was increased beyond 60°, the onset of rotating stall was accompanied by an increase in air noise from the apparatus, with a sharp intensification of the sound at 64° when full rotating stall commenced. For inlet Mach numbers above 0.5, lambda shocks appeared on the upper surface of the airfoils at high nozzle angles and

the occurrence of these shock waves was signalled by a high pitched screaming sound. The rotating stall phenomena at low Mach numbers will be described first, since compressibility effects had a strong influence on the periodicity of the stall pattern.

To obtain satisfactory schlieren pictures, M_1 was required to be at least 0.2. In consequence, a compressor π_m of 0.173 (with M_1 ranging from 0.2 to 0.35) was most suitable for evaluation of rotating stall phenomena at low Mach numbers and extensive testing was carried out at this speed setting of the wind-tunnel compressor. As can be seen from Figure 23f, just before the transition from steady flow to random stall occurred the separation point on the suction surface of the airfoils was approximately 30% of the chord length aft of the leading edge. A 1° increase in angle of attack from this point was sufficient to start random stall.

In this region of operation, the disturbance did not always propagate from blade to blade across the window but would frequently die out before reaching the last blade. Small differences in blade setting may have been responsible for this effect, since the possible variation from the nominal setting was estimated at $\pm 1^\circ$. Figure 24 shows one cycle of stall and unstall in the random-stall regime. Some of the pictures taken in this region of operation showed the airfoils in the window remaining stalled for 20 to 30 milliseconds before unstalling, while others revealed stalls propagating across the window at intervals of 5 to 10 milliseconds. With increasing β_1, the disturbances appeared more regularly until at $\beta_1 = 64^\circ$ the disturbances crossed the window at time intervals ranging from 3.2 to 5.6 milliseconds and could now be properly called

"rotating stall" (Figure 25). An airfoil was now stalled for approximately 40% of the time, and the wave length of the stalls was about six blade-spacings. With further increases in β_1, the stalls appeared more regularly and at $\beta_1 = 67^\circ$ (Figure 26) the time intervals between disturbances varied only from 3.0 to 3.6 milliseconds. From the film records the velocity of propagation could be calculated within 5% and it was found that at any nozzle setting there was little variation in propagation velocity between stall cells, but the average propagation velocity increased from 90 fps to 120 fps as β_1 was increased from 63° to 67°. Due to the variation in the time interval between stalls and the uncertainty in propagation velocity the number of stall cells could only be estimated within ± 1 cell, but there appeared to be approximately nine cells in the cascade at $\beta_1 = 64^\circ$, with the number increasing to eleven at $\beta_1 = 67^\circ$. In Table I on page 38, the measured propagation velocities are tabulated and compared with the results obtained using hot wire equipment.

Over the whole range of inlet angles for which rotating stall was obtained, it was found that the time required to unstall an airfoil was always greater than the time required to stall the airfoil, the former process requiring approximately 0.6 to 0.8 milliseconds, while the latter was completed in 0.4 to 0.5 milliseconds (Figures 24, 25, 26, 27). That this should be so is not surprising when it is considered that the fluid in the separated region can only be removed at its own low velocity after boundary-layer reattachment becomes possible, while the boundary layer can separate from all points of the upper surface of the airfoil when stall occurs and fill the passage very rapidly. At the

higher values of β_1, reversed flow was observed in the channels between airfoils after stall had occurred, so that after the reverse flow had stopped, a slug of initially stationary fluid had to be removed from the channel before good flow could recommence (Figures 26, 27). It can be seen, therefore, that it is impossible to separate the boundary layer time delay from the inertia effect for measurement purposes during the unstalling process since the flow rate through the channel must be changed before the reattached boundary layer can be seen. On the other hand, when the airfoil stalls, flow separation and a decrease in α can take place without necessarily being accompanied by a change in flow rate through the channel, so that the time taken to stall after a change in inlet angle can be used to obtain an upper limit for the boundary layer delay. The average time for stall was approximately 0.5 milliseconds throughout the range of inlet angles; but this is not equal to the boundary layer time delay τ, since for the equivalent exponential-lag system, the minimum time required to attain 95% of the final change in α after a step change in β_1 would be 3τ. An approximate value for τ is therefore 0.16 milliseconds. The inertia time constant L/C_3 was equal to 0.35 milliseconds for this operating condition, since $C_3 = \frac{C_r}{\cos\beta_2} = 230$ fps and the blade chord L = 0.96 inches. Thus, the upper limit to the value of τ was approximately $1/2 \frac{L}{C_3}$ and the true value was certainly smaller than this since the inlet angle did not change instantaneously and the observed response of the boundary layer was therefore slower than the theoretical response to a step-change in inlet angle.

An interesting feature of the photographs is the occasional appearance of what seem to be vortex-planes at the entrance to a channel after

after stall at the moment when the fluid within the channel is stationary and the unstalling process is about to commence (Figure 27). The planes retain their identity in subsequent pictures and move through the channel as good flow is re-established. These planes may be formed by shear action between the deflected main flow and the staionary fluid within the passage, and are visible as sharp lines only when they are perpendicular to the plane of the cascade.

Hot wire equipment was used to check the number of stall cells and the propagation velocity, and also for traversing in the spanwise direction to determine whether the whole passage was affected by rotating stall. The equipment employed was of the type manufactured by the Flow Corporation of Cambridge, Massachusetts and is shown in Figure 28 with the dual-beam oscilloscope, Land Camera, and audio-oscillator. Two hot wire probes were installed behind the cascade at a distance apart of nine blade spacings. The signals from the probes were amplified, fed to the dual-beam DuMont Type 322 oscilloscope, and photographed with a Land Camera to be analyzed later. A time scale was added to each photograph by feeding an oscillatory signal to the beam intensity control of the oscilloscope and thus superimposing a line of blips of any desired frequency on the trace. Since the approximate number of stall cells was already known to be in the neighborhood of 12, two probes set a fixed distance apart were sufficient for determination of the phase lag and it was not necessary to resort to the more complex procedure required for identification of the number of stalls when no other information is available. From the phase lag measurements, the number of stall cells could be calculated, and this information together with the frequency

of the disturbances passing one wire was sufficient for computation of the propagation velocity. The accuracy of this method depends entirely on the regularity of the disturbances since the phase lag can be measured sufficiently closely to pinpoint the number of stall cells only if the phenomenon is periodic. As can be seen from the traces in Figure 29, the variation between stall cells was responsible for an uncertainty of about one cell. For example, at $\beta_1 = 68^\circ$ the estimated number varied from eleven to twelve, with twelve the most likely number. In addition, it is possible that the number of cells changed with time. In Table I below the results of the hot wire measurements are compared with those obtained from schlieren photographs and the agreement is good.

TABLE I

Total Temperature 535°R

Cascade Reynolds Number 240,000

			Schlieren Photographs			Hot Wire Method		
β_2	M_1	C_{r_1} fps	No. of Stalls	Propagation Velocity fps	V/C_{r_1}	No. of Stalls	Propagation Velocity fps	V/C_{r_1}
63.8°	.326	161	9	104	.64	9	99	.62
65.5°	.343	160	10	110	.69	9	112	.70
67.2°	.361	159	11	117	.74	11	116	.74
68.5°	.377	159	--	---	---	12	115	.72

All the testing described above was carried out with a cascade Reynolds number of 240,000. By lowering the pressure at inlet to the wind-tunnel compressors from 20 psia to 10 psia the Reynolds number was lowered to 120,000 without changing the Mach number and velocity. At the

lower Reynolds number rotating stall did not begin until β_1 attained 63°, and the propagation velocity was approximately 15% lower than at the higher Reynolds number. There appeared to be 12 stall cells in the cascade. Since the Reynolds number should affect only the boundary layer delay, and possibly the downstream pressure fluctuations, one would expect only a small change in propagation velocity with Reynolds number.

By traversing the passage with the hot wire probes, the discovery was made that periodic rotating stall existed in a sharply-defined band of about 1/4" depth adjacent to each end-wall of the cascade while the disturbances were still of a random nature over the rest of the cascade. The tip stall began at $\beta_1 = 61^\circ$ and persisted until $\beta_1 = 63^\circ$, after which the periodic stall filled the cascade.

Removal of the boundary layer through the slots after the nozzles had no measurable effect either on the rotating stall characteristics of the cascade or on the C_p versus β_1 curve. If more than 2% of the main flow were removed the cascade pressure rise decreased, indicating that fluid from outside the nozzle boundary layer was lost and that the inlet velocity to the cascade was reduced. The tip stall persisted and may have been caused by corner vortices being shed by the nozzles, as described in Reference 10. Carbon-black patterns showed that the ends of the blades were stalled at $\beta_1 = 56^\circ$.

With increasing Mach number, the hot wire pattern remained periodic until shock waves first appeared, after which a further increase in Mach number was followed by a rapid deterioration in the periodicity of the trace. A high speed film taken at $\beta_1 = 67.2^\circ$ with $M_1 = 0.65$ showed

the stall pattern building up and then collapsing as described below. Following a period of 14 milliseconds with all the airfoils stalled, a brief period of partial unstall moved across the window. Twenty-eight milliseconds later, six cycles of unstall moved past the window, each cycle occupying 1.5 milliseconds. After a further 20.7 milliseconds from the appearance of the cells, the cluster of stalls moved by once again, but there were now eight of them apparently occupying one-half of the circle since they took 12 milliseconds to pass the window and had a propagation velocity of 184 fps, corresponding to a time of 21 milliseconds for one revolution. Another interval of nine milliseconds duration followed, with all the airfoils in the test window fully stalled, and at the end of this time the eight cells came by again, but this time they had apparently sprung apart to fill the cascade since the interval between each cell had doubled. The film terminated at this point, but the hot wire traces indicated that this process was typical of the phenomena at high Mach numbers and was probably followed by collapse and a later reforming of the pattern. A portion of the film is reproduced in Figure 31 and shows strong lambda shocks appearing on the upper surface of the airfoils after the inlet angle increased, with boundary-layer separation behind the shock waves. At this Mach number V/C_r had a value of 0.66.

Pressure fluctuations before and after the cascade were compared by recording the signals from barium titanite crystals connected to static pressure taps. At very low Mach numbers the pressure fluctuations ahead of the cascade were three times as large as those behind the cascade (Figure 30). With increasing Mach number, the relative

magnitude of the pressure fluctuations behind the cascade increased, until at $M_1 = 0.5$ they were as large as those ahead of the blades.

The nozzle-wakes gave a useful indication of the inlet angle to the cascade during rotating stall, and a comparison of the high speed motion pictures with the steady flow spark pictures showed that during the unstalled portion of the cycle the inlet angle was never less than 56°, so that the airfoil was not operating to the left of the peak on the C_p curve at any time during the cycle.

No steady-state hysteresis effects were observed in the cascade response to changes in inlet angle, the pressure coefficient and rotating stall characteristics being dependent only on β_1 and unaffected by the way in which the operating point was approached. This suggests that interference effects between blade-rows are responsible for the hysteresis found in compressor stall characteristics.

3.1.4 Effect of Cascade Solidity on Rotating Stall

With the original blade spacing, the stall cells had the appearance of a cloud of material of fixed identity rolling along the cascade. This illusion of continuity was so strong that, when the film was projected, the observer received the impression that the stall was flowing over and through the blades rather than being propagated from one blade to the next. The position of the boundary of the stall cell was a linear function of time and there was no appearance of discontinuity due to the finite blade spacing. In order to determine the effect of cascade solidity on the appearance, velocity and number of the stalls, every second blade was removed from the cascade so that the solidity σ (defined as $\frac{\text{chord}}{\text{pitch}}$) was reduced to 0.5, and the cascade was tested once

again. In Figure 32, the pressure coefficient is shown for compressor π_m of 0.173 and 0.287, and in Figure 33, β_2 is plotted against β_1. There was now very little turning of the flow and the greater part of the pressure rise was due to the change in radius, which was responsible for a theoretical pressure coefficient of 0.25. The C_p curve still showed the same characteristics as those observed with the higher solidity, with a dip in the curve at $\beta_1 = 49^\circ$, a peak at $\beta_1 = 54^\circ$, a minimum value at $\beta_1 = 60^\circ$ and a second peak at $\beta_1 = 62^\circ$. Rotating stall was observed in the wall boundary layer at the ends of the blades at an inlet angle of 61°, and full rotating stall commenced at 64°. The pressure coefficient and flow deflection were now too small to permit accurate measurement of α, which was approximately 0.9 when rotating stall began.

High speed schlieren photographs taken with an inlet Mach number of 0.35 showed that the number of stall cells was approximately 13, with $\frac{V}{C_r}$ increasing from 0.76 at $\beta_1 = 65^\circ$ to 0.86 at $\beta_1 = 68.6^\circ$. There were now only two airfoils in one wave length of the disturbance, and yet the stalls still moved with uniform velocity along the cascade. Flow separation on the suction surface of one blade commenced when the pressure side of the blade was touched by the stalled region generated by the previous blade (Figures 34, 35). Frequently, the boundary layer reattached on one blade before stall commenced on the blade above it, so that part of the passage had good flow while the upper portion of the passage was still occupied by low-energy fluid. When a blade stalled, a region of flow separation appeared first at the leading edge, then grew and moved back along the blade, requiring approximately 0.5 milli-

seconds to cover the blade. To obtain better definition of the nozzle wakes, a high speed motion picture was taken with an inlet Mach number of 0.45 (Figure 36) and from this it can be seen that the air inlet angle to an airfoil increased sharply just before the airfoil was touched by the stall propagating from the adjacent blade.

A further reduction in solidity to 0.33 was accomplished by removing nine of the remaining blades from the cascade. Only one blade was now visible in the window, but rotating stall still occurred and the turbulent air from the adjacent blade could be seen crossing the window before stall occurred on the blade in the window (Figure 37). The frequency of the disturbances was now almost twice the frequency obtained with a cascade solidity of unity, being 630 cps at $\beta_1 = 68.6^\circ$. Hot wire measurements showed that there were still approximately thirteen stall cells in the cascade, propagating with a velocity of 200 fps.

When nine of the remaining blades were removed (leaving nine blades in the cascade) rotating stall did not appear, and for inlet angles greater than 61° the flow separated from the leading edge as shown in Figure 38. The stalling process was quite abrupt, with the separation point jumping suddenly from the 30% chord position to the leading edge as β_1 was increased from 60° to 61°.

In Figure 39, the frequency of the stalls is plotted against solidity for $\beta_1 = 68.6^\circ$, $M_1 = 0.35$, and on the same diagram the frequency of eddy formation for a single airfoil (Von Karman vortex street) as determined by Fage and Johanson (Reference 11) is shown. The formula for the eddy frequency of a plate or airfoil is $f = 0.155 \frac{V}{b}$, where f is the frequency in cps, V is the free stream velocity fps and b is the component

of chord normal to the free stream (feet). The stall frequency apparently tended towards the single airfoil eddy frequency as the solidity was decreased. When the cascade solidity is too low to permit rotating stall, the airfoils shed eddies, and for the nine airfoils in the cascade an attempt was made to measure the eddy frequency. Accurate determination was difficult because of stream turbulence and because the hot wire could not be traversed to find the position where the disturbances were most regular, but the eddy frequency appeared to be approximately 1,000 cps and this point lay on a smooth curve through the single-airfoil eddy frequency and the rotating stall frequencies. Although accurate determination of the eddy frequency was not possible with the present arrangement of the apparatus, this result suggests that there may be a connection between the eddy frequency in the absence of rotating stall and the frequency of stall cells with small wave lengths. No experimental work has apparently been done on the effect of blade spacing on eddy frequency and it would appear that such a study might shed some light on the relationship (if any) between eddy frequency and rotating stall. The eddy frequency is governed by the same parameters that determine the boundary layer response in rotating stall and the fact that no satisfactory theory of vortex shedding has yet been developed is an indication of the complexity of the problem and the inadequacy of the simple exponential lag representation of the boundary layer response.

3.1.5 Comparison of Theory with Experiment

Using the simple theory with τ assumed negligible, the theoretical propagation velocities were computed from the C_p and β_2 versus β_1

curves for the cascade with solidity unity and one-half. The calculations could be made only in the steady flow region since it is unlikely that the pressure measurements in the rotating stall region represent the steady cascade performance. In consequence, it is not possible to compare the theoretical propagation velocities directly with the experimental results for the same angles. In Figure 40, the computed propagation velocities for 9, 10, 11 and 12 stalls are plotted versus β_1 for $\sigma = 1$, together with the experimental velocities. The broken lines represent the extrapolation of the theoretical curves into the rotating stall regime and it can be seen that most of the experimental points lie within this area, which is as much as could be hoped for from a simple, linearized theory. In this case, omission of the inertia of the fluid within the cascade would result in an error of the order of 100% in the predicted propagation velocity. The propagation velocity with a Reynolds number of 120,000 and twelve stall cells is slightly smaller than that with twelve cells and a Reynolds number of 240,000.

In Figure 40, the computed and observed propagation velocities are shown for the lower solidity, and here the agreement is not as good. The assumption of one-dimensional flow within the passages is certainly not valid for low cascade solidity and the effective inertia of the air within the cascade may be considerably less than the value given by the theory. The good agreement between the experimental results and the simple theory for the high solidity cascade suggests that the boundary layer time delay τ may be considerably smaller than the approximate value calculated earlier, since a value of τ equal to $1/2 \frac{L}{C_3}$ would reduce the predicted propagation velocity by about 30%. From Figure 39,

it can be seen that increasing the cascade solidity beyond 0.75 has little effect on the stall frequency and hence on the propagation velocity. Accordingly, it would appear that the neglect of finite blade-spacing in the theory is justifiable for solidities greater than 0.75.

3.2 The Single-Stage Axial Compressor

An investigation of rotating stall in a single-stage compressor has been carried out by S. R. Montgomery and Lt. J. J. Braun (U.S.N.) and a full report on this work will be available shortly. For comparison with the cascade performance and the theory, some of the results obtained are presented here.

3.2.1 Rotating Stall in the Free-Vortex Rotor

The compressor is a free-vortex machine with a hub-tip ratio of 0.75, and the stage consisted of a row of inlet guide vanes, a rotor, and a set of stator blades. The axial clearance between the rotor and guide vanes was 1.5" and the rotor had an outside diameter of 23.25" and held 44 blades with a mean chord length of 1.5". With the stator removed, an investigation of the rotating stall characteristics of the machine was made using hot wire equipment. For the rotor, the geometry of the blading was quite similar to that of the stationary cascade, with a design-point air inlet angle of 48° at the mean radius.

The performance of the rotor in terms of pressure coefficient and relative outlet angle at the mean radius versus relative inlet angle is shown in Figures 42 and 43. As the mass flow was decreased at 1500 rpm, eight stall cells appeared at $\beta_1 = 67^\circ$, covering the blades from root to tip and propagating at approximately thirty percent of rotor speed relative to the rotor. A further decrease in flow caused a change to

nine cells at $\beta_1 = 71^\circ$, with approximately the same propagation speed. At $\beta_1 = 75^\circ$, the nine cells were replaced by a single stall cell propagating at fifty percent of rotor speed relative to the rotor. Three stall cells appeared at $\beta_1 = 80^\circ$ and four cells at $\beta_1 = 84^\circ$. Throughout the whole rotating stall range, the pressure fluctuations ahead of the inlet guide vanes were less than 25% of the pressure variations between the guide vanes and the rotor, indicating that the effect of the guide vanes on the unsteady flow was substantially as assumed in the analysis. The pressure variations behind the rotor caused by rotating stall (that is, the difference between the fluctuations with and without rotating stall) were less than 25% of those ahead of the rotor throughout the whole flow range in which rotating stall was obtained.

In Figure 44, the predicted and observed values of propagation velocity are plotted on a base of β_1. At the commencement of rotating stall where the linearized theory is most likely to be applicable, the agreement is remarkably good. As in the cascade, the accuracy of the simple theory indicates that the effect of the boundary layer delay on velocity must be small. The change from nine cells to one cell at $\beta_1 = 75^\circ$ was accompanied by a considerable increase in propagation velocity, verifying the prediction that propagation velocity should increase with wave length. The theory comes within 25% in predicting the propagation velocities of the large stall cells, probably because the pressure fluctuations after the rotor were small in this case even for large cells. By considering the flow field after the cascade as a continuum, it is possible to obtain a solution for propagation velocity which reduces to

the Sears-Marble result for large waves with small pressure rise across the cascade (Appendix III). This solution predicts propagation velocities which are much lower than the experimental values both for the stationary cascade and the rotor, showing that neglecting the downstream pressure fluctuations is the better assumption for a single blade row.

4 CONCLUSIONS AND SUGGESTIONS FOR FURTHER RESEARCH

Using the two extreme assumptions for the downstream flow field, solutions for the velocity of stall propagation have been obtained. With the assumption that the downstream field is a continuum, the solution reduces to the Sears-Marble result for the special case considered by Sears and Marble, and does not give good agreement with experiments. The solution obtained by neglecting downstream pressure variations predicts propagation velocities within 25% over a wide range of wave lengths. It may be possible to develop a more realistic model of the downstream field which will cover the whole range of wave lengths and predict downstream interference. In addition, it is desirable to analyze oscillations of finite amplitude, since the linearized solutions are certainly not valid for the large changes in velocity which can occur in rotating stall.

Although a good start has been made in studying the velocity of stall propagation, only the first step has been taken towards predicting the number of stall cells present in a given configuration. A model has been suggested which reproduces the main features of the phenomenon and indicates that the boundary layer response may be of great importance in determining the wave length, but it seems likely that the boundary layer behavior is much more complex than the simple exponential delay used in the analysis. A study of the effect of cascade blade spacing on eddy-shedding may yield some information on stall frequency for the short-wave cells. By decreasing the stagger of the blades in the stationary cascade, it will be possible to test the cascade over a larger portion of the rotating stall region. If transition from a large number of cells to one or two cells (as observed in the

compressor) can be obtained, the schlieren photographs may give some information about the cause of the change.

NOMENCLATURE

A	Area
$a_n(t)$	Functions of time
$b_n(t)$	
b	Half-wave length of the disturbance
c	Velocity
c_x	Steady state velocity in x direction
c_y	Steady state velocity in y direction
c_r	Steady state radial velocity
c_θ	Steady state tangential velocity
C_p	Cascade pressure coefficient = $\frac{p_2 - p_1}{\rho/2\ c_1^2}$
D	Operator $\frac{\partial}{\partial t}$
L	Equivalent chord length of blade
m	Mass flow rate
n	Number of harmonic
M	Mach number
p	Stream pressure
p_o	Total pressure
r	Radius
T_o	Total temperature
u	Total velocity in x (or r) direction
v	Total velocity in y (or θ) direction
V	Velocity of stall propagation
α	Discharge coefficient of cascade
α'	$\frac{d\alpha}{d(\cot\beta_1)}$

β_1	Inlet angle to cascade
β_2	Outlet angle from cascade
λ	Root of characteristic equation
σ	Cascade solidity $\frac{\text{chord}}{\text{pitch}}$
π_m	Compressor rotational speed parameter
ω	Radian frequency
τ	Time constant of boundary layer delay
ρ	Density
Φ	Total velocity potential
φ	Perturbation velocity potential
φ_x	$\frac{\partial \varphi}{\partial x}$
φ_y	$\frac{\partial \varphi}{\partial y}$
φ_t	$\frac{\partial \varphi}{\partial t}$

APPENDIX I

Calculation of α for a Real Cascade

α has been defined as the ratio of the actual mass flow through the cascade to the ideal mass flow for the same $(P_{01} - P_2)$ and flow deflection with no losses. It may be obtained from conventional test results as follows:

(a) Rectilinear cascade

$$\alpha = \frac{\text{Actual mass flow}}{\text{Ideal mass flow for same } (P_{O_1} - P_2)}$$

therefore $$\alpha = \frac{C_1 \cos\beta_1}{(C_2)_{ideal} \cos\beta_2}$$

$$= \frac{C_1 \cos\beta_1}{\cos\beta_2 \sqrt{\frac{2}{\rho}(P_{01} - P_2)}}$$ Since $P_{O_2} = P_{O_1}$ with no losses

$$= \frac{C_1 \cos\beta_1}{\cos\beta_2 \sqrt{\frac{2}{\rho}\left[(P_{01} - P_1) - (P_2 - P_1)\right]}}$$

Thus

$$\alpha = \frac{C_1 \cos\beta_1}{\cos\beta_2 \sqrt{C_1^2 - C_p \cdot C_1^2}}$$

$$= \frac{\cos\beta_1}{\cos\beta_2 \sqrt{1 - C_p}}$$

where

$$C_p = (P_2 - P_1) / \tfrac{1}{2}\rho C_1^2$$

(b) Circular Cascade

$$\alpha = \frac{2\pi r_1 C_1 \cos\beta_1}{2\pi r_2 (C_2)_{id} \cos\beta_2}$$

which reduces to

$$\alpha = \frac{r_1}{r_2} \cdot \frac{\cos\beta_1}{\cos\beta_2 \sqrt{1 - C_p}}$$

APPENDIX II

Stall Propagation in a Circular Cascade

The cascade arrangement is as shown in Figure (10).

Consider disturbances from an incompressible plane source-vortex flow with velocity components $C_\theta = C_{\theta_1} \cdot \frac{r_1}{r}$

$$C_r = C_{r_1} \cdot \frac{r_1}{r}$$

and angle β_1 to the radial direction. The flow before the cascade is irrotational so that a velocity potential can be used.

In the disturbed flow $u = C_{r_1} \cdot \frac{r_1}{r} + \varphi_r$

$$v = C_{\theta_1} \cdot \frac{r_1}{r} + \frac{1}{r}\varphi_\theta$$

From continuity $$\frac{\partial}{\partial r}(ur) + \frac{\partial v}{\partial \theta} = 0$$

Therefore $$r\varphi_{rr} + \varphi_r + \frac{1}{r}\varphi_{\theta\theta} = 0$$

Solutions to this equation are obtained in the form

$$\varphi = \sum_{n=2}^{\infty} \left[a_n(t)\cos n\theta + b_n(t)\sin n\theta\right] r^n$$

satisfying the condition $\varphi_r = \varphi_\theta = 0$ at $r = 0$

For n = 1, the velocity perturbation does not die out at the origin.

From Bernoulli's equation for unsteady flow

$$(\varphi_t)_1 + c_1\delta c_1 + \delta p_1/\rho = 0$$

If inertia effects may be neglected between (1) and (3) then

$$c_1\delta c_1 + \delta p_1/\rho = c_3\delta c_3 + \delta p_3/\rho$$

so that

$$(\varphi_t)_1 + c_3\delta c_3 + \delta p_3/\rho = 0$$

Inertia Effects Within the Cascade

With the assumption that the blades are in the form of logarithmic spirals of small curvature (valid if $\frac{r_2}{r_1}$ is close to unity) the momentum equation along the mean line of the passage (called the ℓ-axis) can be written

$$\frac{\partial c}{\partial t} + c\frac{\partial c}{\partial \ell} + \frac{1}{\rho}\frac{\partial p}{\partial \ell} = 0$$

as for the rectilinear cascade and by a similar process of integration we arrive at the equation

$$L\frac{\partial(\delta c_2)}{\partial t} + (\varphi_t)_1 + c_2\delta c_2 = 0$$

Also,

$$c_2\delta c_2 = \left(\frac{A_3}{A_2}\right)^2 c_3\delta c_3 - \left(\frac{A_3}{A_2}\right)^2 c_3^2\frac{\delta A_2}{A_2}$$

as in the case of the rectilinear cascade. However, α is now given by $\alpha = \frac{r_1}{r_2}\cdot\frac{A_2}{A_3}$, since the outlet area with no separation region is now $\frac{r_2}{r_1}\cdot A_3$.

Therefore, $$c_2\delta c_2 = \frac{1}{\alpha^2}\left(\frac{r_1}{r_2}\right)^2 c_3\delta c_3 - \frac{1}{\alpha^2}\left(\frac{r_1}{r_2}\right)^2 c_3^2\frac{\delta\alpha}{\alpha}$$

$$\frac{\delta\alpha}{\alpha} = \frac{\alpha'}{\alpha}\delta(u/v) = \frac{\alpha'}{\alpha}\frac{v\,du - u\,dv}{v^2}$$

which reduces to

$$\frac{\delta\alpha}{\alpha} = \frac{\alpha'}{\alpha}\frac{\varphi_r - \cot\beta_1\,\varphi_r/r}{c_{\theta 1}}$$

An equation for φ at (1) is obtained in the form

$$\frac{L}{\cos\beta_1}\varphi_{rt} + \frac{1}{\alpha^2}\left(\frac{r_1}{r_2}\right)^2\frac{c_r\varphi_r}{\cos^2\beta_1}\left[1 - \frac{\cot\beta_1\alpha'}{\alpha}\right] + \frac{\alpha'}{\alpha^3}\left(\frac{r_1}{r_2}\right)^2\frac{\cot^2\beta_1\, c_r\varphi_\theta}{\cos^2\beta_2\, r_1} = 0$$

By inserting the solution for φ and separating the terms in cos nθ, sin nθ two differential equations in a_n, b_n are obtained which yield the characteristic equation

$$\left[\left(\frac{L}{\cos\beta_1}+r_1\right)\lambda_n+\frac{n}{\alpha^2}\left(\frac{r_1}{r_2}\right)^2\frac{c_{r1}}{\cos^2\beta_1}\left(1-\frac{\cot\beta_1\alpha'}{\alpha}\right)\right]^2+\left[\frac{n\alpha'}{\alpha^3}\left(\frac{r_1}{r_2}\right)^2\frac{\cot^2\beta_1 c_{r1}}{\cot^2\beta_2}\right]^2=0$$

Stall propagation occurs when $\alpha' = \frac{\alpha}{\cot\beta_1}$ and the velocity of the n^{th} harmonic is given by

$$\frac{V_n}{c_{r1}} = \left(\frac{r_1}{r_2}\right)^2 \frac{\cot\beta_1}{\alpha^2\cos\beta_2\left[\frac{Ln}{r_1}+\cos\beta_2\right]}$$

Thus, if there are m symmetrical stall cells in the circular cascade, the velocity of propagation of the primary component is obtained from

$$\frac{V}{c_{r1}} = \left(\frac{r_1}{r_2}\right)^2 \frac{\cot\beta_1}{\alpha^2\cos\beta_2\left[\frac{Lm}{r_1}+\cos\beta_2\right]}$$

Upstream Interference Effects

If a row of inlet guide vanes is placed before the cascade, with outside radius R, then φ_r will be forced to zero at r = R and a solution is obtained in the form

$$\varphi = \sum_{n=2}^{\infty}\left[a_n(t)\cos n\theta + b_n(t)\sin n\theta\right]\left[r^n + R^{2n}r^{-n}\right]$$

Substituting this solution as before in the differential equation satisfied by φ at (1) and carrying through the rest of the solution we obtain

$$\frac{V}{c_{r1}} = \left(\frac{r_1}{r_2}\right)^2 \frac{\cot\beta_1}{\alpha^2\cos\beta_2\left[\frac{Lm}{r_1}\frac{1-(R/r_1)^{2m}}{1+(R/r_1)^{2m}}+\cos\beta_2\right]}$$

where V is the velocity of propagation of the fundamental component of the wave when there are m symmetric stall cells in the cascade.

APPENDIX III

By assuming that the fluid from each blade passage mixes without pressure recovery immediately after leaving the cascade so that the downstream flow field is a continuum, it is possible to obtain an expression for propagation velocity which reduces to the Sears-Marble value for large waves with small pressure rise across the cascade.

Under these circumstances, the x-component of velocity immediately after the cascade in the unsteady flow will be $C_x + (\varphi_x)_1$ and the y-component of velocity will be $\left[C_x + (\varphi_x)_1\right] \tan\beta_2$

In the downstream flow field, let

$$u = C_x + u' \qquad v = C_x \tan\beta_2 + v'$$

The linearized momentum equations are

$$\frac{1}{\rho}\frac{\partial(\delta p)}{\partial x} + \frac{\partial u'}{\partial t} + C_x \frac{\partial u'}{\partial x} + C_x \frac{\partial u'}{\partial y}\tan\beta_2 = 0$$

$$\frac{1}{\rho}\frac{\partial(\delta p)}{\partial y} + \frac{\partial v'}{\partial t} + C_x \frac{\partial v'}{\partial x} + C_x \frac{\partial v'}{\partial y}\tan\beta_2 = 0$$

Differentiating the x-momentum equation with respect to x, and the y-momentum equation with respect to y and adding we obtain (by using the continuity relation $\frac{\partial u'}{\partial x} + \frac{\partial v'}{\partial y} = 0$)

$$\frac{\partial^2(\delta p)}{\partial x^2} + \frac{\partial^2(\delta p)}{\partial y^2} = 0$$

A solution to this equation may be obtained in the form

$$\frac{\delta p}{\rho} = \sum_{n=1}^{\infty}\left[c_n(t)\cos\frac{n\pi y}{b} + d_n(t)\sin\frac{n\pi y}{b}\right]e^{-\frac{n\pi x}{b}}$$

From the x-momentum equation

$$\frac{1}{\rho}\frac{\partial(\delta p)}{\partial x} + \frac{\partial u'}{\partial t} + C_x \frac{\partial u'}{\partial x} + C_x \tan\beta_2 \frac{\partial u'}{\partial y} = 0$$

But

$$\frac{\partial u'}{\partial x} + \frac{\partial v'}{\partial y} = 0$$

Therefore $$\frac{1}{\rho}\frac{\partial \delta p}{\partial x} + \frac{\partial u'}{\partial t} - c_x \frac{\partial v'}{\partial y} + c_x \tan\beta_2 \frac{\partial u'}{\partial y} = 0$$

At the cascade, $v_2' = u_2' \tan\beta_2$

Therefore $$\frac{1}{\rho}\frac{\partial}{\partial x}\delta p_2 = -\frac{\partial u_2'}{\partial t}$$

$$\frac{\partial u_2'}{\partial t} = \frac{\partial}{\partial x}(\varphi_x)_1 = -\frac{n\pi}{b}\sum_{n=1}^{\infty}\left[\frac{da_n}{dt}\cos\frac{n\pi y}{b} + \frac{db_n}{dt}\sin\frac{n\pi y}{b}\right]$$

$$\frac{1}{\rho}\frac{\partial \delta p_2}{\partial x} = -\frac{n\pi}{b}\sum_{n=1}^{\infty}\left[c_n(t)\cos\frac{n\pi y}{b} + d_n(t)\sin\frac{n\pi y}{b}\right]$$

Therefore $c_n(t) = \frac{da_n}{dt}$ $\quad d_n(t) = \frac{db_n}{dt}$

and $\delta p/\rho$ after the cascade = $\delta p_2/\rho$ may be written as

$$\frac{\delta p_2}{\rho} = \frac{d}{dt}\left(\sum_{n=1}^{\infty}\left[a_n(t)\cos\frac{n\pi y}{b} + b_n(t)\sin\frac{n\pi y}{b}\right]\right)$$
$$= (\varphi_t)_1$$

By substituting this value for $\delta p_2/\rho$ in equation (5) instead of putting $\delta p_2 = 0$, the final expression for propagation velocity is

$$\frac{V}{c_x} = \frac{2(1-c_p)}{\sin 2\beta_1\left[\frac{L}{b}\frac{\pi}{\cos\beta_2} + 2\right]}$$

and this reduces to the Sears-Marble value for Cp = 0 and L/b = 0.

BIBLIOGRAPHY

1. Cheshire, L.J., "The Design and Development of Centrifugal Compressors for Aircraft Gas Turbines", Institution of Mechanical Engineers Proceedings, 1945, Vol. 153.

2. Emmons, H.W., Pearson, C.E. and Grant, H.P., "Compressor Surge and Stall Propagation", A.S.M.E. Annual Meeting, December 1953, Paper No. 53-A-65.

3. Iura, T. and Rannie, W.D., "Experimental Investigation of Rotating Stall in Axial Compressors", Transactions of the A.S.M.E., April 1954.

4. Huppert, M.C. and Benser, W.A., "Some Stall and Surge Phenomena in Axial-Flow Compressors", Journal of the Aeronautical Sciences, December 1953.

5. Sears, W.R., "A Theory of Rotating Stall in Axial-Flow Compressors", Cornell University, Graduate School of Aeronautical Engineering, January 1953.

6. Marble, F.E., "Propagation of Stall in a Compressor Blade Row", California Institute of Technology, Contract AF 18(600)-178, Technical Report No. 4.

7. Stenning, A.H., "Stall Propagation in Cascades of Airfoils", Journal of the Aeronautical Sciences, October 1954.

8. Kriebel, A.R., "A Test Apparatus for Stall Propagation Study", S.M. Thesis, Department of Mechanical Engineering, M.I.T., June 1954.

9. Kriebel, A.R. and Stenning, A.H., "A Cascade Tunnel for Investigation of Rotating Stall", Gas Turbine Laboratory Report No. 26, M.I.T., August 1954.

10. Herzig, H.Z., Hansen, A.G. and Costello, G.R., "Visualization of Secondary-Flow Phenomena in a Blade Row", NACA RM E52F19, 1952.

11. Fage, A. and Johansen, F.C., "On the Flow of Air Behind an Inclined Flat Plate of Infinite Span", Proceedings of the Royal Society, No. 773, September 1927.

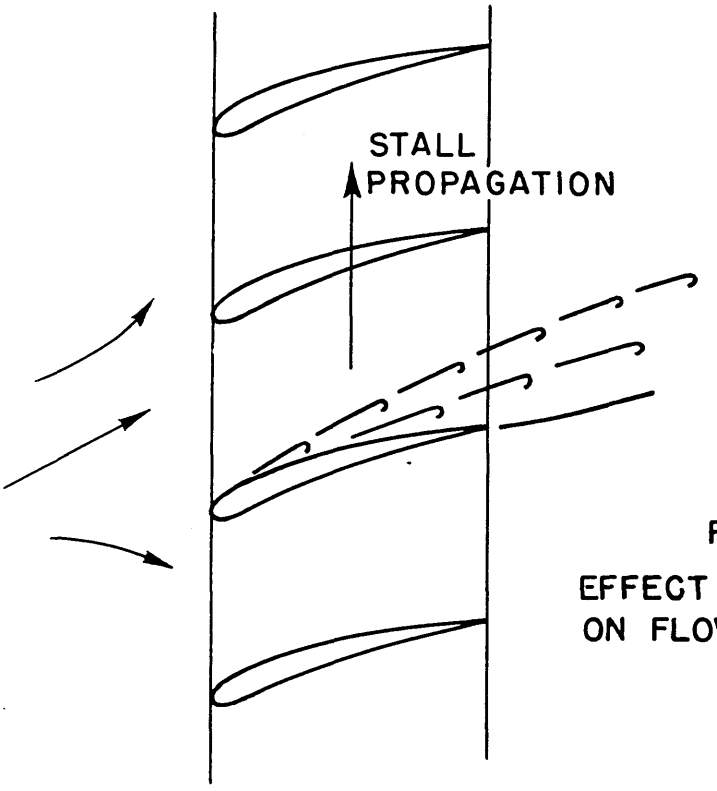

FIG. 1

EFFECT OF STALLED BLADE
ON FLOW ENTERING CASCADE

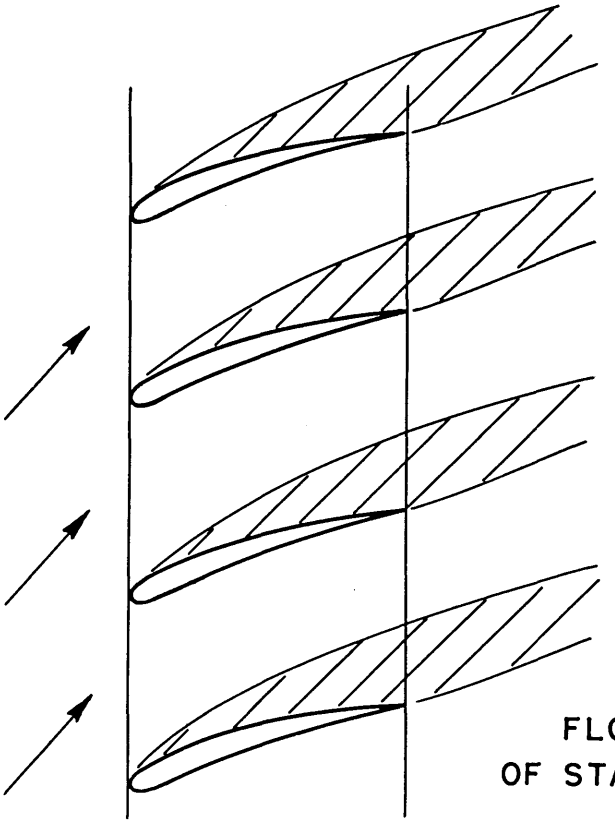

FIG. 2

FLOW FIELD
OF STALLED CASCADE

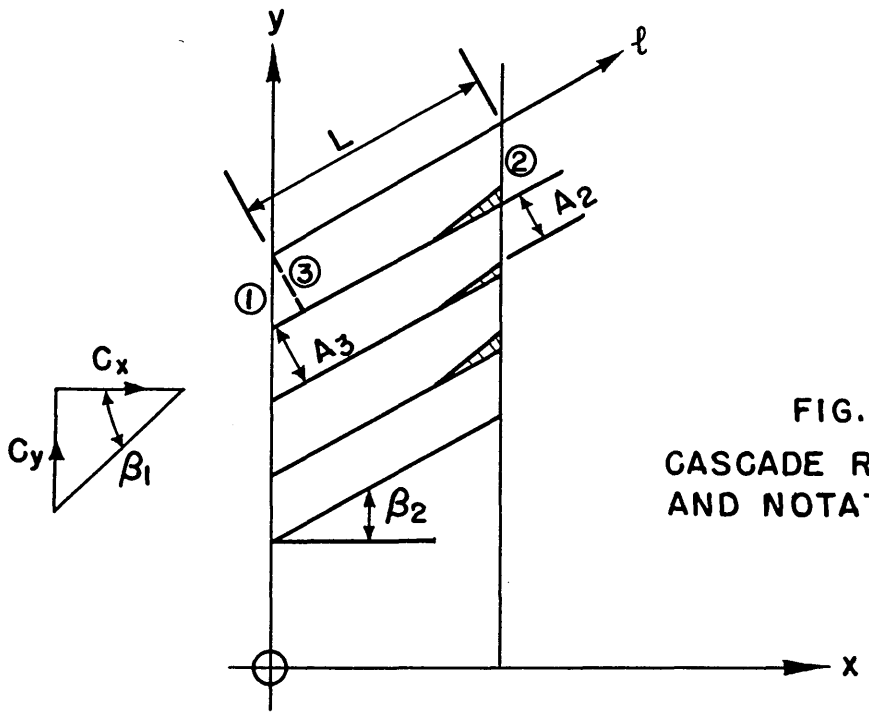

FIG. 3
CASCADE REPRESENTATION AND NOTATION.

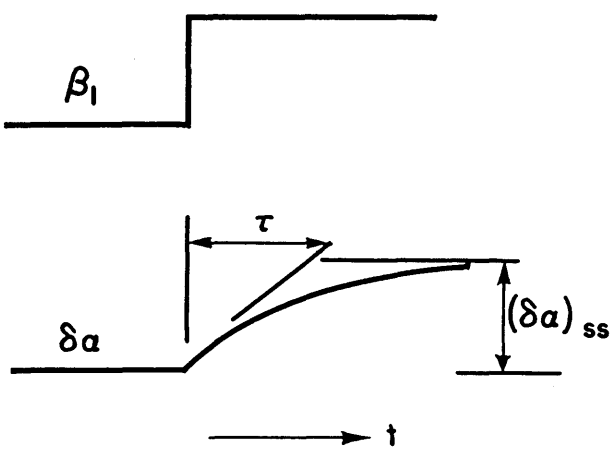

FIG. 4 ASSUMED BOUNDARY LAYER RESPONSE TO STEP CHANGES IN β_1.

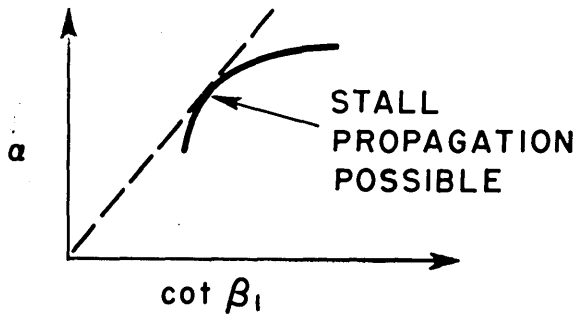

FIG. 5
STABILITY CRITERION
FOR STALL PROPAGATION

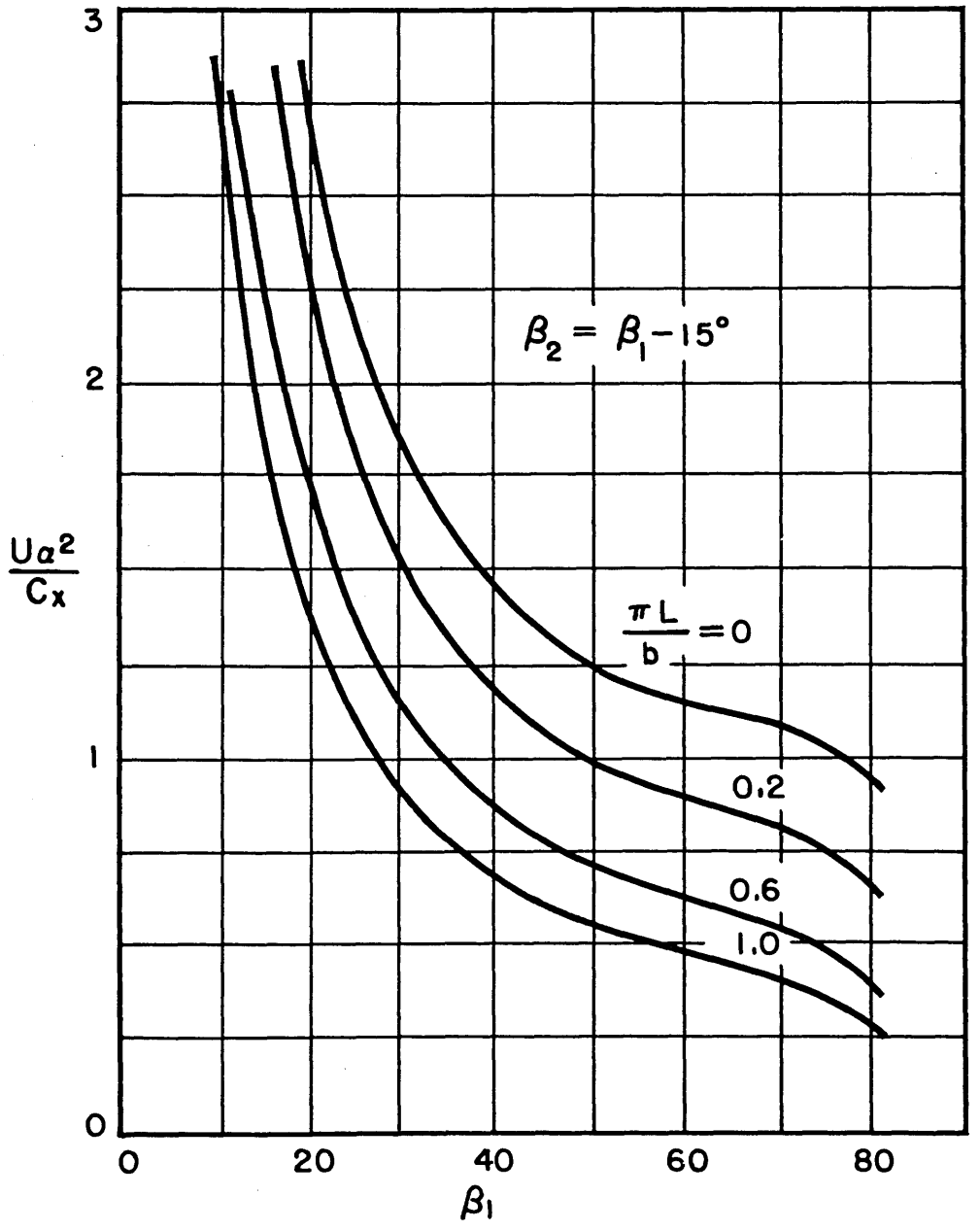

FIG. 6 $\frac{Ua^2}{C_x}$ vs. β_1 FOR CASCADES WITH 15° TURN IN STALLED CONDITION

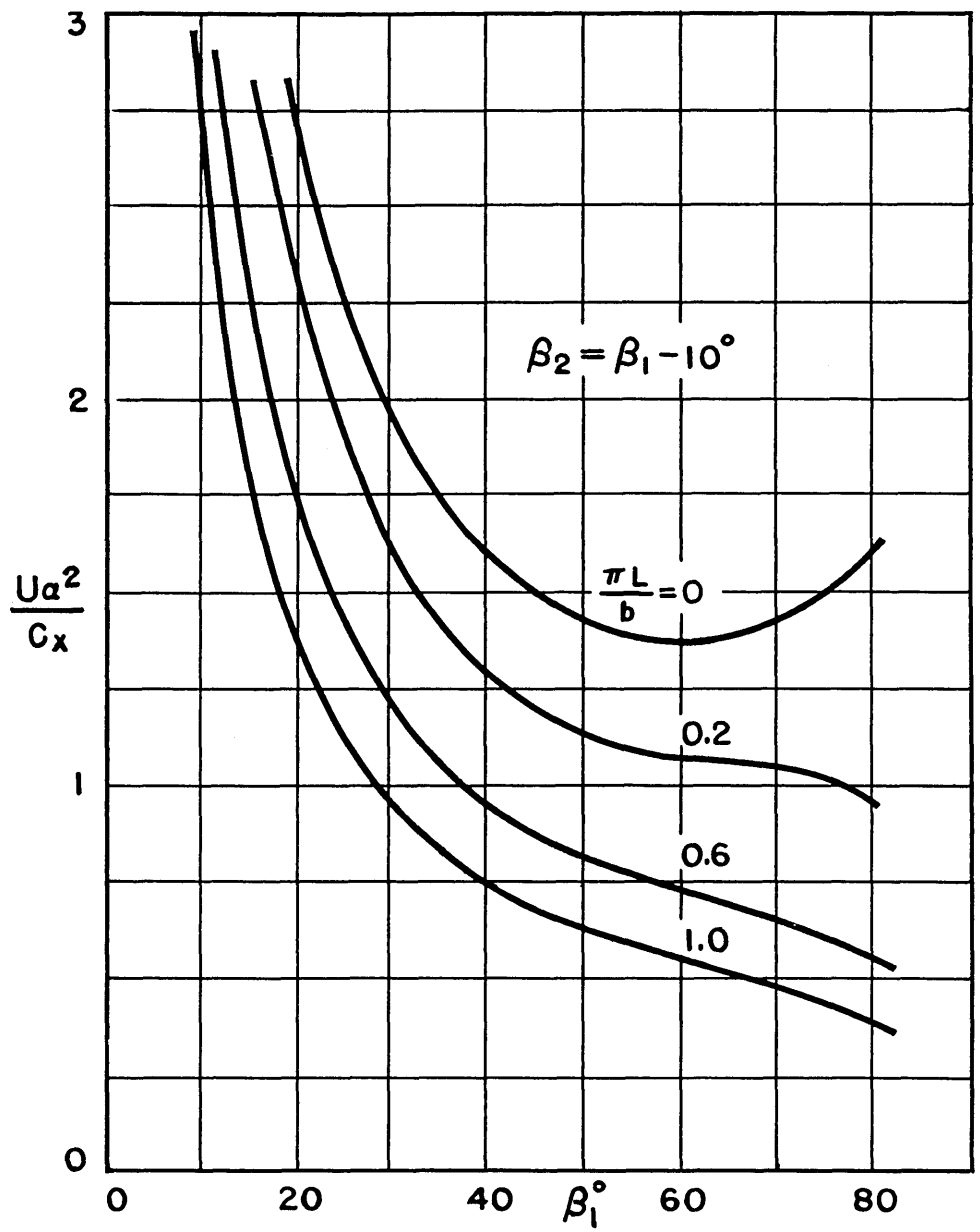

FIG. 7 $\frac{Ua^2}{C_x}$ VS. β_1 FOR CASCADES WITH 10° TURN IN STALLED CONDITION.

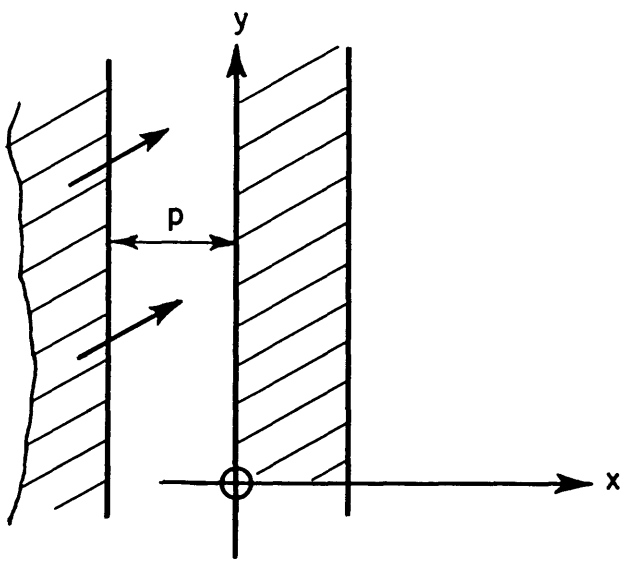

FIG. 8 REPRESENTATION OF CASCADE WITH INLET GUIDE VANES

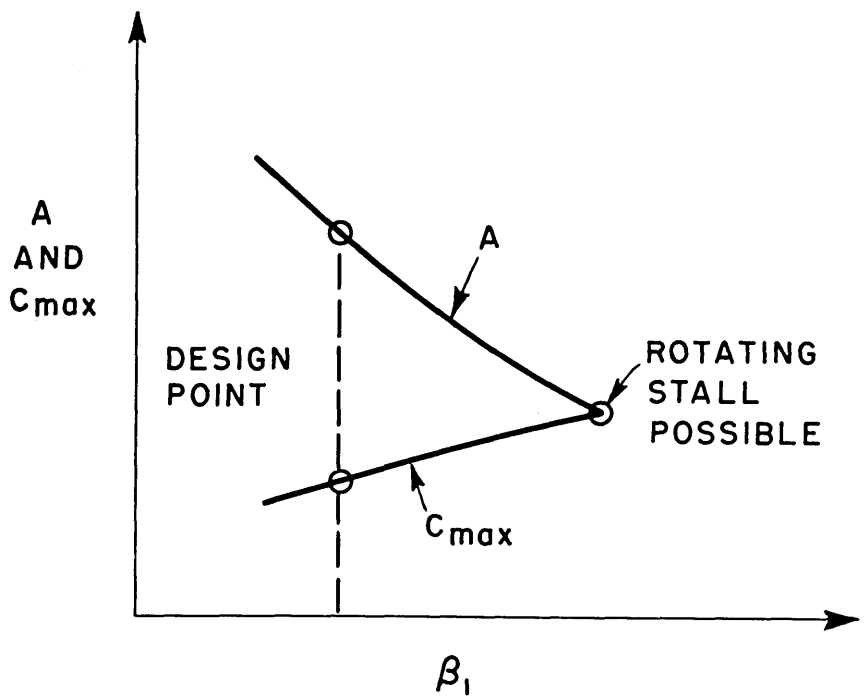

FIG. 9 STABILITY CRITERION WITH BOUNDARY LAYER DELAY

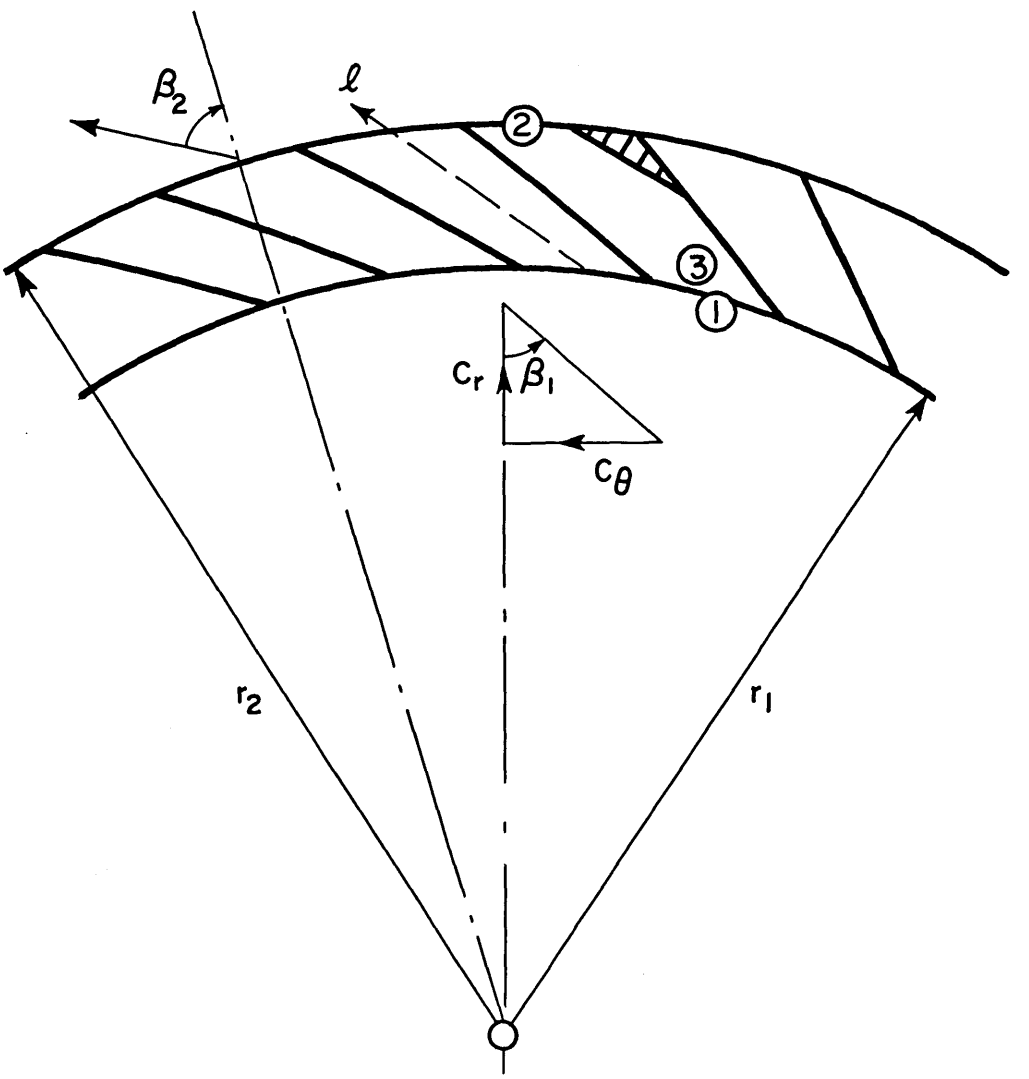

FIG. 10 REPRESENTATION OF CIRCULAR CASCADE

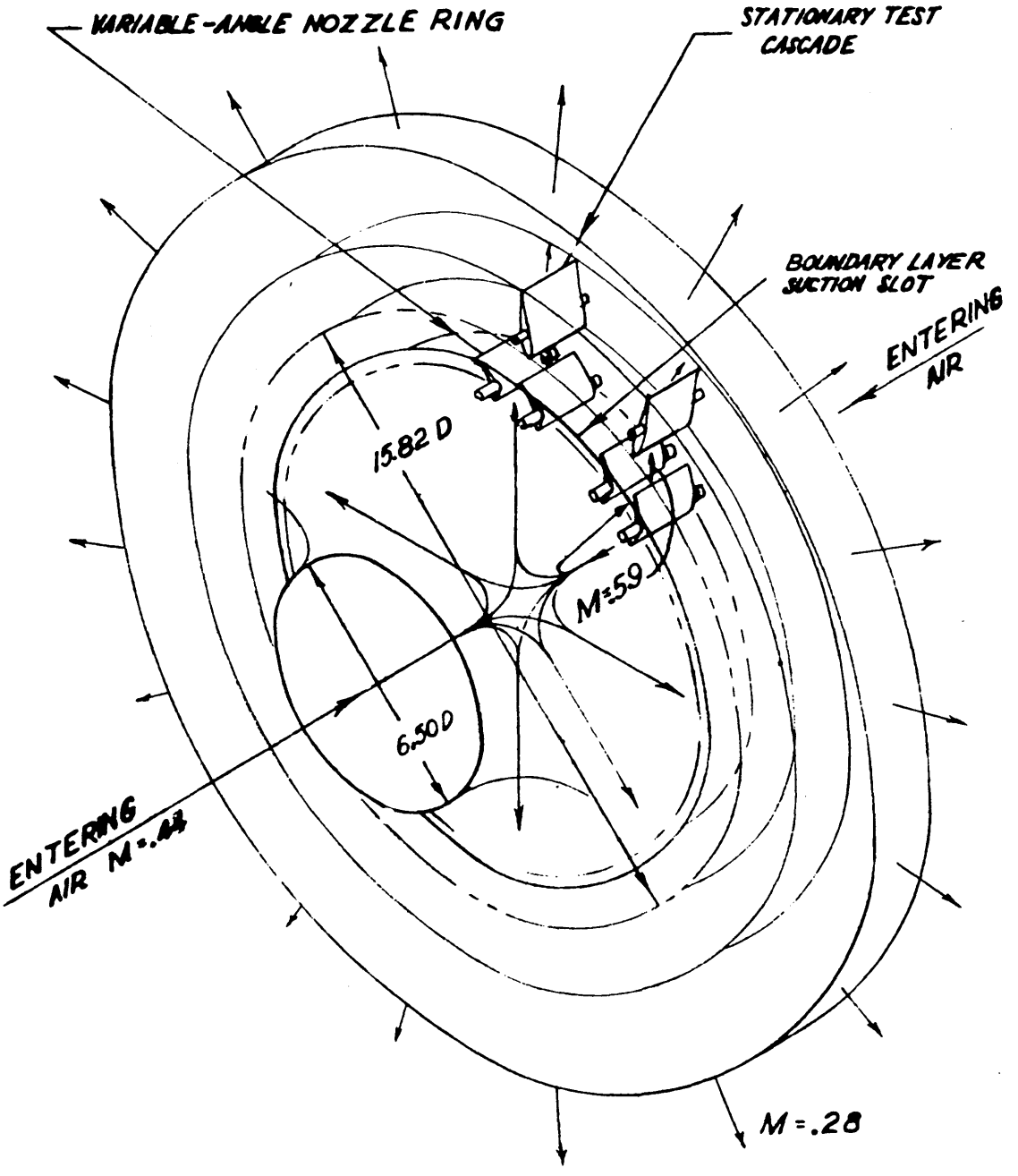

FIG. 11 SCHEMATIC DIAGRAM OF TEST SECTION

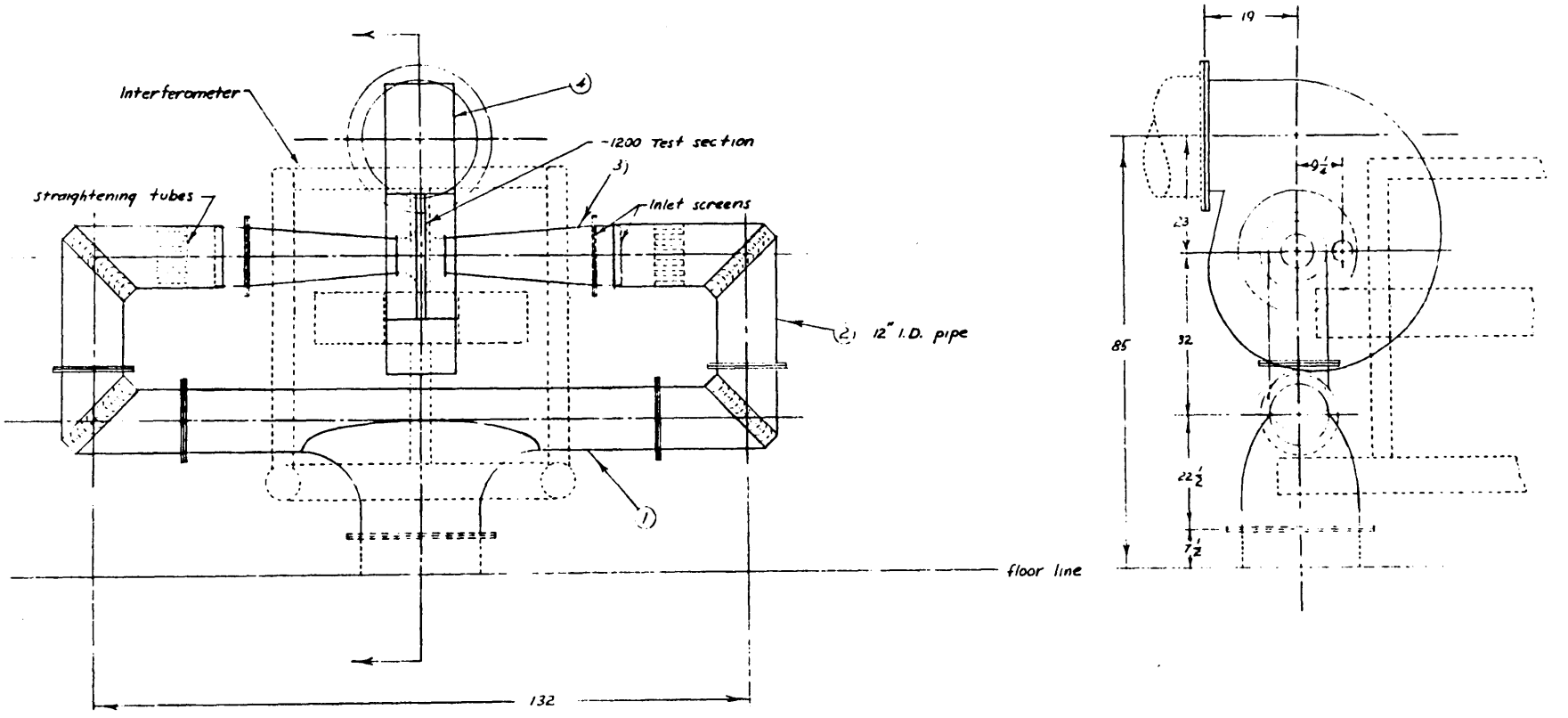

FIG. 12 ASSEMBLY DRAWING OF APPARATUS

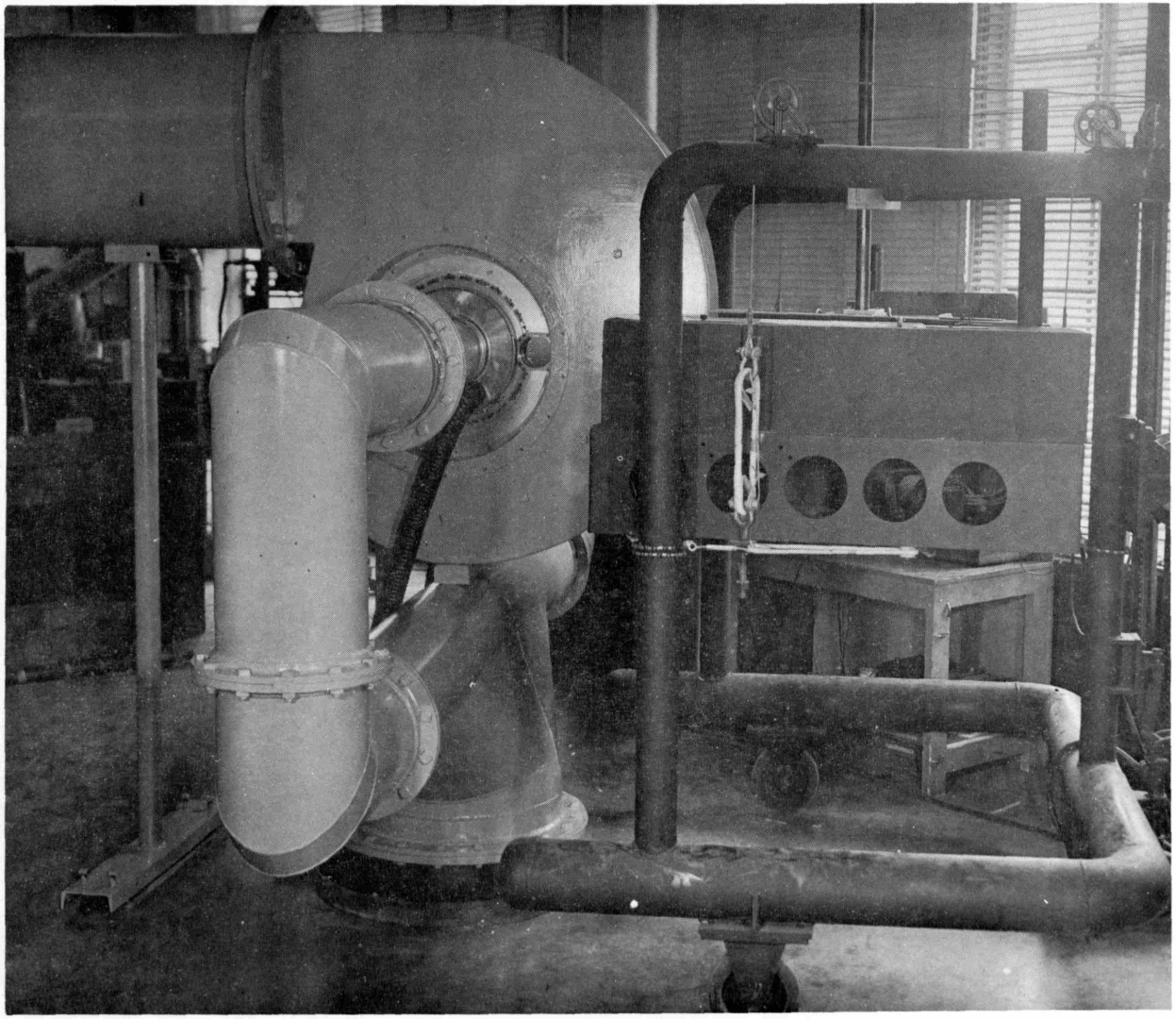

FIG. 13 - CASCADE TUNNEL AND PORTABLE SCHLIEREN

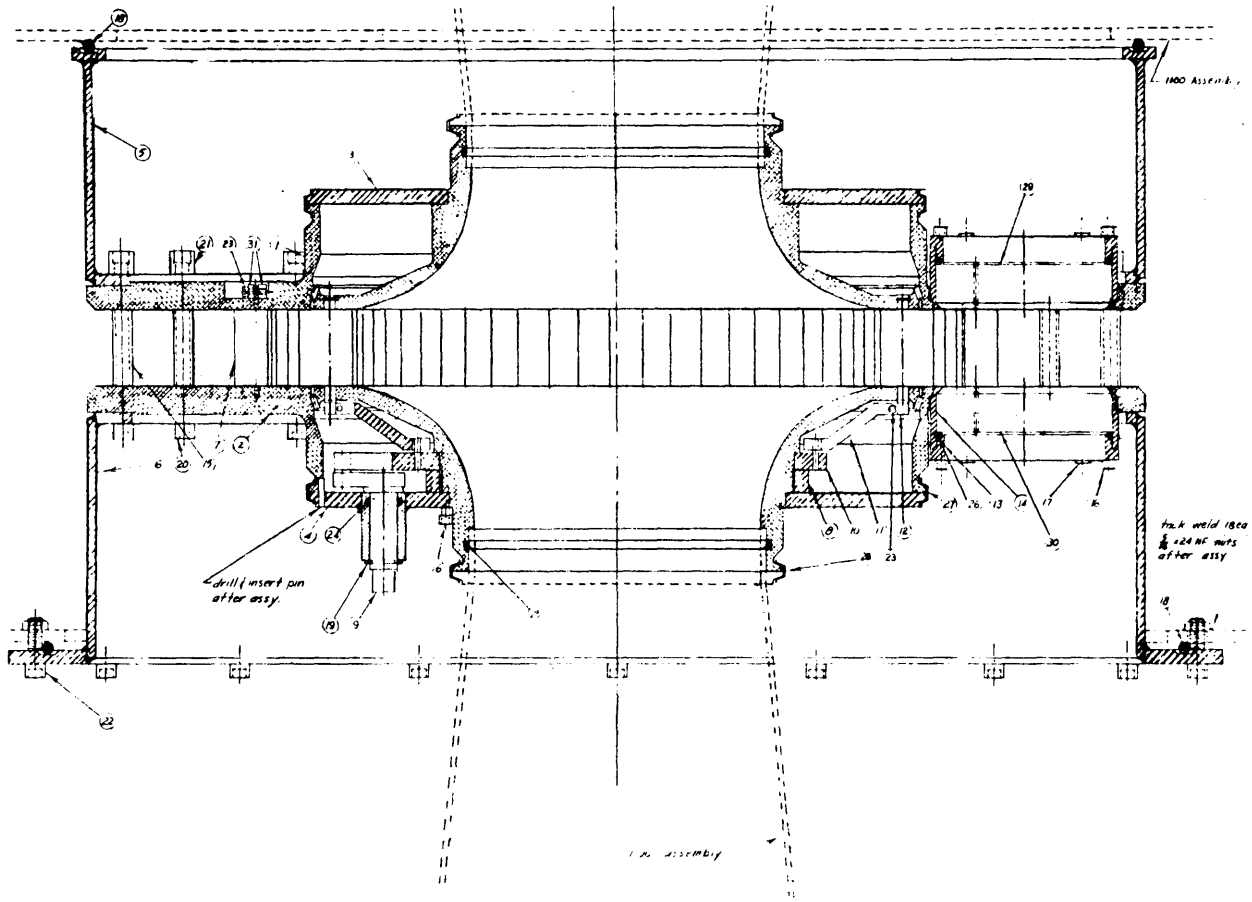

FIG. 14 ASSEMBLY DRAWING OF TEST SECTION

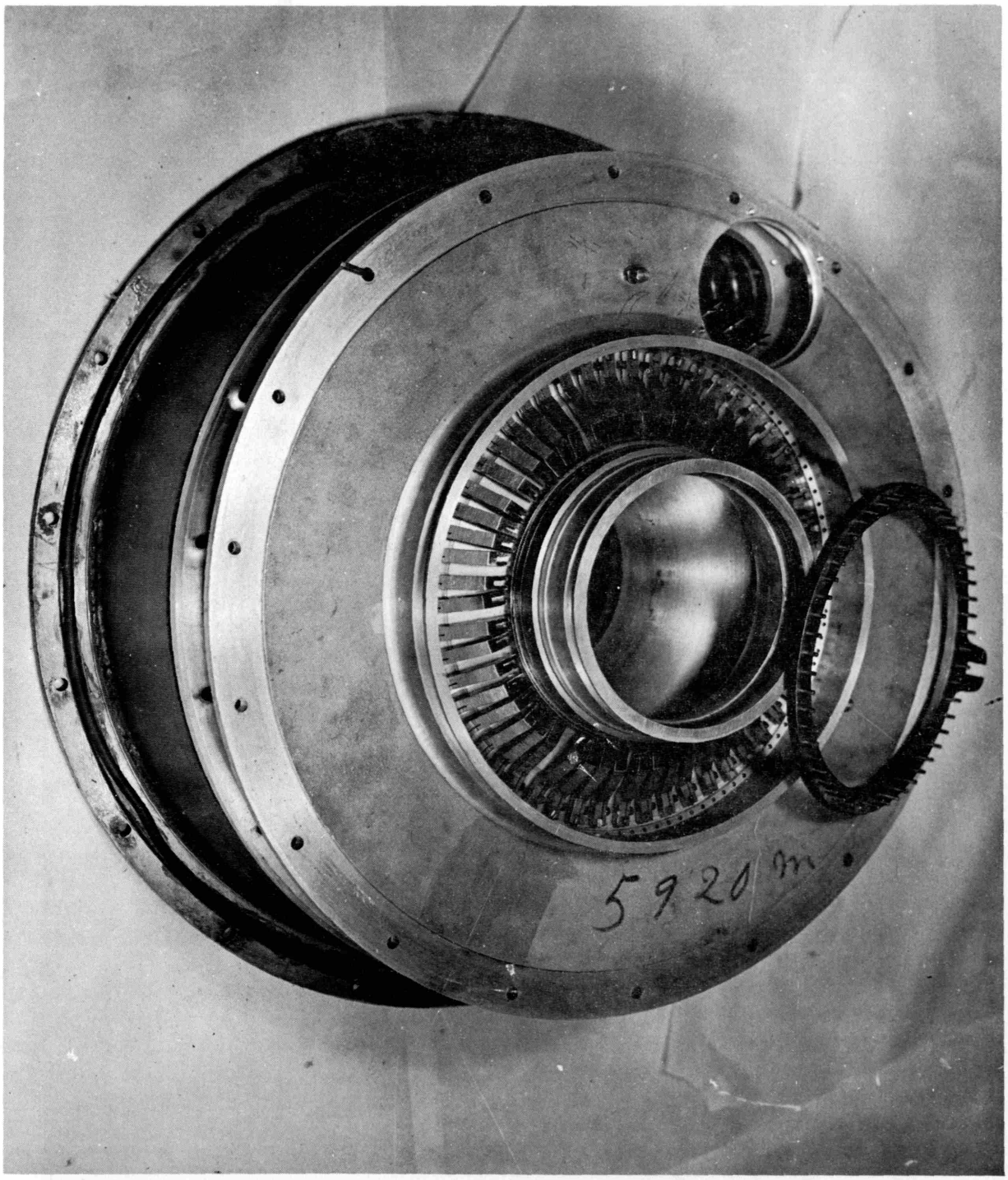

FIG. 15 – TEST SECTION

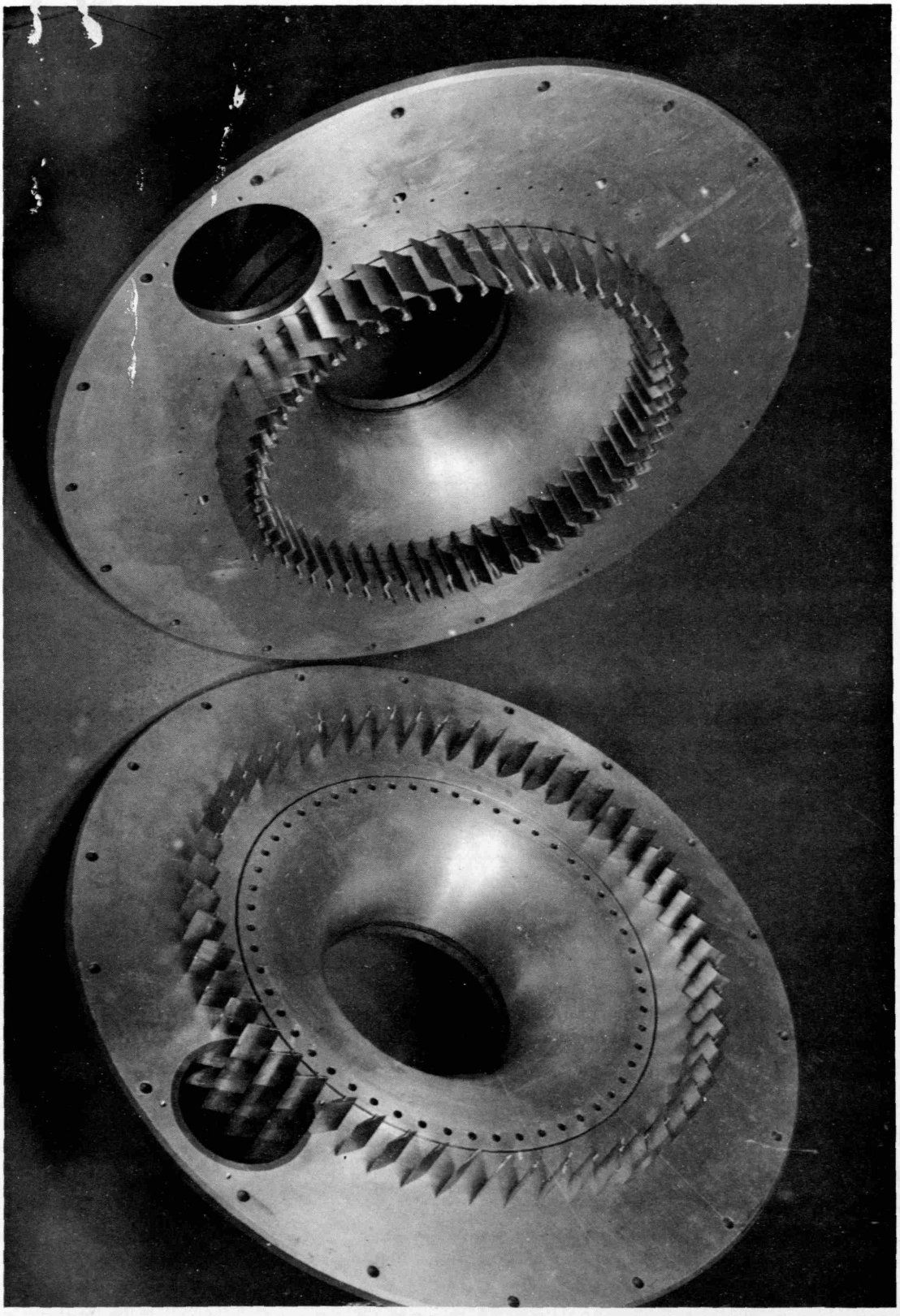

FIG. 16 – TEST SECTION BLADING

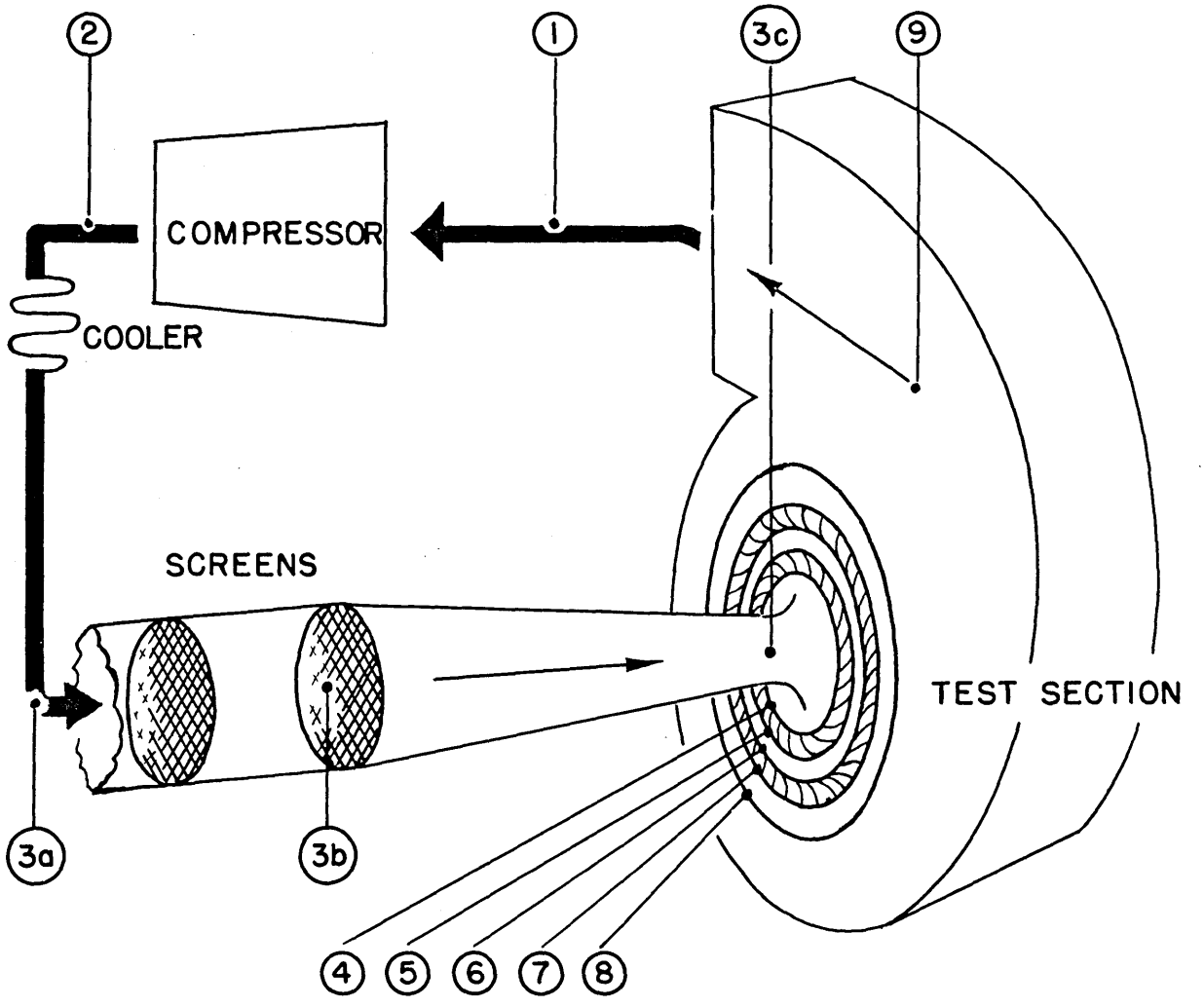

STATION	RADIUS INCH'S	MACH. NO.	VELOCITY F. P. S.	ρ_0 LB-M / FT^3	ρ	P_0 PSIA	P	T °F
1			78	.0712	.0710	14.54	14.49	90
2			62	.0855	.0854	18.09	18.06	90
3a			127	.0814	.0809	16.60	16.47	89
3b			133	.0786	.0781	16.01	15.86	89
3c		.44	498	.0786	.0715	16.01	14.02	70
4	6.0	.45	509	.0786	.0714	16.01	13.93	68
5	7.2	.71	776	.0771	.0608	15.69	11.25	45
6	7.9	.59	658	.0771	.0652	15.69	12.40	54
7	8.7	.39	443	.0759	.0703	15.47	13.93	73
8	12.0	.28	317	.0759	.0730	15.47	14.56	82
9	23.0	.10	115	.0714	.0711	14.56	15.86	89

FIG. 17 AIR CIRCUIT - SCHEMATIC DIAGRAM AND TABULATED PROPERTIES.

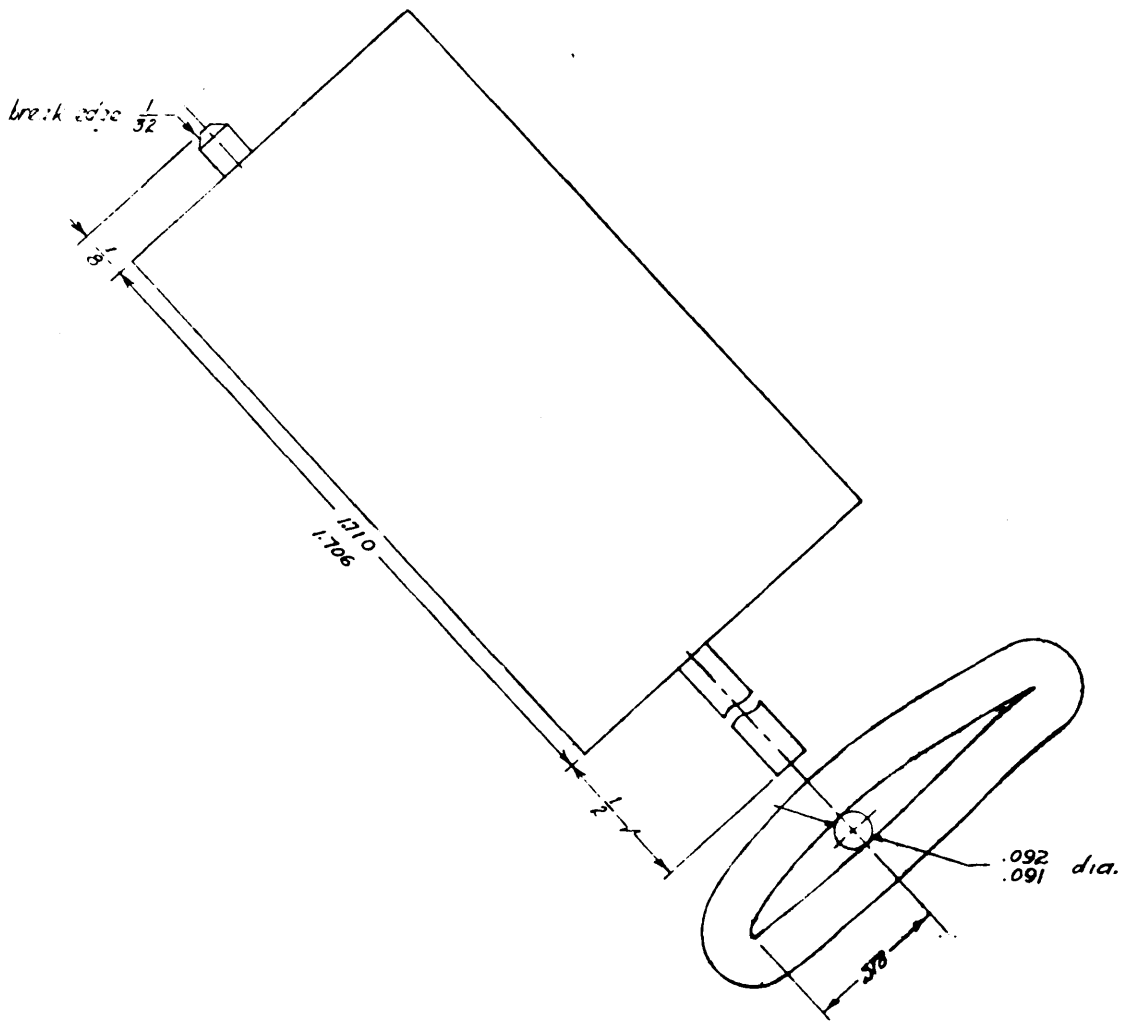

FIG. 18 COMPRESSOR CASCADE AIRFOIL

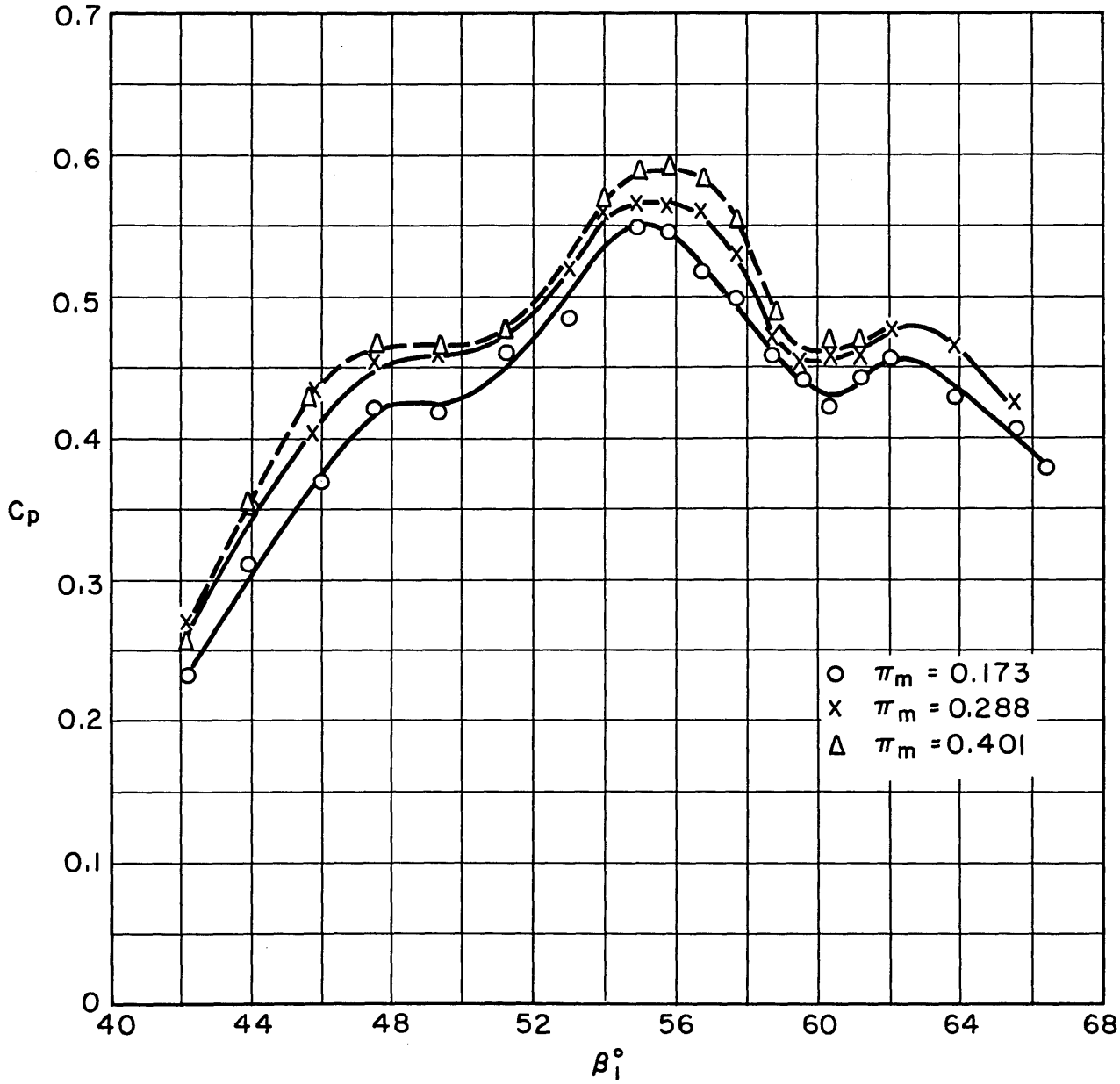

FIG. 19 CASCADE PERFORMANCE
PRESSURE COEFFICIENT VS β_1 FOR σ = 1.0

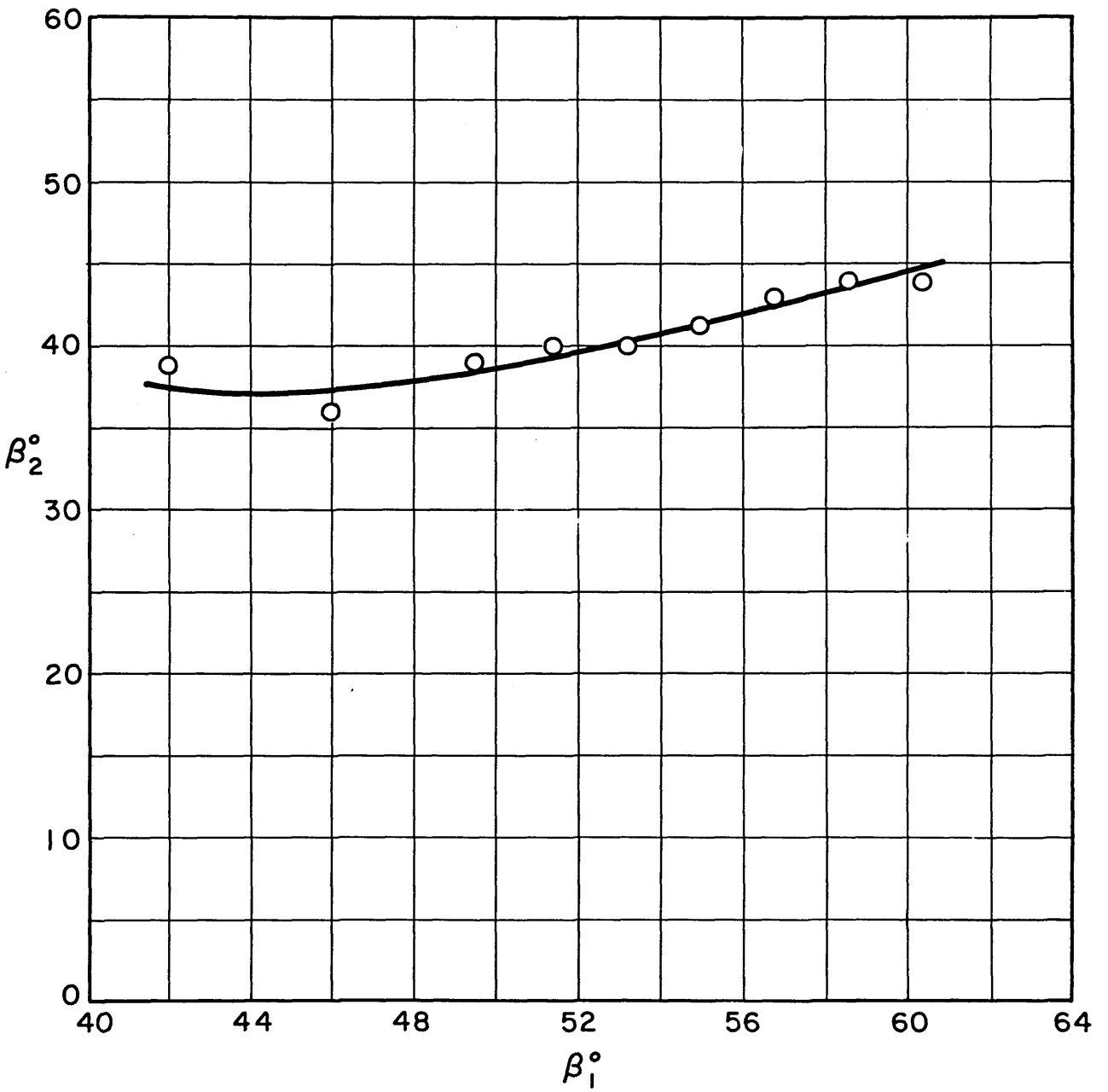

FIG. 20 CASCADE PERFORMANCE β_2 VS β_1 FOR $\sigma = 1.0$

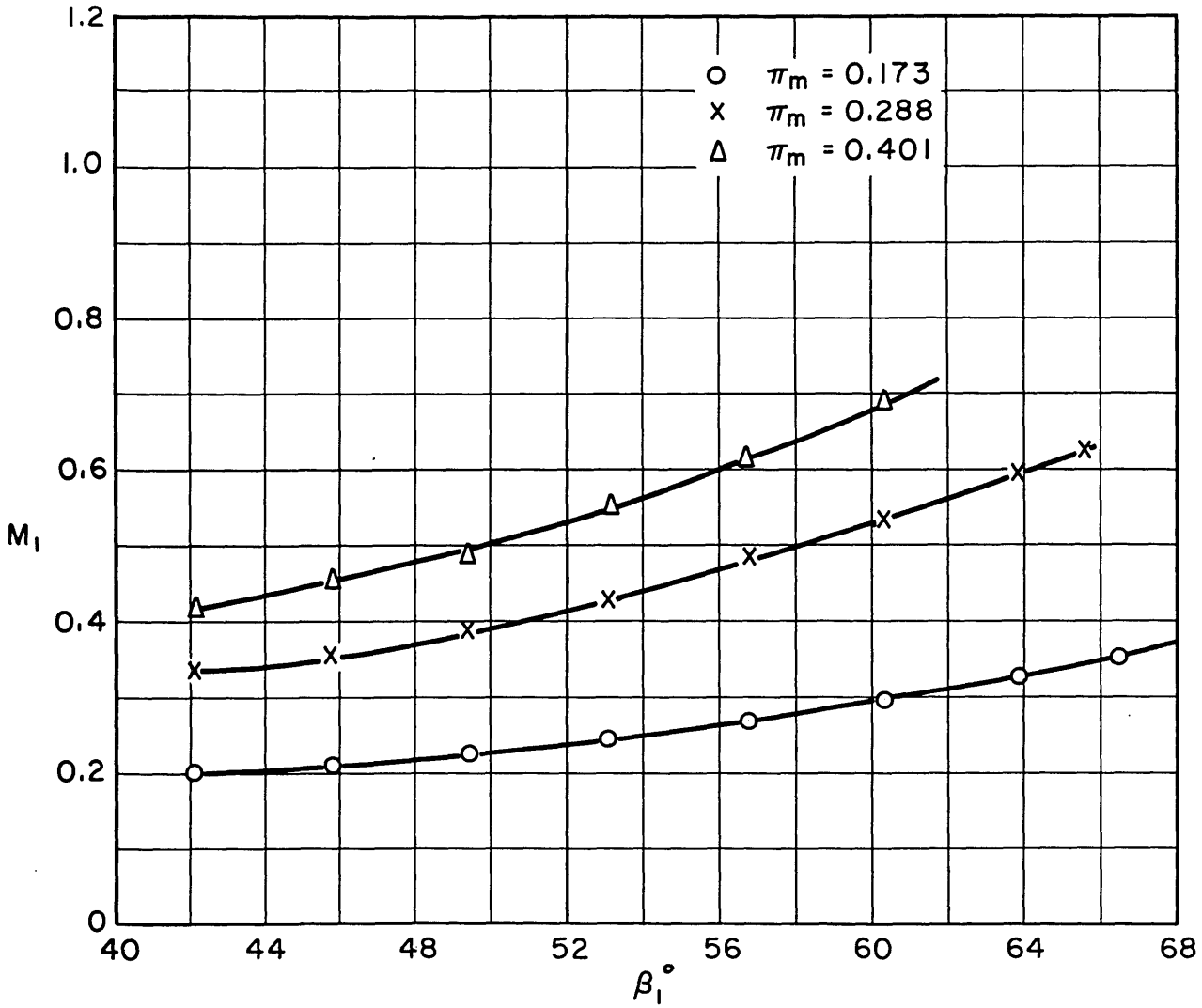

FIG. 21 MACH NUMBER ENTERING CASCADE VS β_1

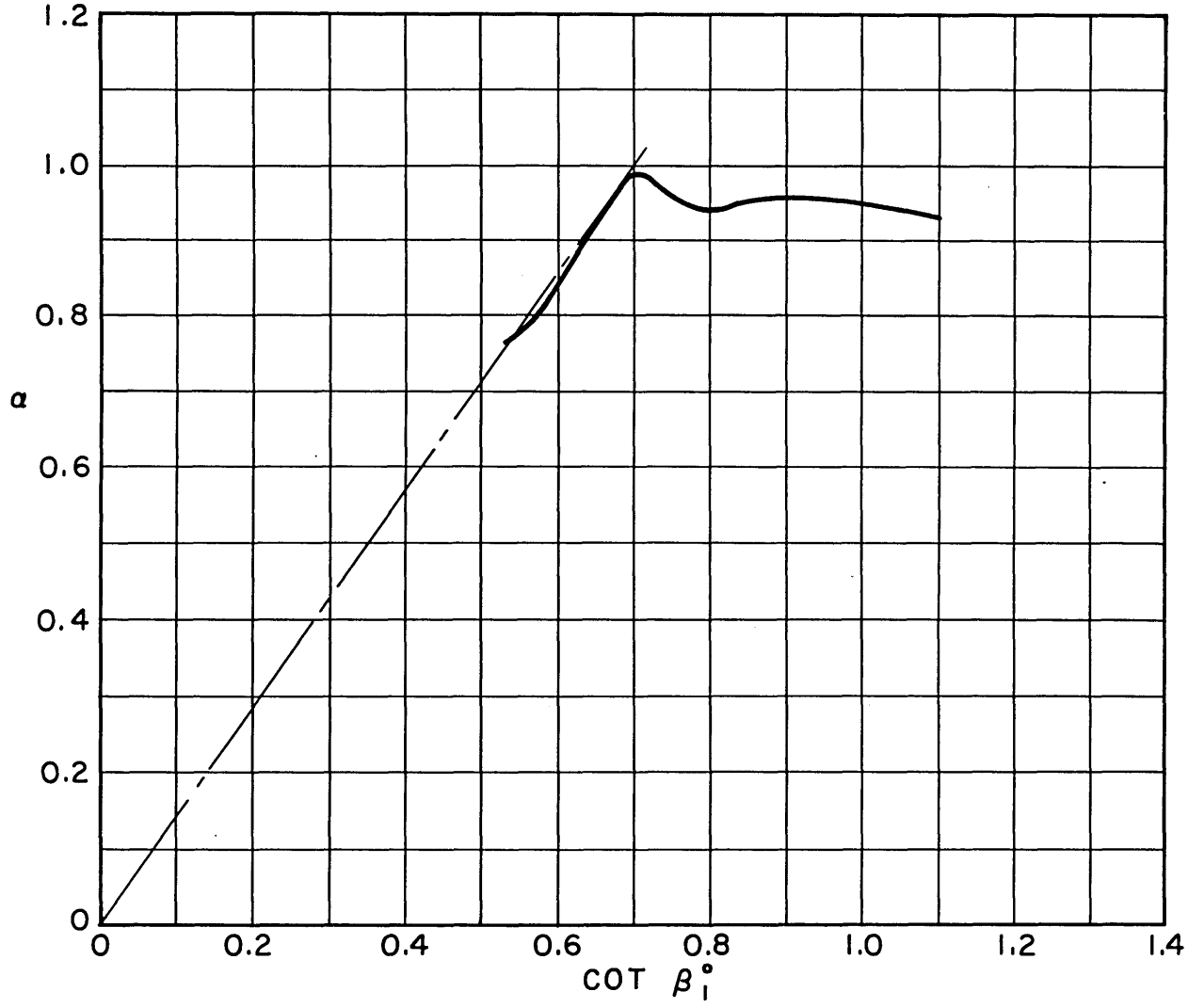

FIG. 22 CASCADE PERFORMANCE — α VS COT β_1 FOR $\sigma = 1.0$

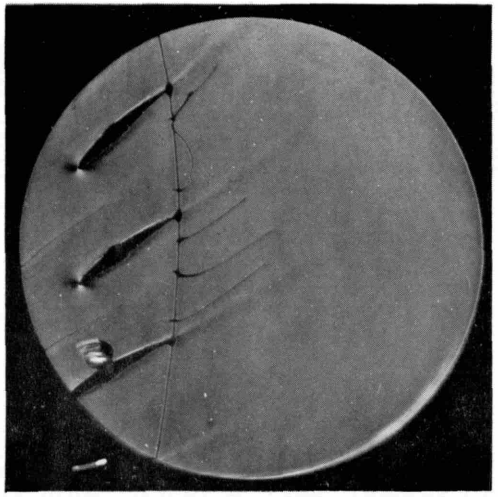

(a)
$\beta_1 = 42°$

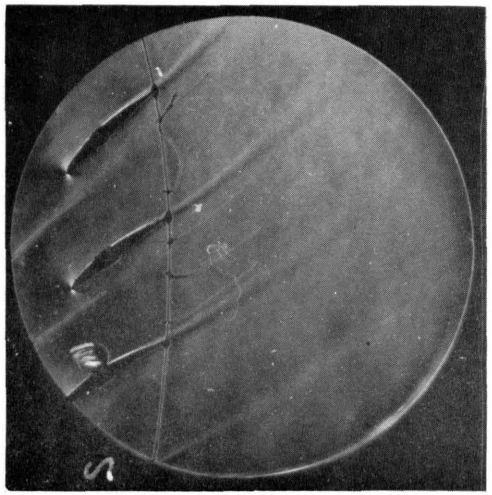

(b)
$\beta_1 = 46°$

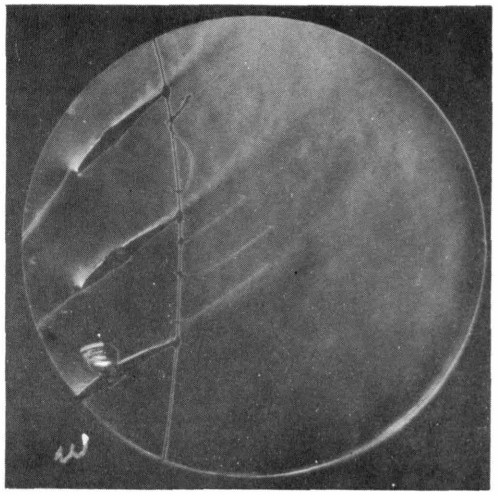

(c)
$\beta_1 = 49.5°$

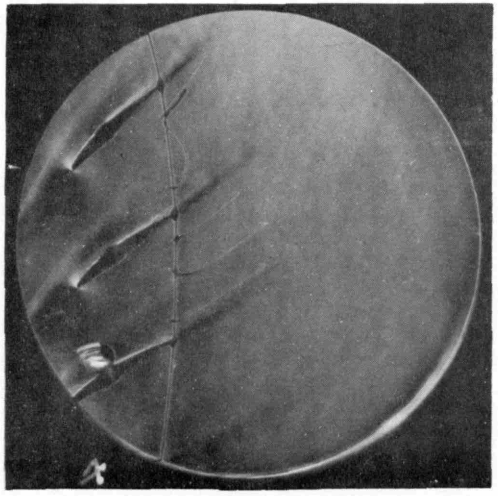

(d)
$\beta_1 = 53.2°$

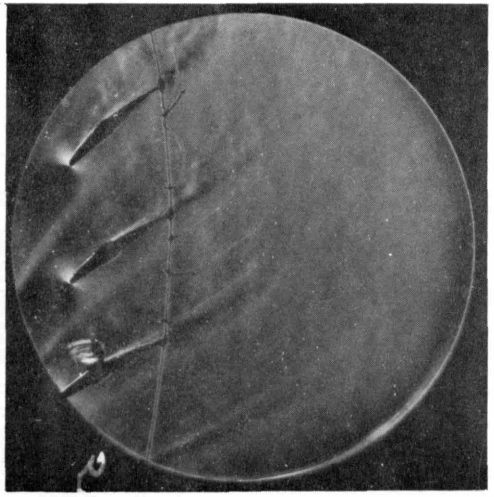

(e)
$\beta_1 = 56.8°$

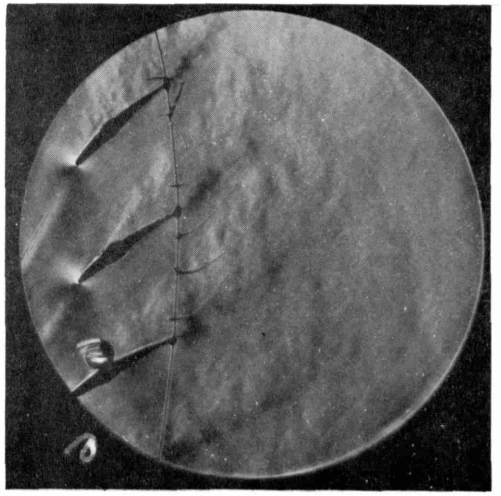

(f)
$\beta_1 = 60.4°$

FIG. 23 SCHLIEREN PHOTOGRAPHS OF THE CASCADE IN STEADY FLOW

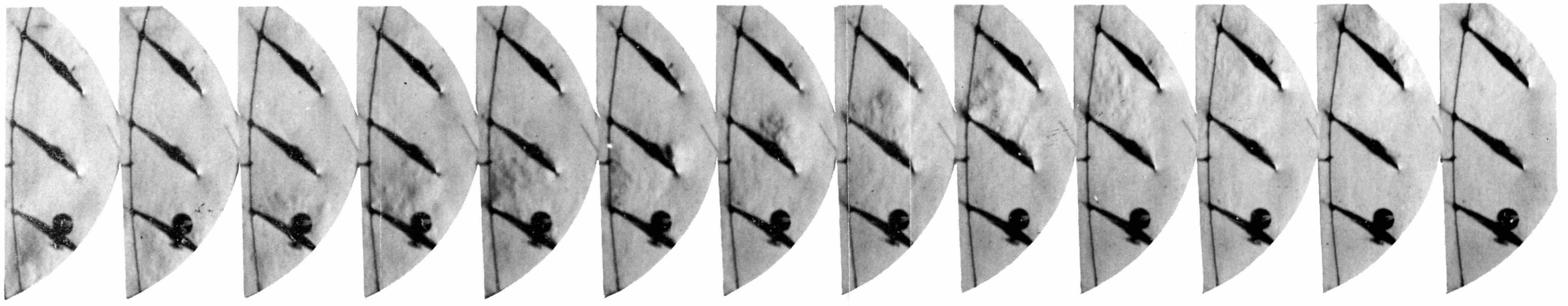

TIME

FIG. 24 ROTATING STALL. 5000 FRAMES/SEC.

$\beta_1 = 63°$ $M_1 = 0.32$ $\sigma = 1.0$

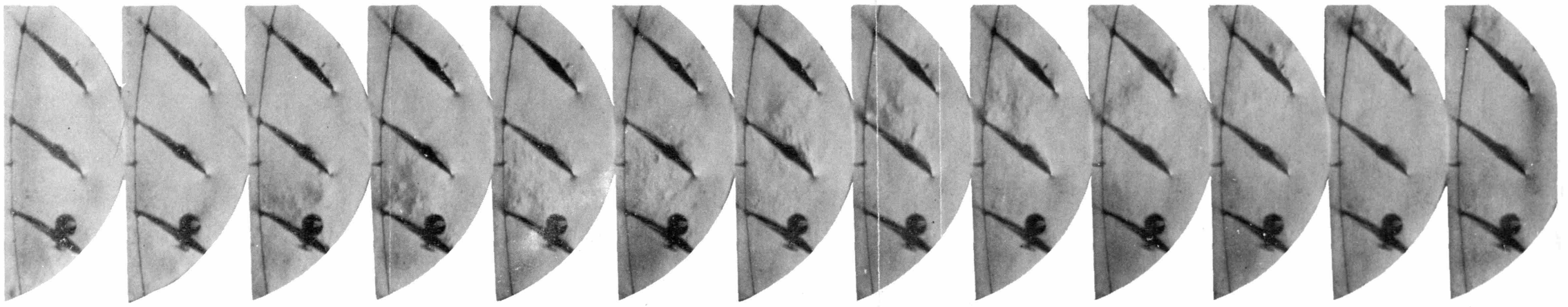

TIME

FIG. 25 ROTATING STALL. 5000 FRAMES/SEC.

$\beta_1 = 64°$ $M_1 = 0.33$ $\sigma = 1.0$

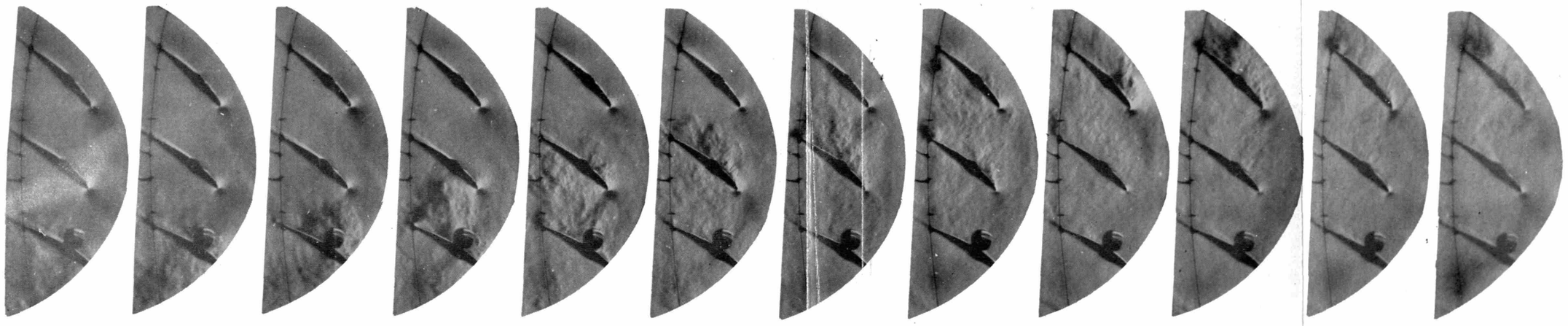

TIME ⟶

FIG. 26 ROTATING STALL. 5000 FRAMES/SEC.
$\beta_1 = 67°$ $M_1 = 0.35$ $\sigma = 1.0$

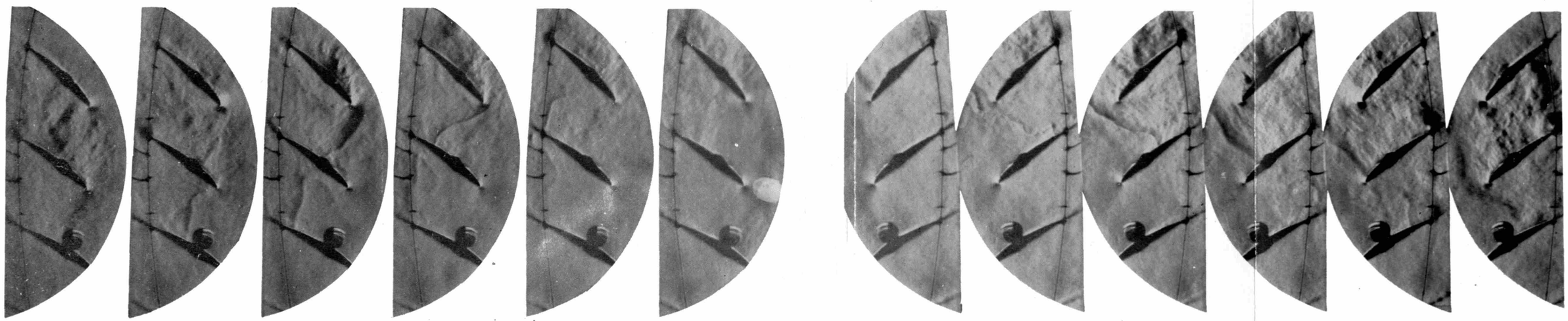

(a) ⟶ TIME (b) ⟵ TIME

FIG. 27 VORTEX PLANES IN THE CASCADE. 5000 FRAMES/SEC.
$\beta_1 = 67°$ $M_1 = 0.35$ $\sigma = 1.0$

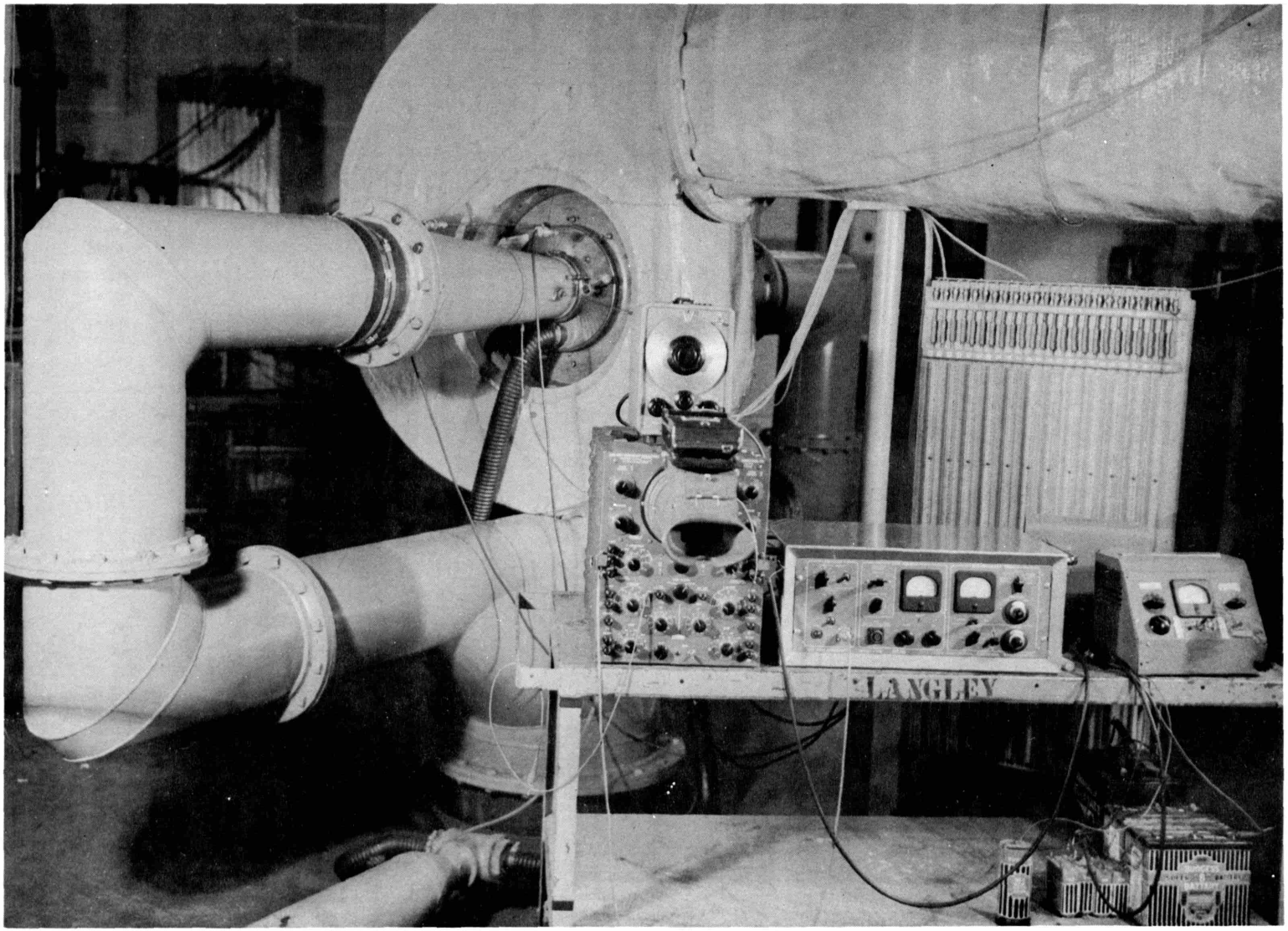

FIG. 28– HOT-WIRE EQUIPMENT AND CASCADE TUNNEL

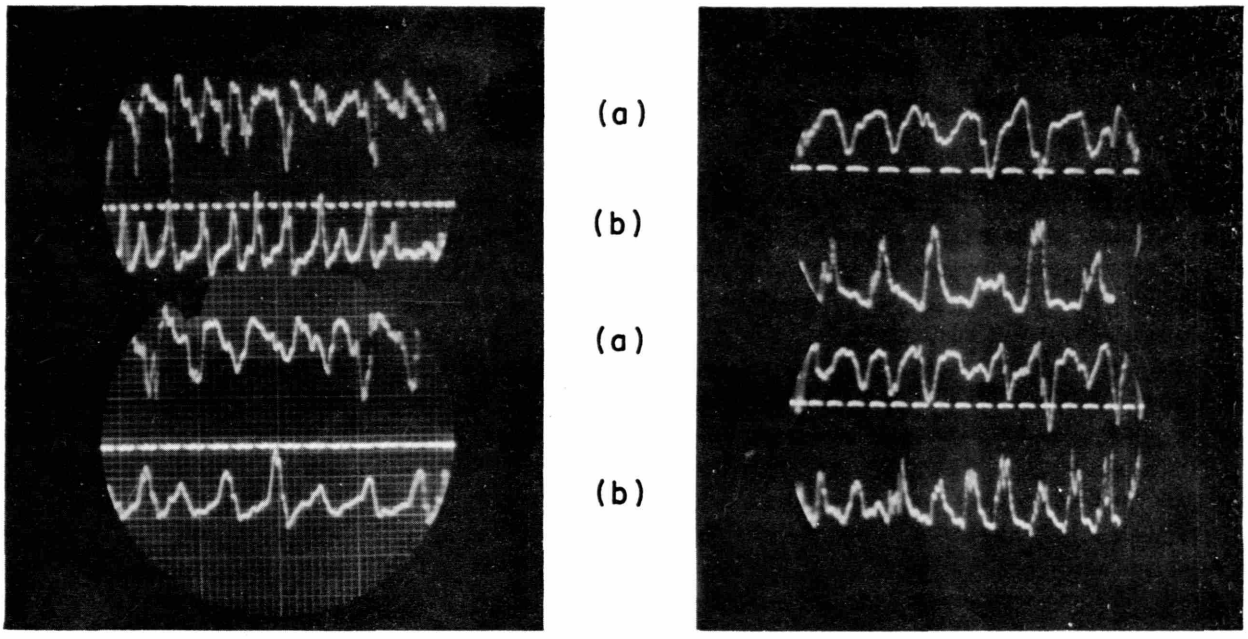

$\beta_1 = 65.5°$ $M_1 = 0.34$ $\beta_1 = 68°$ $M_1 = 0.35$

500 CPS TIMING SIGNALS
VELOCITY INCREASING TOWARDS CENTER
PROBE (b) SEES STALL FIRST

FIG.29 HOT WIRE TRACES FROM TWO PROBES AHEAD OF THE CASCADE, 9 BLADES APART

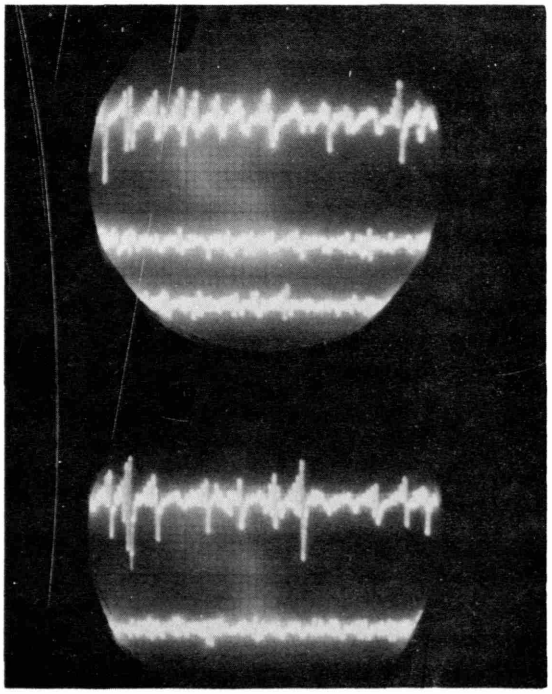

FIG. 30

PRESSURE FLUCTUATIONS BEFORE AND AFTER THE CASCADE.

$\beta_1 = 68.5°$ $M_1 = 0.22$

(a) BEFORE (b) AFTER

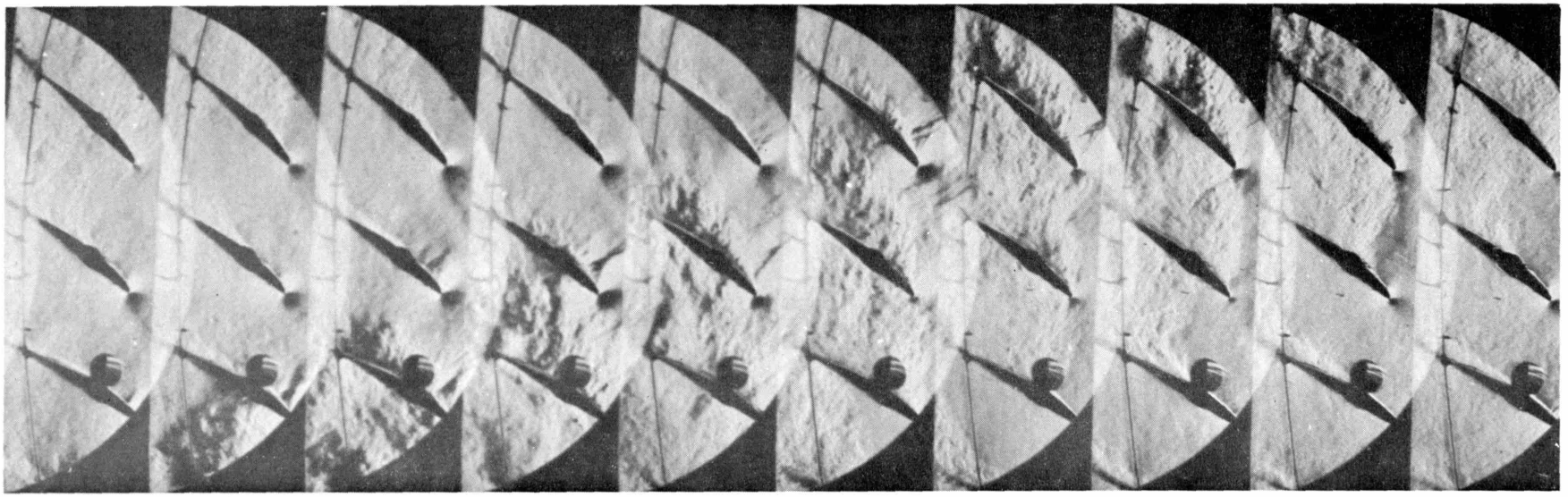

→ TIME

FIG. 31 ROTATING STALL. 6000 FRAMES/SEC.

$\beta_1 = 67°$ $M_1 = 0.65$ $\sigma = 1.0$

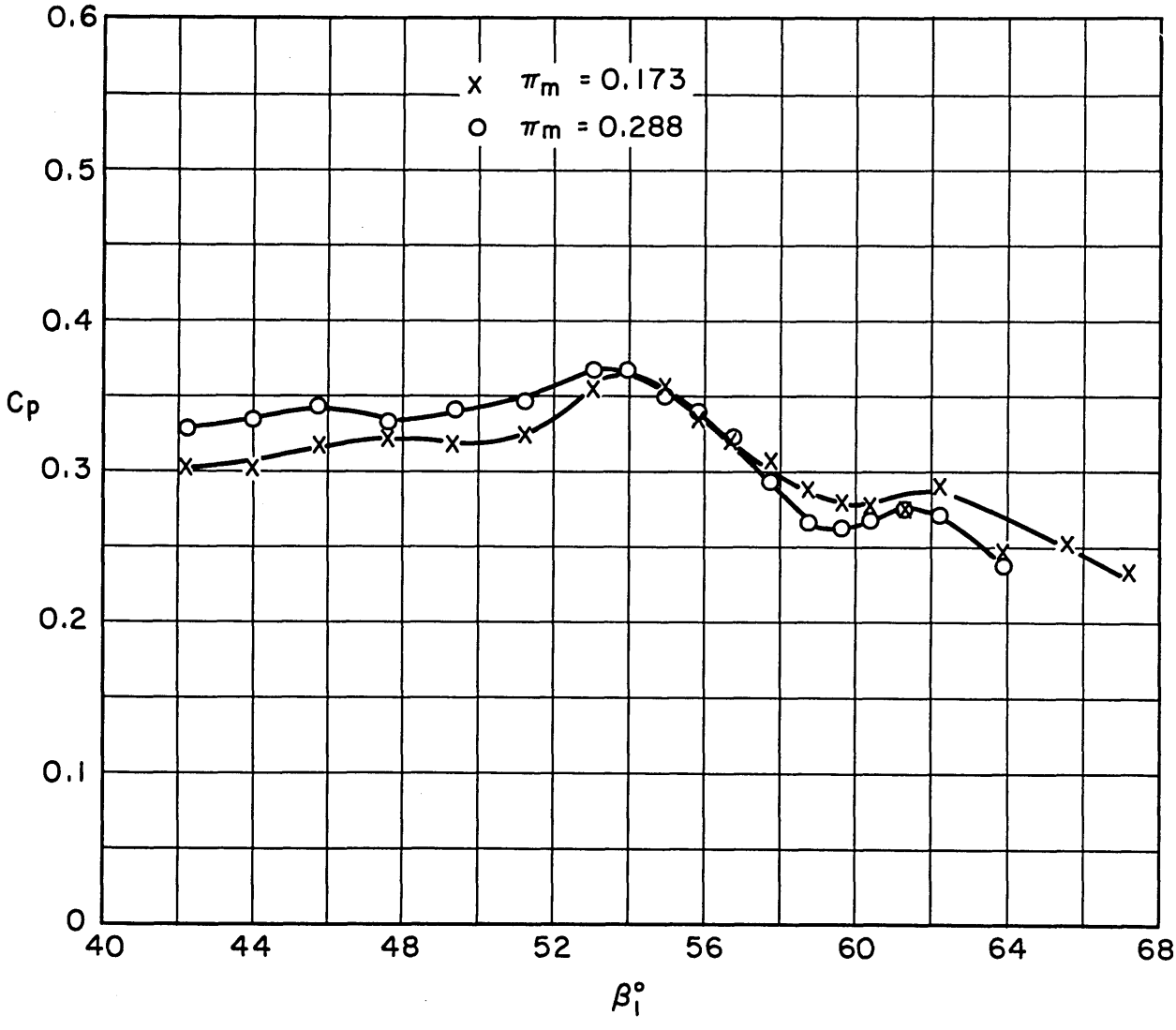

FIG. 32 CASCADE PRESSURE COEFFICIENT VS. β_1 FOR $\sigma = 0.5$

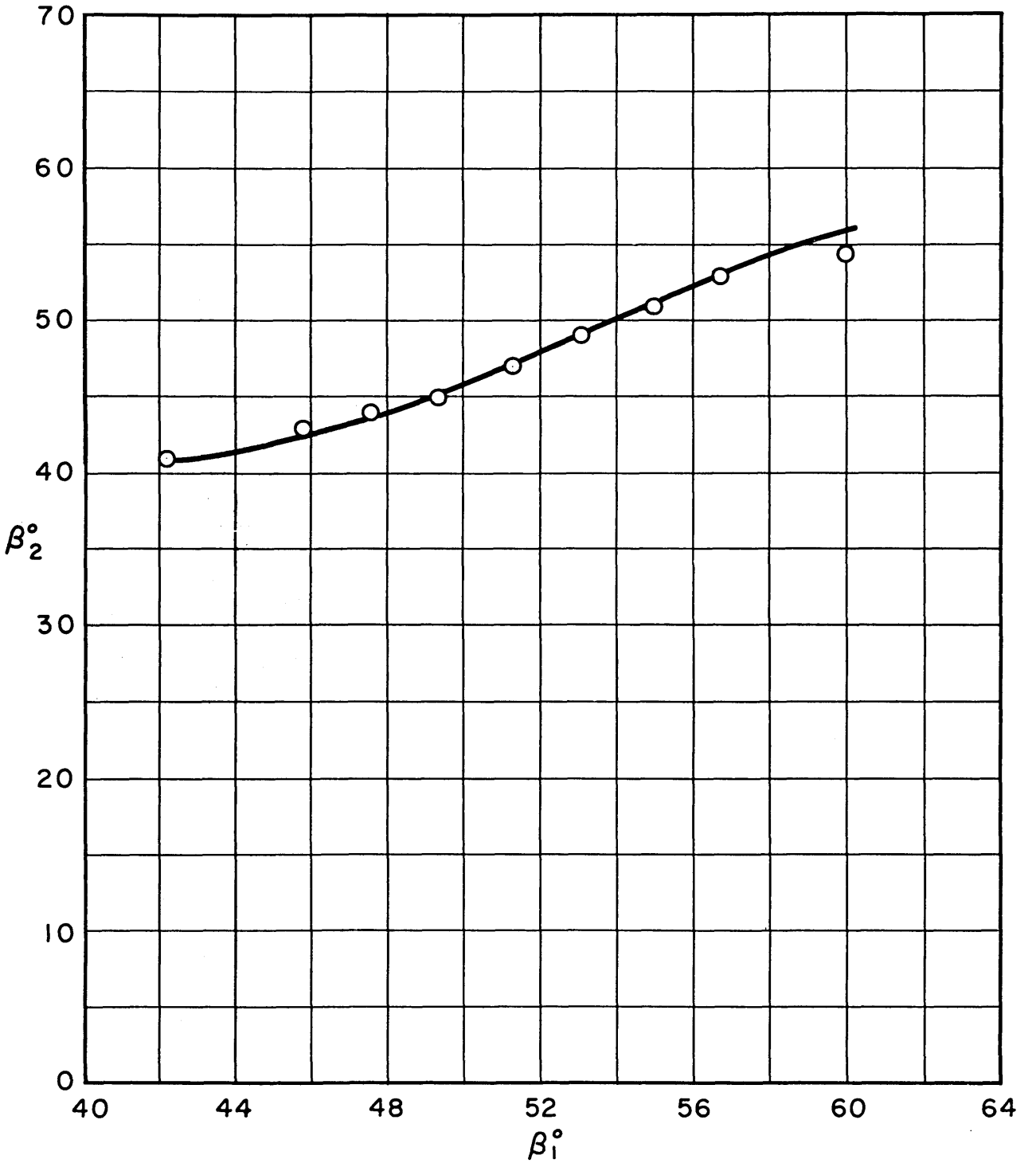

FIG. 33 CASCADE PERFORMANCE β_2 VS. β_1 FOR $\sigma = 0.5$

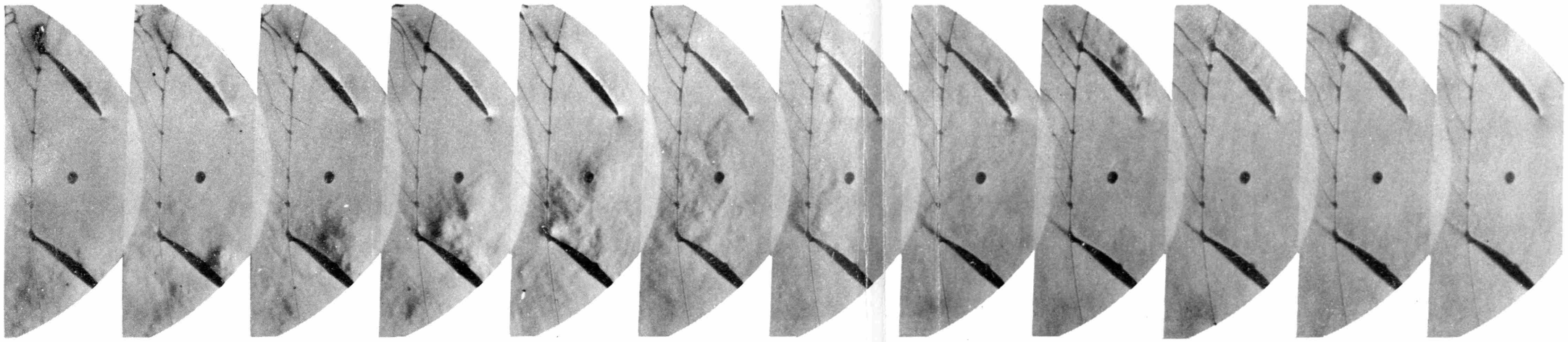

TIME

FIG. 34. ROTATING STALL. 5000 FRAMES/SEC

$\beta_1 = 65°$ $M_1 = 0.34$ $\sigma = 0.5$

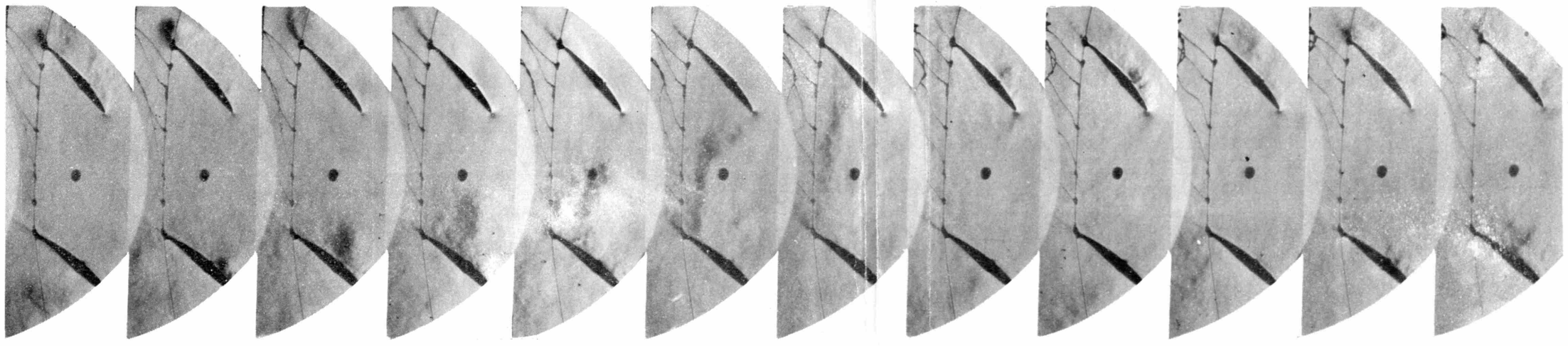

TIME

FIG. 35. ROTATING STALL. 5000 FRAMES/SEC.

$\beta_1 = 68.5°$ $M_1 = 0.35$ $\sigma = 0.5$

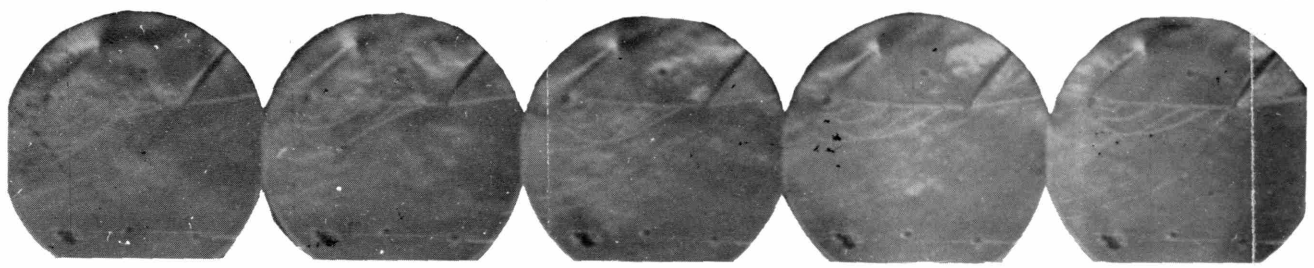

← TIME

FIG. 36. ROTATING STALL.
$\beta_1 = 68.5°$ $M_1 = 0.45$
16 mm. FASTAX CAMERA

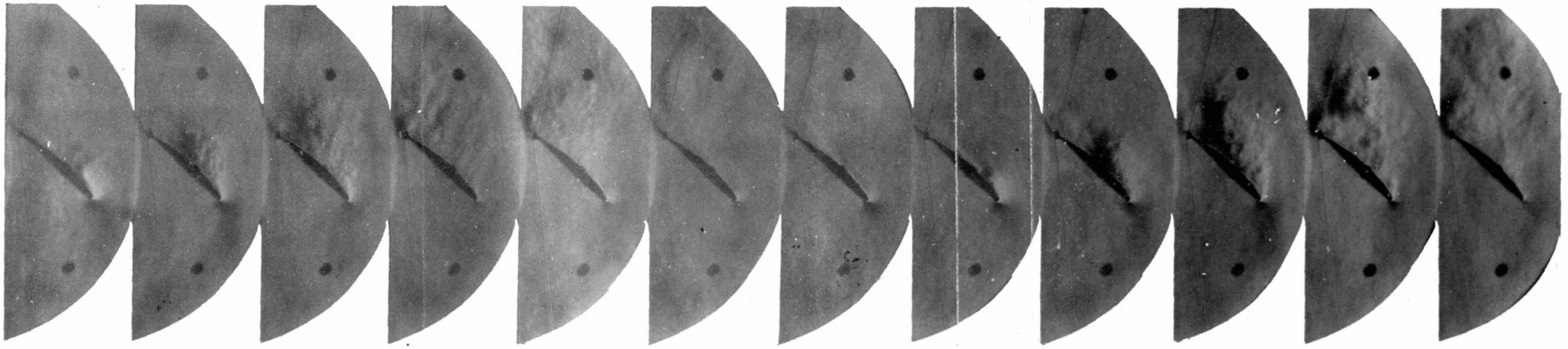

TIME →

FIG. 37. ROTATING STALL. 5000 FRAMES/SEC.
$\beta_1 = 68.5°$ $M_1 = 0.35$ $\sigma = 0.33$

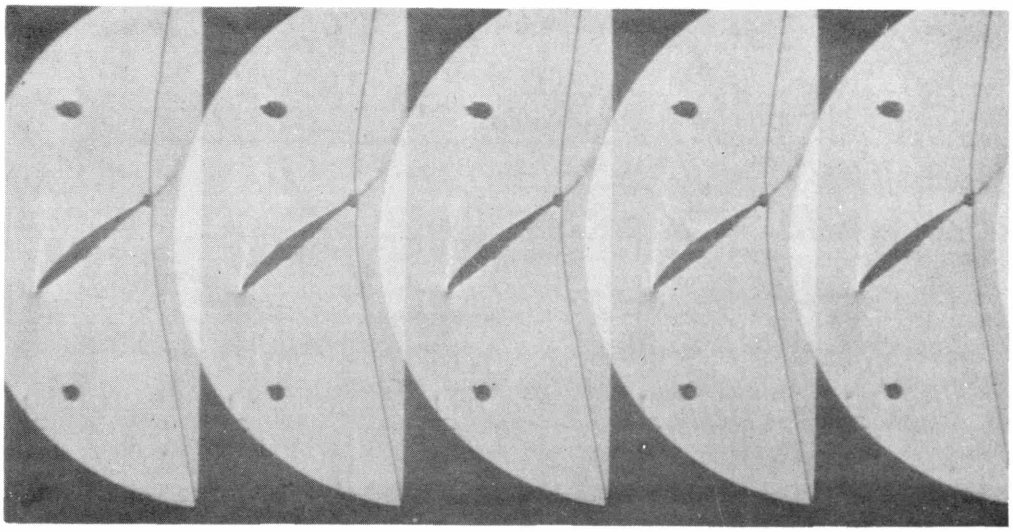

FIG. 38 STALLED AIRFOIL 5000 FRAMES/SEC.

$\beta_1 = 68.5°$ $M_1 = 0.35$ $\sigma = 0.16$

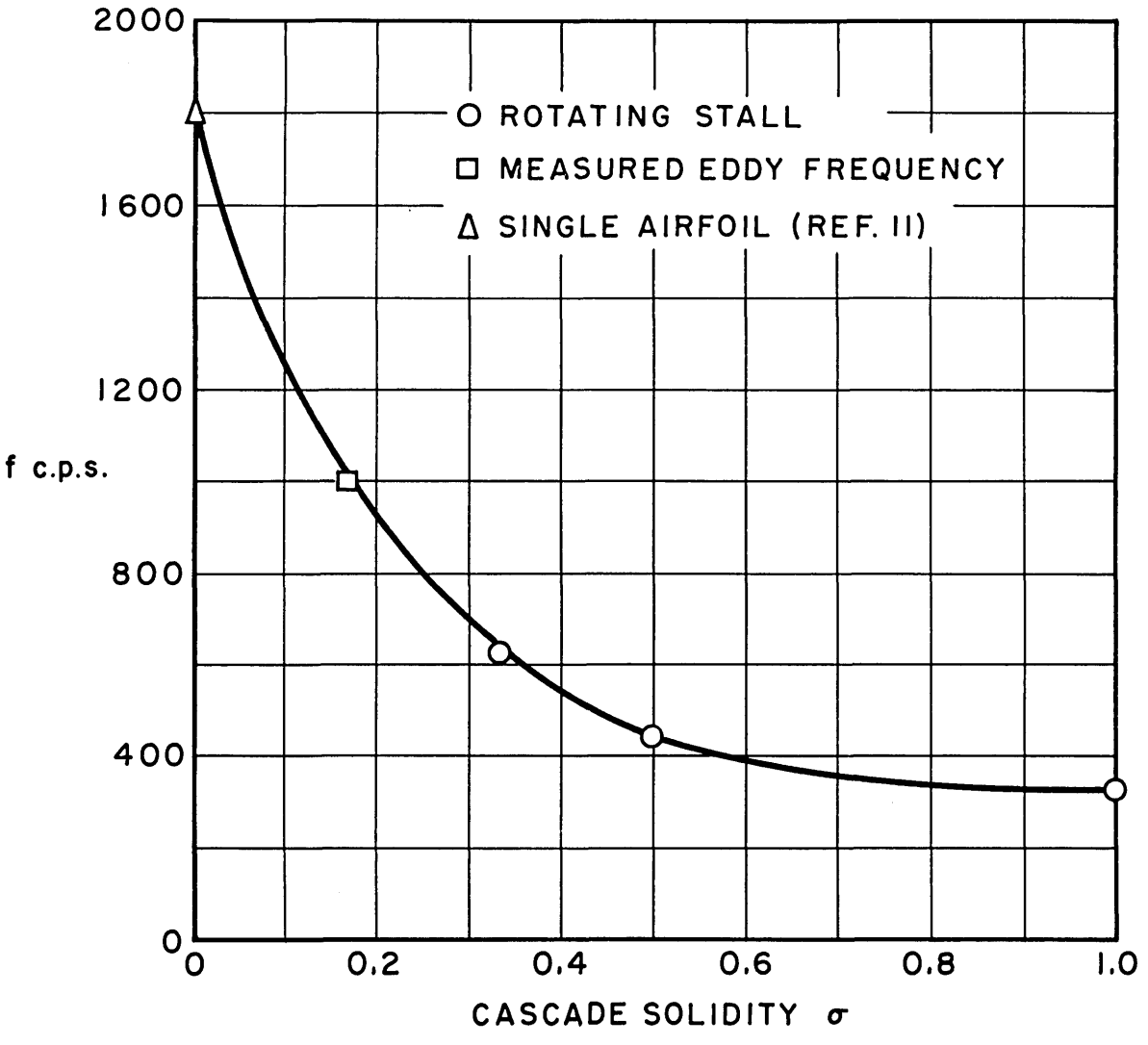

FIG. 39 FREQUENCY OF OSCILLATIONS VS. SOLIDITY

$\beta_1 = 68.5°$ $M_1 = 0.35$

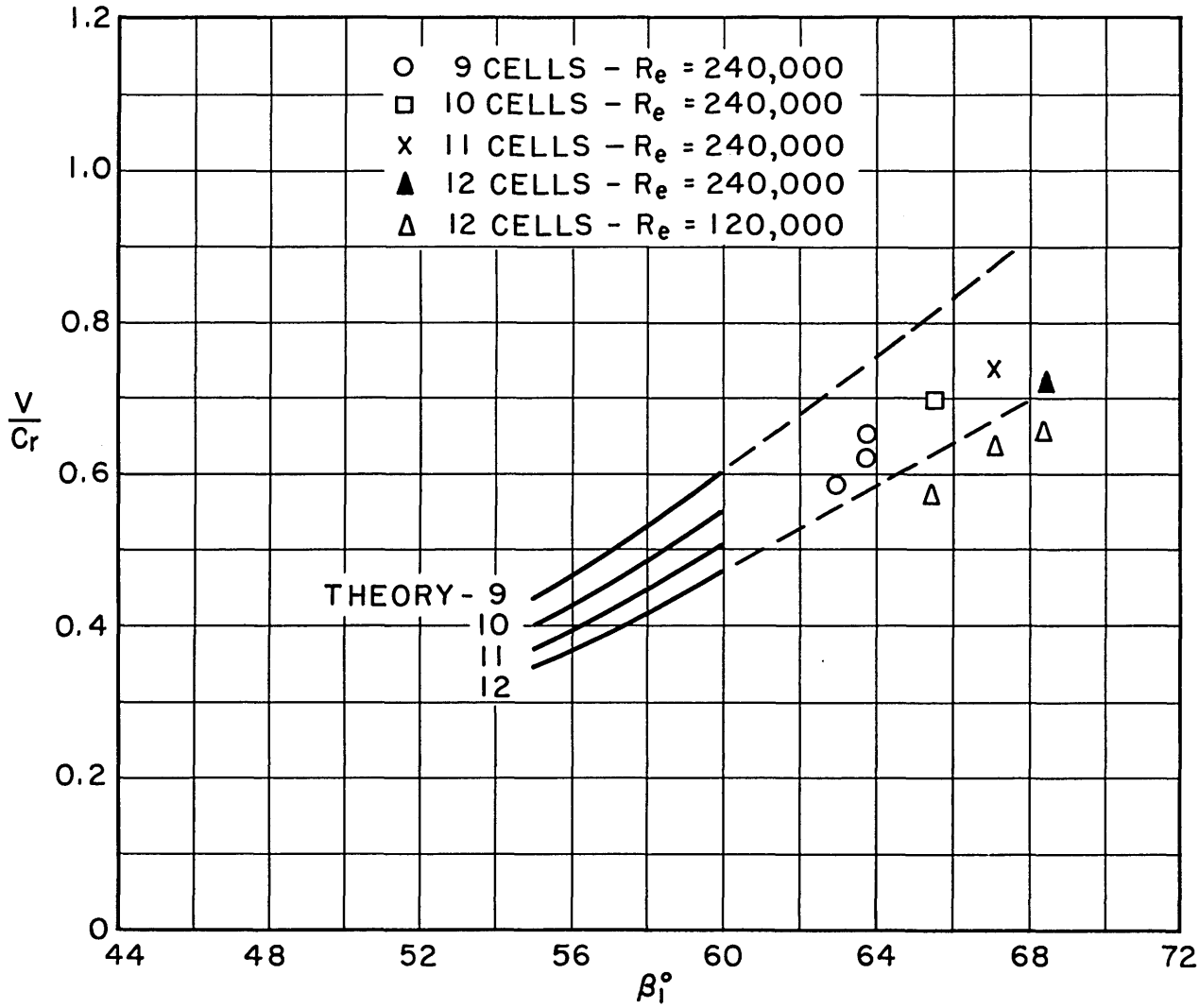

FIG. 40 THEORETICAL AND EXPERIMENTAL VALUES OF PROPAGATION VELOCITY. $\sigma = 1.0$

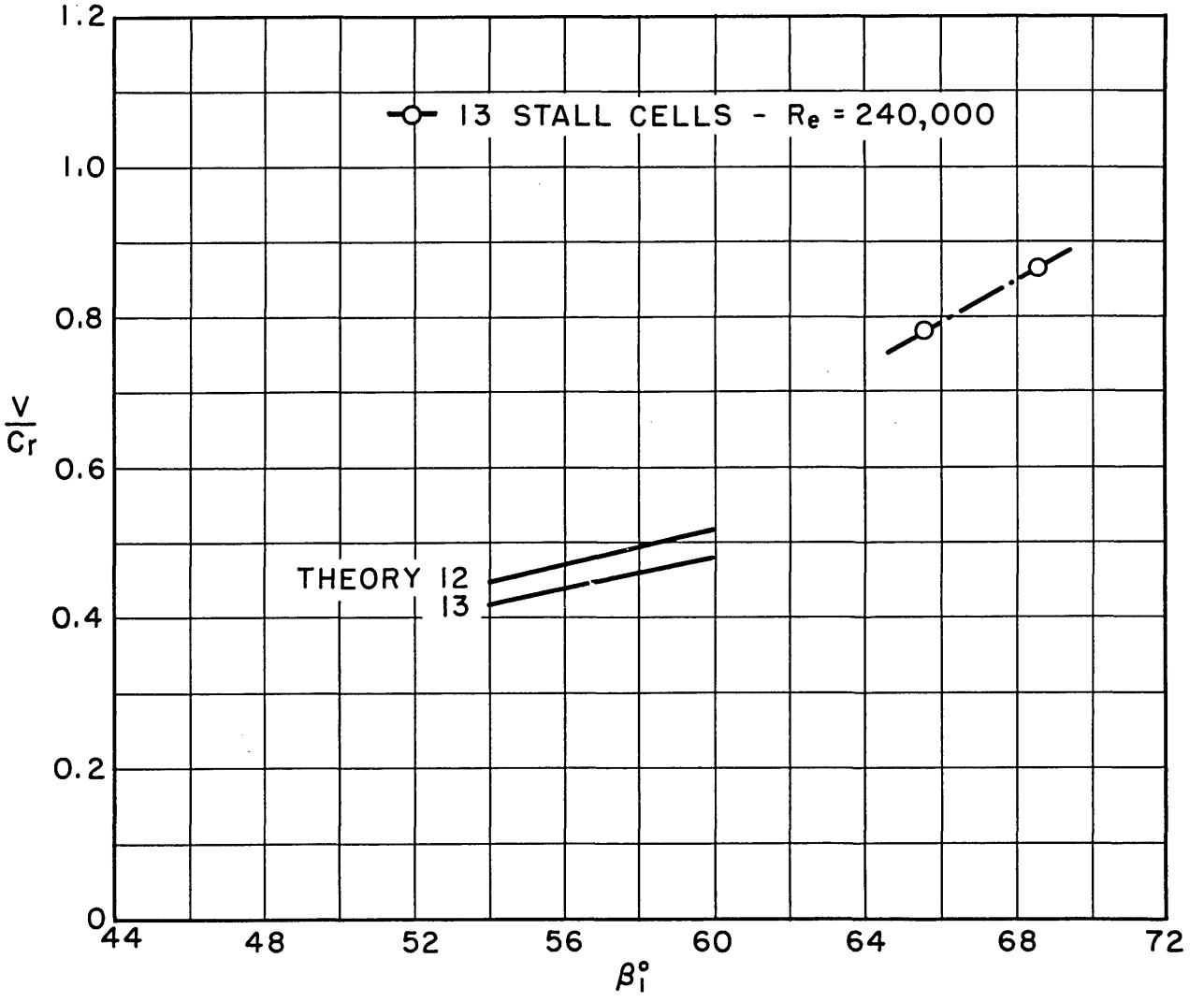

FIG. 41 - THEORETICAL AND EXPERIMENTAL VALUES OF PROPAGATION VELOCITY. $\sigma = 0.5$

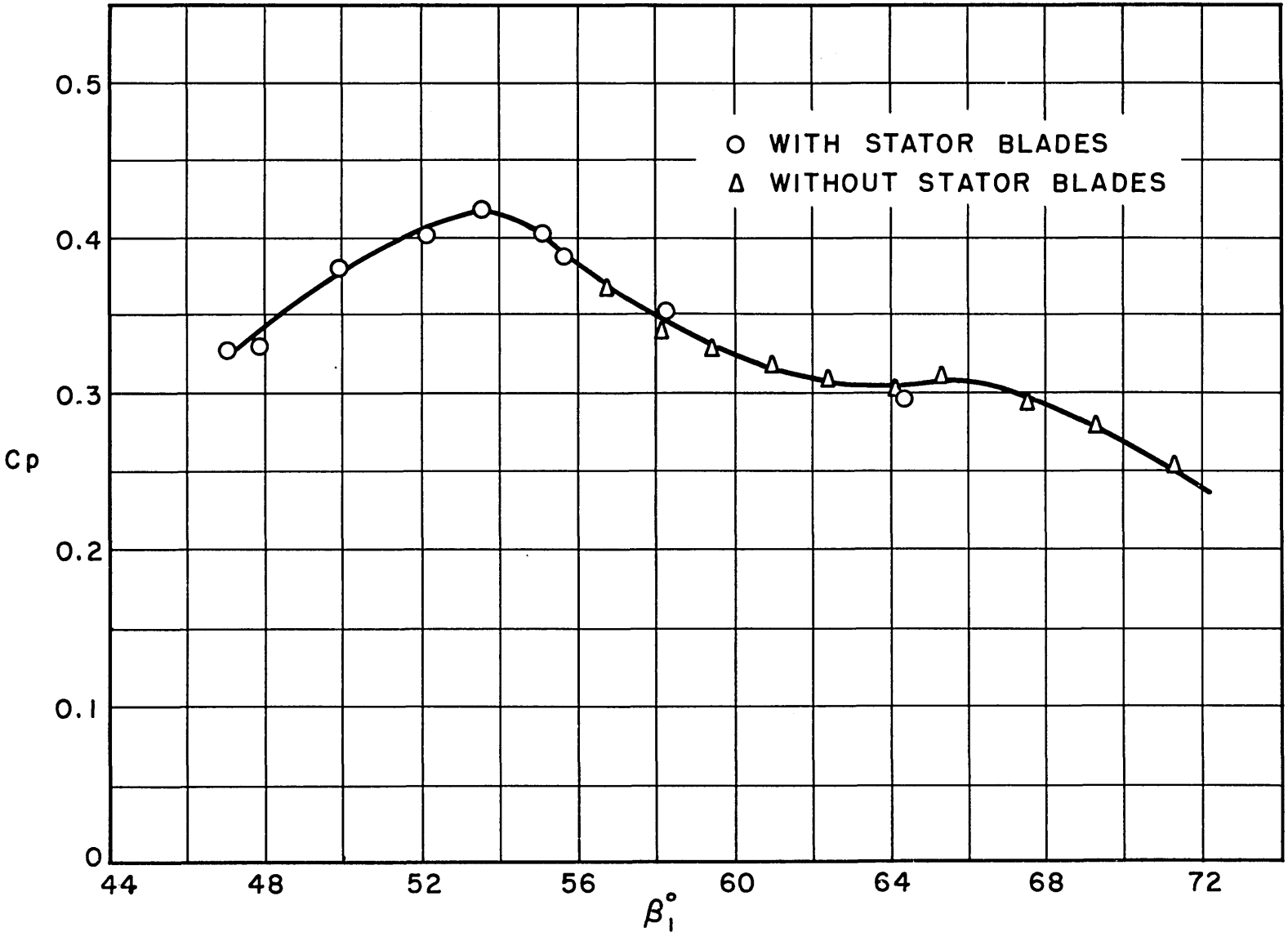

FIG. 42 ROTOR PERFORMANCE. PRESSURE COEFFICIENT VS. β_1

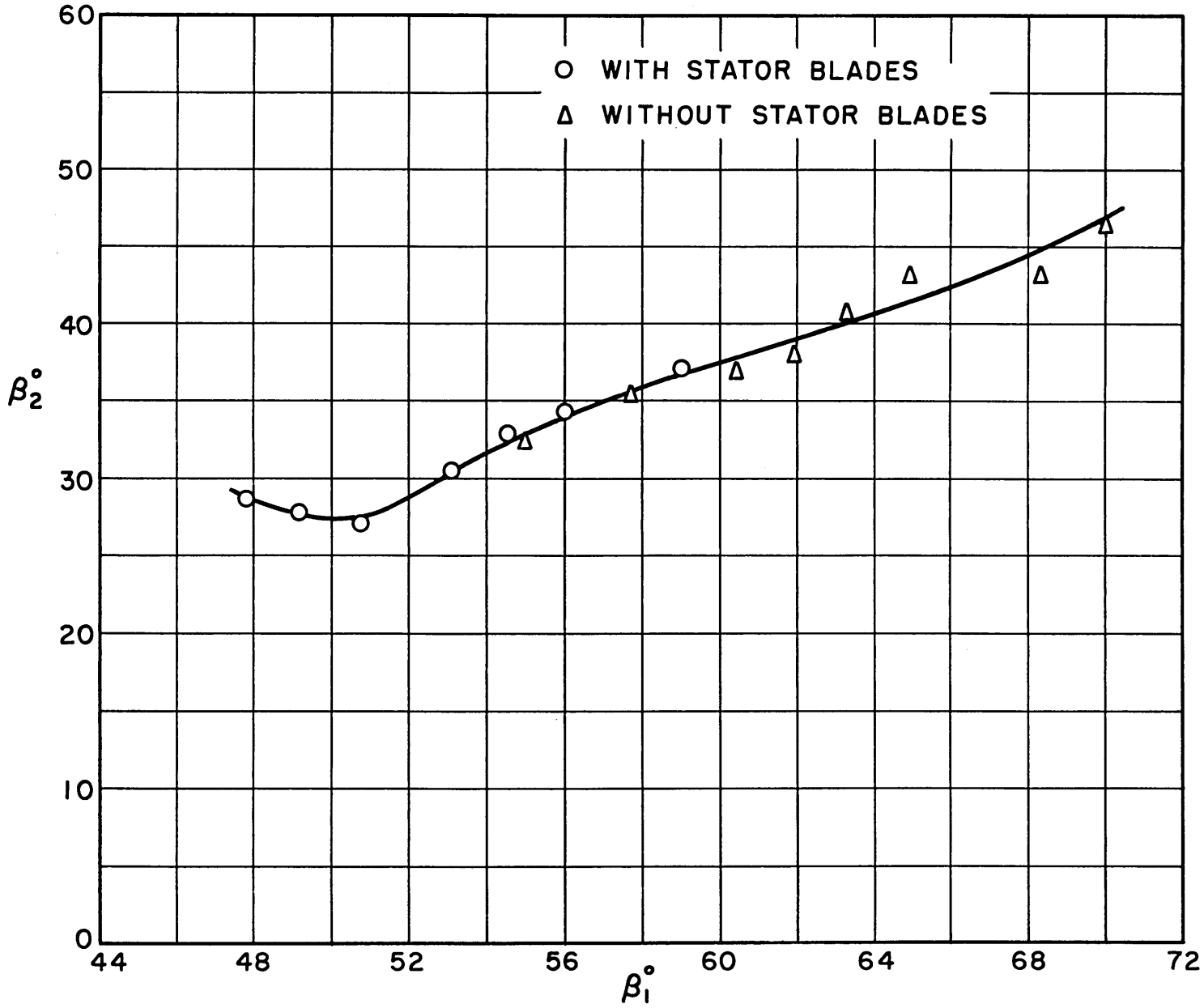

FIG. 43 ROTOR PERFORMANCE. β_2 VS. β_1

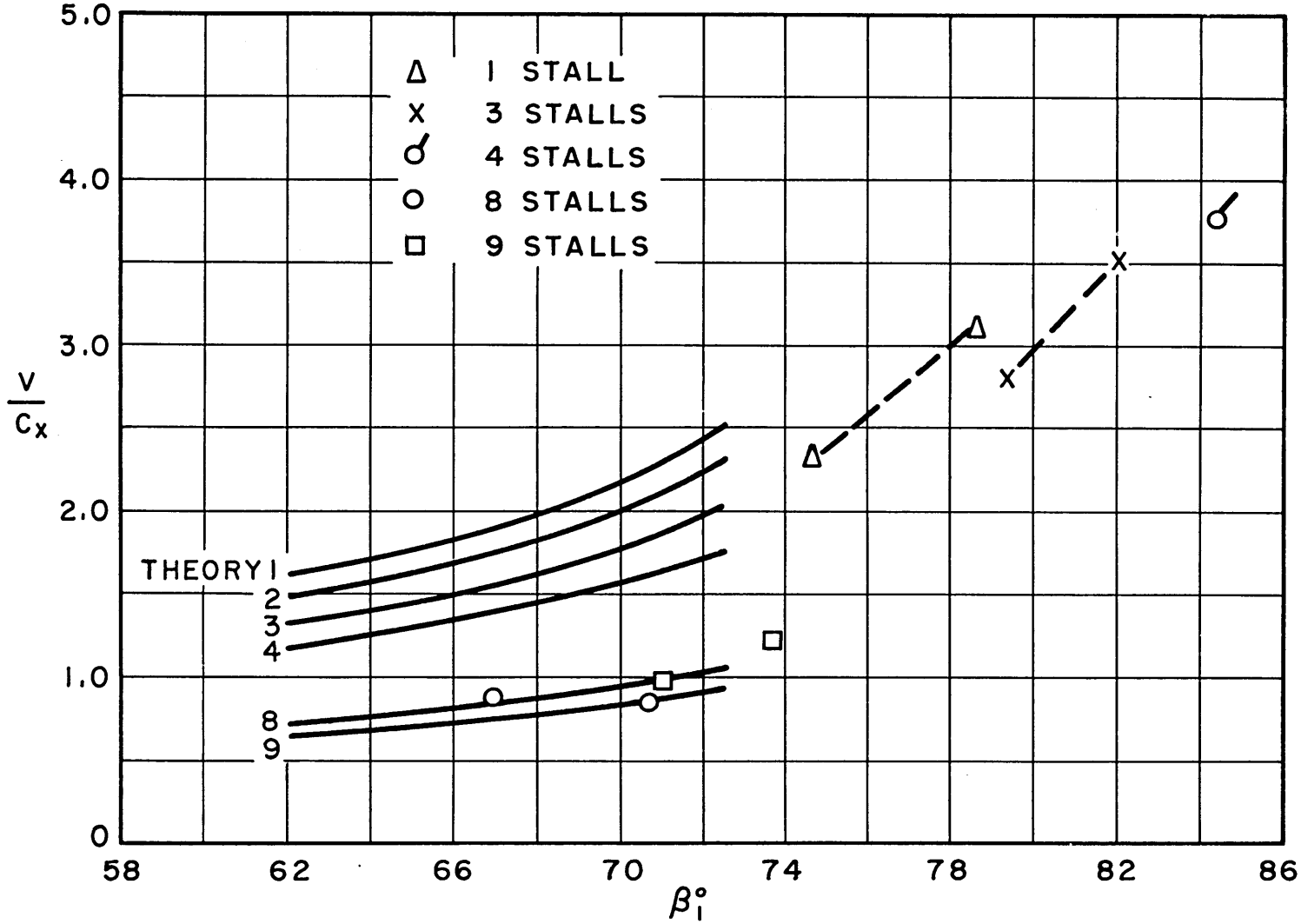

FIG. 44 THEORETICAL AND EXPERIMENTAL PROPAGATION VELOCITIES FOR THE ROTOR.

BIOGRAPHY

The author was born on October 2, 1928, in London, England. After graduating from Allan Glen's School in Glasgow, he attended the University of Glasgow and received the degree of B.Sc. in Mechanical Engineering, in 1950. He was awarded the Thomas Gray travelling scholarship, came to M.I.T. in September 1950, and worked in the Gas Turbine Laboratory as a research assistant until September 1951, at which time he received the S.M. degree.

From 1951 to 1952 the author was employed on guided missile development by the Canadian Defense Research Board at Quebec. He returned to M.I.T. in September 1952, first as a research engineer and later as an instructor, and was responsible for the design and development of turbines for guided missile power supplies at the Dynamic Analysis and Control Laboratory. Other projects included analog simulation of jet engines for control system studies.

In July 1954 he was appointed to the staff of the Gas Turbine Laboratory as Assistant Professor, teaching courses on thermodynamics and propulsion and carrying out research on fluid machinery.